12-2018

A Multidimensional Approach to Understand Chemotaxis and Motility in *Azospirillum brasilense*

Tanmoy Mukherjee
University of Tennessee, tmukherj@vols.utk.edu

To the Graduate Council:

I am submitting herewith a dissertation written by Tanmoy Mukherjee entitled "A Multidimensional Approach to Understand Chemotaxis and Motility in *Azospirillum brasilense*." I have examined the final electronic copy of this dissertation for form and content and recommend that it be accepted in partial fulfillment of the requirements for the degree of Doctor of Philosophy, with a major in Biochemistry and Cellular and Molecular Biology.

<div align="right">Gladys Alexandre, Major Professor</div>

We have read this dissertation and recommend its acceptance:

Elizabeth Fozo, Tian Hong, Andreas Nebenführ, Daniel Roberts

<div align="right">Accepted for the Council:
<u>Carolyn R. Hodges</u></div>

<div align="right">Vice Provost and Dean of the Graduate School</div>

(Original signatures are on file with official student records.)

A Multidimensional Approach to Understand Chemotaxis and Motility in *Azospirillum brasilense*

A Dissertation Presented for the

Doctor of Philosophy

Degree

The University of Tennessee, Knoxville

Tanmoy Mukherjee

December 2018

DEDICATION

I dedicate my work to my Grandmaa, Maa, Baba and my Brother.

ACKNOWLEDGEMENTS

First and foremost, I would like to extend my sincere gratitude to my PhD mentor, Dr. Gladys Alexandre, who has been supportive throughout the course of my research at the University of Tennessee, Knoxville. I feel really lucky to have her as my mentor and guide who has been so much patient and encouraging throughout my PhD career. I am indebted to all the people with whom I have had the pleasure to work with during my dissertation research. Besides my advisor, I would like to thank the rest of my dissertation committee members Dr. Tian Hong, Dr. Elizabeth Fozo, Dr. Andreas Nebenführ, and Dr. Daniel Roberts for their great support and invaluable advice. Each of my dissertation committee members have provided me with extensive professional guidance and have shaped the way I think about scientific research. I would like to especially thank Dr. Hong for the collaboration and support he has provided for the project on swimming behavior of *Azospirillum brasilense.* I am also thankful to my friend Dr. Mustafa Elmas for developing the MATLAB code for high throughput tracking of swimming cells.

 I am grateful to all the undergraduate for their countless hours in the lab spent in helping me with my research. I would like to specially thank Lam Vo who has been an exceptional support as a friend and colleague in the lab.

Nobody has been more important to me than my family during this journey. I would like to thank my parents who provided unconditional love, guidance and support in all my endeavors. I would like to thank my friends Rahul, Avik, Rani, JP, Pawel, and Divyani

who have lent me their support and faith in me in the most testing times. Last but not the

least I would like to thank my fiancée Sreejata for her exceptional support and belief in me.

ABSTRACT

Bacterial chemotaxis is a key survival strategy in diverse environments. It is also an important behavior that allows motile bacteria to colonize new niches. *Azospirillum brasilense* are motile diazotrophic bacteria of agricultural interests due to the ability of several strains to promote growth of a variety of plants upon inoculation. The genome of *A. brasilense* is predicted to encode four chemotaxis pathways, two of which (Che2 and Che3) do not control the chemotaxis response. The chemotaxis system, named Che1, was shown in previous work to regulate transient changes in swimming velocity that occur during chemotaxis. However, Che1 had a minor role in controlling changes in the probability of reversals in the direction of swimming which are also hallmark of the chemotaxis response of motile *A. brasilense* cells. In this dissertation, using genetic and behavioral assays, we demonstrate that the Che4 chemotaxis system regulates the probability of swimming reversals and is the major signaling pathway for chemotaxis and wheat root surface colonization in *A. brasilense*. We also showed that Che1 and Che4 function together to coordinate changes in the swimming motility pattern and that the effect of Che1 on swimming speed functions to enhance the chemotactic response. In the latter half of this dissertation, we focused on the motility and the role of different CheY homologs in chemotaxis and motility of *A. brasilense*. We used high throughput single cell tracking to analyze the swimming pattern of motile *A. brasilense* and identified three different swimming patterns: run-reverse, run-pause and run-reverse-flick "like" pattern. We also

showed that different CheY homologs differently affect the probability of transient pauses during swimming and obtain evidence that the transient pauses are controlled by chemotaxis signaling. These diverse swimming patterns may be advantageous to navigate the heterogeneous and porous environment of the soil. Collectively, our findings illustrate novel mechanisms by which motile bacteria utilize two chemotaxis systems to regulate speed and reversal frequency, and transient pauses during swimming to enhance chemotaxis.

TABLE OF CONTENTS

LIST OF TABLES

LIST OF FIGURES

CHAPTER I

LITERATURE REVIEW

BACTERIAL FLAGELLA AND DIVERSITY IN FLAGELLATION

Bacteria are motile due to the presence of a flagellum on their body. The flagellum is a supramolecular complex that can be 30-50 nm in diameter with over 30 different proteins, some of which are present as a single copy while others are present as several thousand copies (1). From a structural perspective, the flagellum can be divided into three main parts i) the filament ii) the hook and, iii) the basal body (Fig. 1). In most motile bacteria, the flagellar filament is a rigid and extracellular structure that is about 10 µm in length (2, 3). The flagellar basal body comprises a rotary motor whereas the hook and filament work as a universal joint and a propeller respectively. Spirochetes are unique as they can have 1-100s of periplasmic flagella anchored near each end of the bacterium (Fig. 2) (4). The intracellular flagella in spirochetes function not only in motility but also provide these bacteria with their distinct cell shape and serve a skeletal function (5, 6).

FLAGELLAR MOTOR

The bacterial flagellar motor (BFM) is one of the three known biological rotary complexes that also include the two motors of the F_1F_O ATPase complex. While the F_1 motor is driven by ATP hydrolysis, the BFM and F_O are powered by an ion gradient across the cytoplasmic membrane (7). In case of the BFM, the ions are either protons as in *Escherichia coli* and *Salmonella enterica* serovar Typhimurium (8) or sodium ions, the latter being found in marine *Vibrio* and extremely alkalophilic *Bacillus* (9).
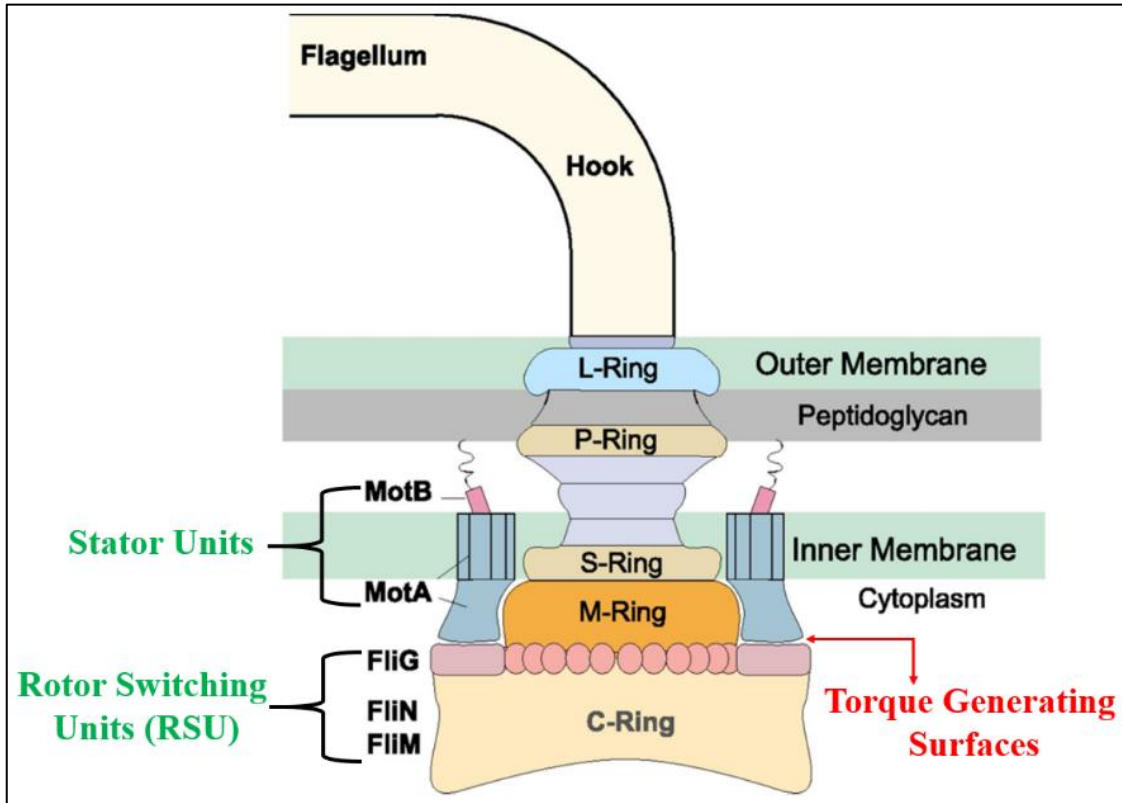
Figure 1. Schematic representation showing the components of the BFM.

The rotor contains the M, S, and C rings of the basal body. FliG around the periphery of the C ring interact with the MotA of the stator complex to generate torque and rotate the flagella. MotA and MotB together form the stator modified from Mandadapu *et al* (10).
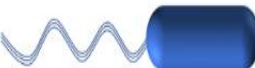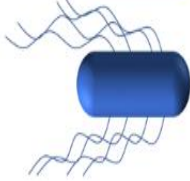
Figure 2. Bacterial flagellation pattern.

Different types of flagellation pattern observed in bacteria are shown here with known examples. The list is not exhaustive. In case of *B. burgdoferi*, the flagella are periplasmic and seen here in fine red lines. Flagellum is shown as blue wavy line/s.

The BFM in *E. coli* is part of the basal body that comprises a stator and a rotor (6). The rotor of the BFM contains four concentric rings namely L Ring, P ring, MS ring and the C ring connected by a rod like structure. The L and P ring sits in the lipopolysaccharide outer membrane and peptidoglycan cell wall, respectively. The MS ring is in the membrane and supramembranal region while the C ring is in the cytoplasm. In *E. coli*, the C ring is comprised of three different proteins, FliG, FliM and FliN that exist as 26 copies (FliG), 34 copies (FliM) and more than 100 copies (FliN), respectively (11). FliG, FliM, and FliN together form a rotor switching unit (RSU). In *E. coli*, the stator complex of the BFM is comprised of two proteins, MotA (4 copies) and MotB (2 copies). The BFM can accommodate 1-17 stator complexes depending on the load on the BFM and the bacterial species (Fig. 1)(12). The stator complex forms a proton channel to couple proton flow through the channel with torque generation. It is the movement of ions through the stator-rotor interface that generates the necessary torque for rotation of the BFM. Torque is generated by the electrostatic and steric interactions between amino acid residues in MotA and FliG in *E. coli* (10, 13).

The BFMs of motile bacteria are mostly bi-directional in that they can rotate both clockwise (CW) and counter-clockwise (CCW). Very few species have unidirectional motors as seen in *Rhodobacter sphaeroides* and *Sinorhizobium meliloti* (14, 15) and the lateral flagellar motor of *Vibrio alginolyticus* (16). Different BFMs produce different torque, and increased torque causes increased swimming speed (17) (18). The torque generated by the BFM can range from ~4,000 pN·nm (19) in the sodium driven motor of

Vibrio spp. to ∼350 pN.nm in *Caulobacter crescentus* (20). The sodium-driven motors are much faster and can rotate at ∼1700 Hz, while the proton-driven motors rotate at ∼300 Hz (7). The diversity in torque generated by different motors is also attributed to the wider base of the BFM: bacteria swim faster as the size of the flagellar basal body increases (12). Bacteria display diverse types of flagellation (Fig. 2). The placement of the flagellum on the cell body varies in different bacterial species. It can be polar (either one or both cell poles) or lateral (peritrichous flagella along the cell body). Many bacteria rely on a single flagellar system. However, a handful of bacteria such as *Vibrio parahaemolyticus*, *V. alginolyticus*, some *Aeromonas* spp., *Rhodospirillum centenum* and *Azospirillum brasilense* possess a dual flagellar system (21). The polar flagella are expressed constitutively and permit swimming in a liquid medium. The lateral flagellar system is expressed only when grown on solid surfaces to facilitate swarming (21, 22).

DIVERSITY IN SWIMMING PATTERN

The most extensively studied bacterium, *E. coli*, has a swimming behavior characterized by straight runs that alternate with brief tumbles, in which the cells re-orient in a new swimming direction. The duration and length of the straight runs increase (a second or so) when the bacteria move towards higher concentrations of an attractant and decrease when moving toward higher concentrations of a repellent (23, 24). The *E. coli* flagella are arranged as peritrichous appendages, and they form a bundle to propel cell's swimming during a run (Fig. 2 and 3). When forming a bundle, all flagella motors rotate in the CCW direction. Owing to its peritrichous flagella, *E. coli* tumbles when one of the several

6

flagellar motors changes the direction of rotation from CCW to CW, which disrupts the helical bundle (24). During a tumbling event, the cell re-orients itself, usually within 0.1s, due to Brownian motion before resuming a "run" towards a higher concentration of an attractant (Fig. 3A).

Many bacteria are monotrichous or lophotrichous including 90% of motile marine bacteria (25, 26). For most of these bacteria, the swimming pattern and control of flagella coordination is poorly understood and typically limited to general descriptions. In the few bacteria with monotrichous flagella and bi-directional motors that have been studied till date, their swimming pattern deviates from the *E. coli* "run and tumble" (27). In the case of monotrichous bacteria, the cell moves forward when the BFM rotates CCW, and the flagellum "pushes" the cell body in the direction of movement which leads to a forward run. When the BFM starts rotating in the CW direction it "pulls" the cell in the backward direction leading to backtracking of the cell trajectories leading to a backward or reverse run (Fig. 3C). This "push and pull" mechanism of swimming is common to monotrichous and lophotrichous bacteria. The monotrichously flagellated *V. alginolyticus*, on the other hand, adds an additional step of flicking its polar flagellum to randomize the direction of swimming leading to a "run–reverse-flick" type of swimming (Fig. 3 D)(28, 29). Thus *V. alginolyticus* swims in a cyclic three-step pattern where forward run followed by motor reversal leads to a backward run. The angle distribution from this forward run to backward run is always centred around ~180° (28). When changing from a backward run to a forward run, *V. alginolyticus* uses its flagella to "flick" so that the cell reorients with a broad

distribution around an angle of 90˚. Subsequently, it was proposed that after the onset of a forward run, the flagellum buckles at the hook due to load from compression (30) as well as the probability of flicking depending on cell size and speed (30, 31).

R. sphaeroides possesses a unidirectional motor that rotates only in the CCW direction (32). *R. sphaeroides* changes swimming direction by briefly stopping motor rotation before re-starting rotation of its single lateral flagellum in a new direction, owing to random re-orientation of the cell body by Brownian motion during the stop (Fig. 3B) (33). *S. meliloti* swims using a polar flagellar tuft powered by unidirectional motors that rotate in the CW direction. In *S. meliloti*, the cells change swimming direction by briefly slowing down, but not completely stopping the unidirectional motor (34). Together, these few examples illustrate the diversity of mechanisms that seem to underlie the ability of flagellated motile cells to change swimming direction. However, because the swimming patterns of motile and polarly flagellated bacteria have not been characterized in most bacteria, the extent of this diversity is yet to be fully appreciated.

ADAPTATIONS TO ECOLOGICAL NICHES THROUGH MOTILITY

Millions of years of evolution have made bacteria adapt to diverse environments and niches, and this is reflected phenotypically and structurally in the BFM and thus, in the swimming ability and patterns.
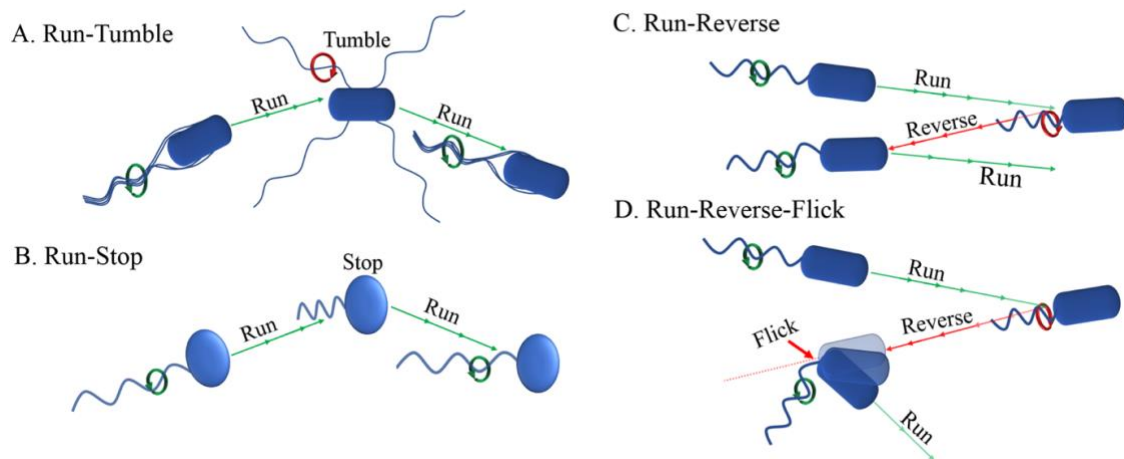
Figure 3. Bacterial swimming patterns.

A). *E. coli* swims in a two-step run and tumble pattern. During run, the flagellar motors rotate in a CCW direction forming a flagellar bundle pushing the cell body forward. Tumbling happens when any of the motors rotate in a CW direction and the flagellar bundle falls apart. This causes the cell to reorient in a random direction. **B).** *R. sphaeroides* swims in two steps run and stop pattern **C).** *P. aeruginosa* swims in run and reverse pattern. **D).** *V. alginolyticus* swims in a cyclic three step run-reverse-flick fashion. Notice the buckling of the flagella (red arrow) that leads to change in direction around ~90˚. Green arrowhead lines denote forward path whereas red arrowhead depicts backward movement. CW rotation is shown in red circular arrow while CCW is shown in green circular arrow.

Adaptations to ecological niches through Flagellar motor

The speed of rotation of the BFM was shown to increase linearly with membrane potential which in turn is a component of the proton motive force (35). This proton motive force generated is also necessary to generate the torque required for rotating the BFM thus defining the swimming speed of the bacterium. The BFM is considered highly efficient if the torque generated to proton motive force ratio approaches unity during its rotation i.e. the BFM can convert all of the proton motive force generated to torque to drive the motor (20). However, the torque-speed relationship of the motor shows two regimes and is concave down in nature (Fig. 4). In the first regime, the torque remains unchanged with increases in the motor speed. This constant torque regime is considered the most efficient regime where efficiency approaches unity (20). Above a motor speed threshold, called the knee zone (Fig. 4), the torque decreases linearly with the motor speed and the efficiency of the motor also sharply decreases. Hence, bacteria which are found to swim at a speed above the knee rate are not considered as efficient swimmer.

The motor in *C. crescentus* operates at 100% efficiency whereas that of *E. coli* operates at nearly 80% efficiency as the swimming speed is very close to the knee zone (Fig. 4). It is noteworthy that the motor in *V. alginolyticus* operates far from the knee zone and at only 20% efficiency (20). Although, the energy consumed by BFM during swimming is negligibly low and can be neglected in rich medium, it can have considerable effect on the energy budget if the bacterium is swimming in a low nutrient medium (20). Consistent with this notion, *C. crescentus* cells which possess highly efficient motors are also found in low
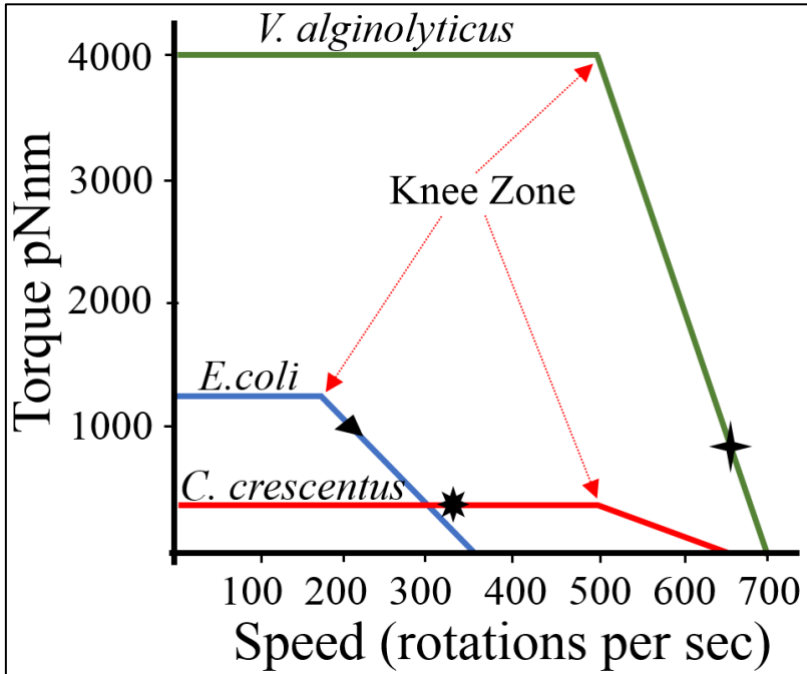
Figure 4. Torque-speed relationship of the flagellar motor in three bidirectional flagellar motors.

The measured torque and speed of the motor for freely swimming cells are denoted by triangle for *E. coli*, star for *V. alginolyticus*, and sun for *C. crescentus*. Adapted from (20).

nutrient environments, and the genome of this bacterial species encodes multiple clusters of genes for proteins essential for survival in nutrient scarce habitats (36). *C. crescentus* generates more torque during a backward than a forward movement which can help them to quickly backtrack toward (37) nearly missed nutrient source peaks. On the other hand, *V. alginolyticus* that swims with a sodium driven motor in their marine settings can afford to operate their motors at a low efficiency of 20%. This is because the BFM of *V. aliginolyticus,* a marine bacterium, is powered by sodium ions and there is no dearth of sodium ions in the marine environment to power the BFM in this bacterium. The same argument can be extended to the motor of *Campylobacter jejuni*, a bacterium from the epsilon(ε)proteobacteria family, found in the high nutrient environment of the animal mucus layers, and that generates a high torque at high efficiency (38).

Apart from the example of the energetic cost of motility being influenced by the flagellar motor torque, another example of adaptation to ecological niches is evidenced from the structure of the BFM. The BFM of *C. jejuni* can pierce through highly viscous mucus layers and has likely evolved to swim in high-viscosity media that would generally immobilize swimming *E. coli* or *Vibrio* cells. In a detailed review on the motility of ε-proteobacteria, Beeby notes that ε-proteobacteria which usually have one or more polar flagella can swim much faster in high viscosity environments (39). In their earlier work they had found that accessory proteins are added to the BFM that can increase the C ring size (12). Beeby *et al*. used Cryo Electron Microscopy (CryoEM) to show that *C. jejuni* had 17 flagellar stators as compared to the 11 found in *Salmonella enterica* subsp. enterica

serovar Typhimurium and thus a wider C ring of 26 nm as compared to 23 nm of *S. enterica* subsp. enterica serovar Typhimurium. This structure, in turn, generates increased torque and thus helps promote swimming in viscous environment (12). n the follow up paper they used phylogenetic analysis coupled with CryoEM to decode likely evolutionary path of the *Campylobacter* motor and speculate the selective advantage of each step in the path (12). They found that the inner- and outer-membrane associated structures of the BFM may have evolved multiple times independently to form the high-torque generating *Campylobacter* motor (38) to enable them swim in highly viscous environment.

Adaptations to ecological niches through different swimming parameters

The energetic cost of motility is high and includes maintenance of flagella and their rotation (40). Various swimming patterns and speed can lead to better foraging, especially during chemotaxis, where chemotactic precision, as defined by faster gradient climbing and better steady-state accumulation at resource, peaks (41). Thus, it is highly desirable for bacteria living under scarce nutrient conditions to optimize their motility. For example, *C. crescentus* adapts to nutrient poor environment not only through efficient motor torque but also through the adoption of a helical swimming pattern that enhances its motility (42). Helical trajectories are also shown to be important for spirochetes and for a pathogen such as *Helicobacter pylori* as these swimming patterns enhance motility to enhance motility, pathogenesis, and survival within host (4, 43). Helical trajectories were shown to generate thrust that enhances their forward motion in all the above cases. Thrust generated by the

13

cork screw motion of the helical trajectories help *H. pylori* and spirochetes to pierce their way through host environment (4, 43). In the case of *C. crescentus,* thrust generated by helical trajectories provides a propulsive force to move in forward direction. Liu *et al.* further determined that this propulsive force was less in the backward direction (42). Usually there is a correlation between cell body rotation and the swimming speed of the bacterium. However, in the case of *C. crescentus,* it was found that when the cell changes from pusher to puller mode, the cell body rotation increased by 100% without any increase in the overall swimming speed irrespective of the cell length and average swimming speed (42). On closer examination Liu *et al.* found that the cell body forms a helical trajectory that is more pronounced in pusher mode than puller mode and the degree of helicity was dependent on the rotational phase of the cell. They further showed through theoretical calculations and analysis of the helical trajectory that the angular force from the flagellar motion and the anisotropic drag force leads to the helical trajectory of *C. crescentus* in pusher mode generating more thrust than the puller mode (42).

While flagellated bacteria have distinct swimming patterns, the exact potential advantage(s) these various patterns provide cells with is largely unknown. One way towards addressing these is to analyze and compare the swimming patterns of phylogenetically closely related bacteria found in distinct ecological niches. *Pseudomonas* is a very diverse genus that includes Plant Growth Promoting Rhizobacteria, (PGPR) (e.g., *Pseudomonas fluorescens, P. putida*) as well as plant (e.g., *Pseudomonas syringae)* and animal pathogens (e.g., *P. aeruginosa*). The swimming patterns of *P. fluorescens, P.*

putida, and *P. aeruginosa* have been studied to date, and all three species display swimming strategies distinct from each other and from that of *E. coli*. Flagellation in these three *Pseudomonas* species ranges from monotrichous in *P. aeruginosa* and *P. fluorescens* to lophotrichous in *P. putida*. *P. fluorescens* swims by a "run-flip-backup-hover" mechanism (44). During swimming, *P. fluorescens* cells occasionally display a series of continuous rocking that produce a "flip" like motion or standstill for a while (hover). In both the flip or the hover there is no net displacement (44). *P. aeruginosa* and *P. putida* were shown to adopt a "run-reverse-turn" trajectory (45). *P. putida* swiftly changes direction while swimming forward and five different swimming patterns were identified when tracked through 3D holography (46, 47). The run-tumble motility pattern of the peritrichously flagellated bacterium *E. coli* is rarely seen in marine environments, suggesting this motility pattern is not selected for in marine bacterial species (48).

Whether different swimming patterns relate to physical constraints imposed on the cell body and/or to effects of flagellar arrangement on fluid mechanics, have also not been addressed to date, because of the difficulty in setting adequate experiments. Indeed, a combination of factors that includes swimming speeds, cell size, type of chemotaxis and gradient length (49, 50) can affect swimming patterns as well. A combination of mathematical modeling and wet lab experiments has recently attempted to address this issue (50-52). In an attractant gradient, *V. aliginolyticus* was shown to be migrating faster than *E. coli* (28). Simply scaling up the speed of *E. coli* to the speed of *V. aliginolyticus* in a mathematical model failed to recapitulate the chemotactic performance of *V.*

aliginolyticus (28), underscoring the importance of overall swimming pattern in the chemotaxis response. Similar swimming speed dependent chemotactic precision was reported for bacteria with even higher speeds, such as the marine bacterium *P. haloplanktis* (53), suggesting that the nature of the swimming pattern impacts chemotaxis performance in other species.

BACTERIAL CHEMOTAXIS BACKGROUND

Flagella endow bacteria with motility but also permit chemotaxis. Flagellum contains thousands of individual protein subunits which makes the entire flagellum structure totaling almost 50kDa. Expression and assembly of flagellum/flagella is a highly controlled hierarchical energetically costly feature (54). In fact, chemotaxis is considered to be one of the fundamental functions of motility, as it is not always energetically favorable (55). Chemotaxis is the process by which a motile organism responds to a chemical stimulus in the environment and directs its movement to move toward higher (attractant) or lower (repellent) concentration of the chemicals. Bacteria use chemotaxis to bias their swimming direction toward favorable niches in the environment (56). It is thus not surprising that in most pathogenic motile bacteria, motility and chemotaxis promote colonization of preferred sites in hosts (57). The most extensively studied model organism, *E. coli,* possesses a single chemotaxis signal transduction system. In *E. coli*, the chemotaxis signal transduction system controls the probability of changes in swimming directions to bias the swimming pattern, resulting in what is known as "the biased random walk (56)." The chemotaxis signal transduction pathway comprises periplasmic chemoreceptors that sense

16

environmental cues, and a set of cytoplasmic proteins that couple signal sensing with changes in swimming direction by acting on the flagellar motors. In a gradient of a repellent, chemoreceptors activate the cytoplasmic chemotaxis protein CheA, which is a histidine kinase, and cause its autophosphorylation via ATP. Phosphorylated CheA then transfers its phosphate group to a response regulator protein, called CheY. CheY, upon phosphorylation, has an increased affinity for a specific protein in the flagellar motor, FliM. Interaction of phosphorylated CheY (CheY-P) with FliM leads to switching of the direction of rotation of the BFM and thus, the swimming direction. Therefore, by modulating the phosphorylation of CheY through chemotaxis signaling, *E. coli* alters the affinity of CheY to the BFM, which alters the direction of rotation of the flagellar motors.

THE CONFORMATIONAL SPREAD MODEL OF FLAGELLAR MOTOR SWITCHING

Like all rotary motors, the structural parts of the bacterial flagellar motor can be divided into two categories - the rotors are the rotating portion while the stators are the nonrotating components of the BFM. The rotational switch unit is composed of approximately 1 FliG, 1 FliM and a tetramer of FliN with each RSU containing a single binding site for CheY~P (58). The symmetry mismatch between the number of FliM (34-45 monomers), FliN (34-45 tetramers) and FliG (26 monomers) that make up the RSUs and the number of RSUs (34) have been a long-standing conundrum in the field (Fig. 1 and Fig. 5A). When the motor is rotating CW, it was shown to have fewer FliM (34 monomers) and FliN (34 tetramers) in the RSU (59, 60). However, when the concentration of CheY~P is low and

the BFM is rotating exclusively in CCW, it recruits more FliM (45 monomers) and FliN (45 tetramers) in the RSUs (59, 60). This helps in creating more binding sites for CheY~P and thus switching from CCW to CW rotation (59, 60). Adaptation of the BFM is reflected by how much time the motor spends in either CCW or CW rotating state and is dependent on the FliM/FliN ratio but not on the CheY~P concentration (61). The ability of the BFM to adapt by dynamically changing its components depending on the direction of rotation is unique to the BFM. Though the symmetry mismatch between components of the RSUs have been attributed to the unusual conformational plasticity of FliG (62), the mechanisms by which the BFM functionally adapts to the variable number of FliM and FliN monomers in different rotating states is not completely understood. Switching of the BFM from CCW to CW is a highly sensitive to CheY-P concentration that occur at a narrow concentration range (3mM for *E. coli* motor) of CheY-P (61, 63). The ultrasensitivity of the BFM to CheY~P concentration can be explained through the conformational spread model which relies on a highly cooperative switching mechanism (64). The authors proposed that the highly cooperative nature of the switch can be explained by the differential affinity of CheY~P for CCW and CW rotating motors and by the size of the BFM (58, 64). In this model, each of the identical RSUs can exist in the CCW or the CW state which in turn, depends on i) the conformations of its nearest neighbors in the C ring and ii) the RSU bound state to CheY~P (58). The above two conditions generate four states for a single RSU: CCW/inactive (bound or unbound CheY~P) and CW/active (bound or unbound CheY~P). Each of the four states have only two other states available to them for

18

transition depending on their energy level (58). The bound inactive state (RSU in CCW state with bound CheY~P) was presumed to have higher energy and to be less stable than the unbound inactive state. In contrast, the unbound active state (RSU in CW state with no CheY~P bound) was proposed to have higher energy and to be less stable than the bound active state (58). Higher energy and reduced stability would cause individual RSUs to be more likely to transition into one of the two states available to them. Furthermore, the interaction between adjacent RSUs are expected to be more favorable for those RSUs in the same state, irrespective of CheY~P binding (58). The conformational spread model of switching is based on the interaction between the neighboring RSUs and the stochastic shrinkage or growth of the inactive and active individual RSUs from an initial nucleation site on the C ring. Switches typically would occur following a single nucleation event at one of the RSUs that spreads conformationally to the adjacent RSUs, leading to a coherent state for almost all the RSUs of the C ring (58). This conformational spread model captured experimental data and recapitulated some of the properties of the BFM, including i) high cooperativity and ultrasensitivity of the motor and non-linear dependence of the switch on CheY~P concentration and, ii) the equilibrium between CW and CCW locked states. The model was later refined to include the fine dynamics of the switching behavior that includes measurement of intervals for two of the locked state (CW and CCW) and the size of the ring that depends on number of RSUs present at any given time in the C ring (65).

At the molecular level, CheY~P binds to a flexible segment near the N terminus of FliM (66). This event leads to a series of conformational changes within the RSU. The first binding event of CheY~P to FliM leads to interaction of CheY~P with a hydrophobic patch on FliN (67). This interaction is thought to lead to subtle shuffling of FliN relative to FliM (68). Eventually, the CheY~P binding signal is transmitted to FliG. As FliG forms the torque generating surface with MotA, a conformational change in FliG leads to torque generation (Fig. 5A)(69, 70). This conformational change in one of the RSUs is then transmitted to the neighboring RSUs. When 13 ± 7 RSUs are in bound state with CheY~P, the BFM switches from CCW to CW (71) (Fig. 5B – Upper panel). If the threshold number of CheY~P binding is not reached, the RSU can switch back to its default state, without switching. This has been speculated to be the cause for pauses observed during motor rotation in *E. coli* (Fig. 5B – Lower panel) (58).
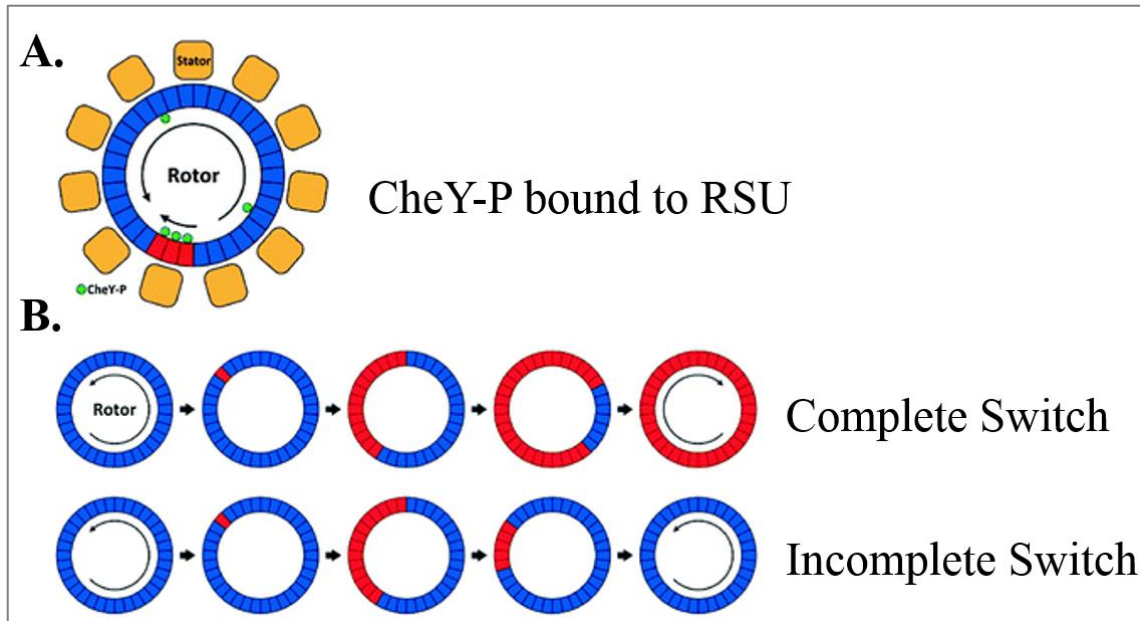
Figure 5. Graphical representation of conformational spread model of flagellar motor switching

A) Shown here are the 34 rotational switch units of the *E. coli* motor existing in CCW state (blue) or CW state (red). Conversion of individual RSUs from CCW (blue) to CW (red) state occurs after binding of CheY-P (bright green solid circle). B) Nucleation of CCW to CW state can occur at single RSU level and conformationally spread to nearby RSUs leading to complete switch (upper panel). Additionally, RSUs in the CW state can revert back or shrink to complete CCW state (Upper panel) The later condition is considered as incomplete switch and manifested as pause during swimming. Adapted from (58).

ROLE OF CHEYS IN CHEMOTAXIS

CheY overview and architecture

CheY is a response regulator (RR) protein with a single receiver domain (REC) and no output domain. As indicated above, during chemotaxis CheY interacts with CheA, FliM (a motor protein) and it also interacts with CheZ (a phosphatase). Interaction with each of these proteins is central to chemotaxis. While interaction with CheA and FliM is important for signal output (changes in the direction of rotation of the BFM), the interaction of CheZ is required for signal termination. It has been proposed that the same region in CheY is important for interaction with all these three proteins which partially overlaps with each other (72).

CheY structure from *E. coli* consists of 5 alternating β-strands and α-sheets giving a $(\beta\alpha)_5$ topology (73) and other structures solved since then show a similar structure. The hydrophobic core is formed by five parallel beta sheets. On one side of this hydrophobic core there are two alpha helices, and on the other side, there are three more alpha helices (Fig. 6). The active site of CheY contains D (aspartate)12, D13 and D57 which binds a bivalent cation and is required for phosphorylation and dephosphorylation at D57. T(threonine) 87 and K(lysine) 109 are required for phosphorylation-dependent conformational change.
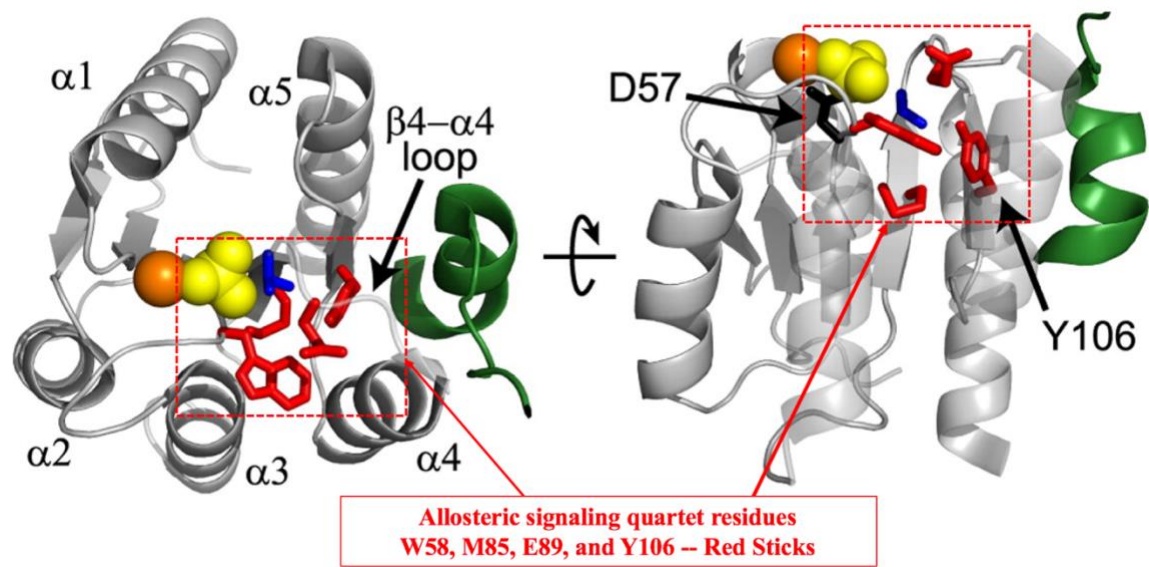
Figure 6. Cartoon depicting the residues important for conformational change in CheY from *E. coli*.

Site of phosphorylation, D57 is shown in black, FliM is shown in green, BeF$_x$ is shown in yellow, Mg^{2+} is shown in orange bound to crystal structure of CheY(1F4V)(74). The allosteric quartet of W58, M85, E89 and Y106 are shown in red and T87 in blue. Adapted from (75).

CheY activation mechanism

The phosphorylation event at D57 of the *E. coli* CheY converts it into an active form where tyrosine (Y106) switches from solvent exposed to a buried state under the β4-α4 loop (76). The β4-α4 loop also undergoes a major displacement after the phosphorylation event. The highly conserved T(threonine) 87 separates D57 and Y106 in inactive form, but after phosphorylation, T87 moves towards the phosphorylation site due to hydrogen bonding. This event then leads to creation of more space where Y106 gets buried. Hence, this mechanism was called Y-T coupling (76).

Role of multiple response regulators in other species

Chemotaxis in *E. coli* relies on a single CheY. However, many bacteria sequenced till date possess more than one chemotaxis operon and many also possess more than one CheY encoded in their genome (77). The best studied bacteria with multiple chemotaxis operons are *R. sphaeroides*, *S. meliloti*, *P. aeruginosa* each having more than one CheY. *R. sphaeroides* and *C. crescentus* have as many as six CheYs (78, 79), whereas *S. meliloti* has two CheYs (80). At least two of the *R. sphaeroides* CheYs are absolutely needed for chemotaxis at any time with CheY6 being indispensable, and either CheY3 or CheY4 also needed for chemotaxis (78). In the case of *S. meliloti,* CheY2 slows down the unidirectional motor while CheY1 acts as the phosphate "sink" to promote signal termination (80, 81).

AZOSPIRILLUM BRASILENSE - A MODEL ORGANISM WITH MULTIPLE CHEMOTAXIS OPERONS AND COMPLEX SWIMMING PATTERNS

As more bacterial genome sequences become available, it's clear that many bacteria possess multiple chemotaxis systems and additional chemotaxis proteins that are not found in *E. coli* (77). For example, *R. sphaeroides* has four chemotaxis systems; *P. aeruginosa* has five whereas *Myxoccoccus xanthus* has nine chemotaxis systems (82). Some of these chemotaxis systems have been shown to have functions other than flagellar motility, called alternate cellular functions (ACF)(77).

A. brasilense which is the model organism I study during my Ph.D. has four chemotaxis like systems. *A. brasilense* is a free-living soil bacterium considered a plant growth-promoting rhizobacteria (PGPR) and included in many commercially available biofertilizers. *A. brasilense* swims using a single polar flagellum with a bi-directional motor that can rotate CW or CCW (83). Out of the four chemotaxis systems in *A. brasilense*, two of them (Che2 and Che3) do not control chemotaxis (O'Neal Unpublished)(84). Che1 has been shown to regulate transient changes in swimming speed (ref) whereas, when this research was initiated, the role of Che4 was unknown. In this work, I show (Chapter 2) that the swimming reversal frequency, the rate at which the bacteria changes swimming direction, is controlled by the Che4 pathway while Che1 functions to enhance chemotaxis performance through transient changes in speed (85, 86). At this time, the mechanism by which Che1 affects the swimming speed is not known. The

25

role each of the CheYs plays in modulating the swimming pattern of *A. brasilense* was also

unknown when my research was initiated and is presented in Chapter 3 and 4.

CHAPTER II

AZOSPIRILLUM BRASILENSE CHEMOTAXIS DEPENDS ON TWO SIGNALING PATHWAYS REGULATING DISTINCT MOTILITY PARAMETERS

ABSTRACT

The genomes of most motile bacteria encode two or more chemotaxis (Che) systems but their functions have been characterized in a handful of model systems. *Azospirillum brasilense* are motile soil alphaproteobacteria able to colonize the rhizosphere of cereals. In response to an attractant, motile *A. brasilense* cells transiently increase swimming speed and suppress reversals in the swimming direction. The Che1 chemotaxis pathway was previously shown to regulate changes in the swimming speed but it has a minor role in chemotaxis and root surface colonization. Here, we show that a second chemotaxis system, named Che4, regulates the probability of reversals in the swimming direction and is the major signaling pathway for chemotaxis and wheat root surface colonization. Experimental evidence indicates that Che1 and Che4 are functionally linked to coordinate changes in the swimming motility pattern in response to attractants. The effect of Che1 on swimming speed is shown to enhance the chemotactic response of *A. brasilense* in oxygen gradients, likely providing the cells with a competitive advantage in the rhizosphere. Together, the results illustrate a novel mechanism by which motile bacteria utilize two chemotaxis

pathways regulating distinct motility parameters to alter movement in gradients and enhance the chemotactic advantage.

Importance. Chemotaxis provides motile bacteria with a competitive advantage in the colonization of diverse niches and is a function enriched in rhizosphere bacterial communities, with most species possessing at least two chemotaxis systems. Here, we identify the mechanism by which cells may derive a significant chemotactic advantage using two chemotaxis pathways that ultimately regulate distinct motility parameters.

<u>INTRODUCTION</u>

Bacterial chemotaxis provides a competitive advantage by guiding motile cells in gradients of chemoeffectors toward environments that support growth and metabolism. Chemotaxis contributes to the establishment of various associations of bacteria with eukaryotic hosts (animals, insects, and plants) and promotes virulence, symbiosis and the establishment of microbial communities (87). Bacterial chemotaxis and motility are widespread traits encoded in the genomes of bacteria inhabiting diverse environments and these functions are specifically enriched in microorganisms found in soils (88), suggesting that they provide a significant competitive advantage in this environment. Consistent with this findings, comparative genome analysis of chemotaxis in diverse motile bacteria suggested that most bacteria possess two chemotaxis systems and soil–dwelling bacteria have more than two chemotaxis systems (89).

The molecular mechanism of chemotaxis signal transduction has been deciphered in most details in the model organism, *Escherichia coli*, which possesses a single chemotaxis system. In *E. coli*, the chemotaxis signal transduction pathway consists of membrane bound receptors clustered in dense arrays at the cell poles where their C-terminal domains associate with cytoplasmic CheA kinase and the CheW scaffolding protein. When stimulated by a repellent, CheA autophosphorylates on a conserved Histidine residue (H48) using ATP and transfers its phosphate to the CheY response regulator (56). Phospho-CheY binding to flagella motors with high affinity triggers a switch in the direction of flagella motor rotation from counterclockwise to clockwise and a change in the swimming direction of the cell, or a tumble (56). A phosphatase, CheZ assists signal termination by acting on phospho-CheY (56). In addition, a receptor-specific methyltransferase, CheR and a receptor-specific methylesterase CheB activated by phosphotransfer from phospho-CheA, differentially methylate the receptors to reset sensitivity (56). This basic set of chemotaxis proteins comprises a signaling pathway that is generally conserved across bacterial species (77). However, there are notable exceptions to this paradigm such as the absence of CheB and CheR in some species, the existence of multiple CheY response regulators in others or the presence of ancillary chemotaxis proteins not found in *E. coli* (56). Another variation on this theme is the presence of multiple chemotaxis pathways in the genomes of most motile bacteria (77). Some of these additional chemotaxis pathways regulate type IV pili-dependent motility or alternative cellular functions (ACF) and they can be identified due to their unique structure (89). The largest numbers of chemotaxis pathways found in

bacterial genomes are predicted to regulate flagellar motility patterns. The contribution of multiple chemotaxis systems to the regulation of changes in swimming direction was demonstrated in some species. For example, in *Rhodobacter sphaeroides*, two chemotaxis systems together control the probability of stops in flagellar rotation (78).

Azospirillum brasilense are motile soil bacteria that inhabit the rhizosphere of diverse plants. *A. brasilense* cells swim using a single polar flagellum and change swimming direction when the direction of flagellar rotation briefly reverses, causing cells' movement to be re-directed in a different direction (83). In addition to regulating the probability of reversals in swimming direction, motile *A. brasilense* cells navigating an attractant gradient can transiently increases swimming speed (85). The chemotaxis pathway that regulates transient increases in swimming speed in response to attractants has been identified as Che1 (85). However, the chemotaxis pathway(s) responsible for controlling changes in the direction of flagellar rotation to trigger swimming reversals is not yet known. The existence of a distinct pathway for controlling swimming reversals comes from the observation that inactivation of *cheB1* or *cheR1* from the Che1 pathway affected the ability to increase the swimming speed in response to an attractant, as expected but these mutations, but not those in *che1*, *cheA1* or *cheY1*, also impaired the ability to regulate reversals in the swimming direction (90). These data were interpreted to suggest that Che1 functionally interacts with the unidentified pathway controlling the probability of changes in swimming reversals (85). The available genome sequence of *A. brasilense* indicates the presence of four distinct chemotaxis operons, three of which (Che1, Che2 and Che3) are also encoded in the

genomes of all *Azospirillum* strains sequenced to date as well as in the genome of the closely related *Rhodospirillum centenum* (91-94), suggesting they were present in the last common ancestors of these two genera (Fig.7). The role of Che2 in *A. brasilense* is unknown but it is a homolog to the Che2 operon controlling flagellar biosynthesis in *R. centenum* (94). In *A. brasilense*, *che2* does not appear to be expressed under standard laboratory conditions (Xie and Alexandre, unpublished). Che3 is a chemotaxis-like ACF pathway that was recently implicated in the control of flocculation in *A. brasilense* (84).
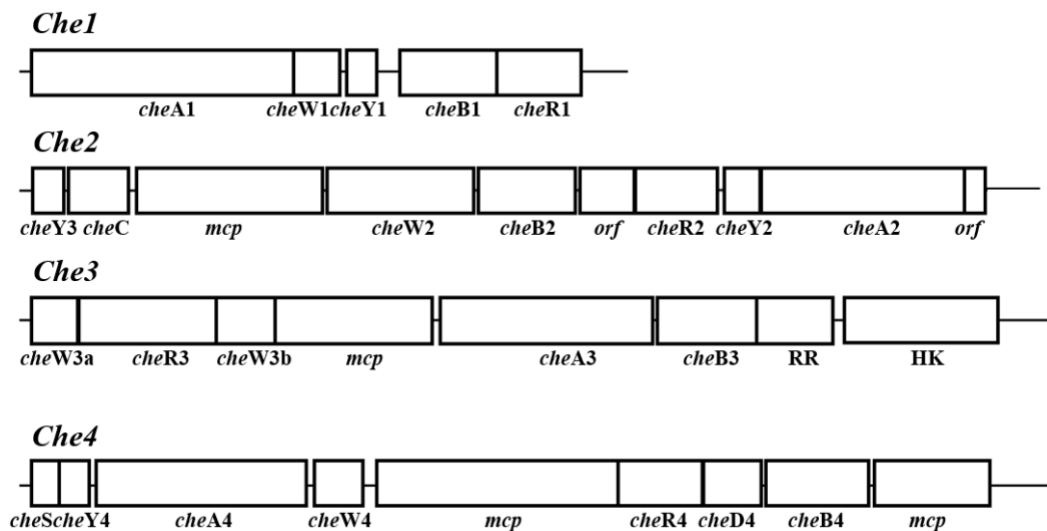
Figure 7. Chemotaxis gene clusters encoded within the *A. brasilense* genome.

Boxes represent open reading frames and are drawn relative to scale. The chemotaxis genes within each cluster were either previously characterized or identified by homology searches. RR: response regulator; HK: histidine kinase; mcp: methyl-accepting chemotaxis protein.

32

Che4 is present in the genome of all *Azospirillum* strains sequenced to date, but absent from the *R. centenum* genome. In *R. centenum*, the Che1 chemotaxis system controls all chemotaxis responses (95) in contrast to its homolog in *A. brasilense* (Che1) that controls swimming speed and has only a minor role in chemotaxis. The Che4 system is thus the most likely candidate for controlling the probability of reversals in the swimming direction in this species. Here, we show that Che4 is essential for all chemotaxis responses in *A. brasilense* and for competitive wheat root surface colonization. We demonstrate that the signaling output from Che4 directly modulates the probability of swimming reversals and that signaling from Che1 and Che4 is integrated during chemotaxis to produce an enhanced response to attractants. These results illustrate a novel mechanism by which motile bacteria utilize two chemotaxis pathways regulating distinct motility parameters to alter movement in gradients and increase their chemotactic advantage.

RESULTS

che4 **mutants lack chemotaxis and aerotaxis**

Genome sequence analysis predicted that Che4 is the major chemotaxis system controlling movement of *A. brasilense* cells in gradients of chemoeffectors. To test this hypothesis, we constructed strains lacking *cheA4* ($\Delta cheA4$, strain AB401), *cheY4* ($\Delta cheY4$, strain AB402) or the entire *che4* cluster ($\Delta che4$, strain AB403) and tested their chemotaxis and aerotaxis abilities using spatial gradient assays (Fig. 8). All mutants were motile and grew at similar rates under various media and incubation conditions (data not shown). While the $\Delta cheA4$ mutant was null for chemotaxis and aerotaxis, the $\Delta cheY4$ and $\Delta che4$ mutants were null

33

for aerotaxis but displayed residual chemotaxis in the soft agar assay (Fig. 8A-8B). Similar patterns were observed when other carbon sources were used in the soft agar assay (data not shown). The different phenotypes of some of these mutants in chemotaxis versus aerotaxis were intriguing. The discrepancy between the behavior of the Δ*cheY4* and Δ*che4* mutants in the aerotaxis versus the chemotaxis assay could be due to the different incubation times and conditions under which these assays are conducted. The aerotaxis assay is performed using a suspension of free-swimming cells placed into a capillary tube and the aerotactic band typically formed within 2-3 minutes and remain stable for at least 25 minutes. The chemotaxis rings are formed in soft agar plates and are observed after at least 24-48 hours of growth. One possibility is that the rings observed in the soft agar plates are the result of pseudotaxis responses, since these have been reported under similar conditions in several bacterial species (96-98). The taxis defects of the Δ*cheA4* and Δ*cheY4* could be complemented by expressing a parental gene from a broad host range plasmid but not by expressing a variant allele of *cheA4* or *cheY4* carrying a single mutation on the predicted phosphorylatable histidine (H54Q in CheA4) and asparate (D57N CheY4) residues, respectively (Figs. 8C-8D). These data suggest that conserved phosphorylatable residues on CheY4 and CheA4 must be present for signaling to occur, suggesting that a phosphorylation cascade between CheA4 and CheY4 triggers changes in the direction of flagellar rotation that cause swimming reversals. Together, these results identify CheA4 as the major histidine kinase mediating aerotaxis and chemotaxis in *A. brasilense* and they

34

Figure 8. Taxis behaviors of *A. brasilense* and its *che4* mutant derivatives.

(A) Chemotaxis in the soft agar plate assay containing malate (10mM) and ammonium chloride (18.7 mM) as carbon and nitrogen sources, respectively. The strains tested are indicated at the top of each plates. The pictures were taken, after 48 h incubation, at 28 ºC. Representative images from at least 5 different assays are shown. (B) Aerotaxis in the spatial gradient assay. The air gradient is established by diffusion in the direction indicated by the arrow, into the capillary tubes filled with a suspension of motile cells to be tested. The number of cells were equivalent in all tubes and all strains were motile. The formation of a stable band of motile cells is indicated by *. The images were taken 5 minutes after placing the cells within the capillary tubes. (C) Functional complementation of the chemotaxis defect of the *ΔcheA4* mutant in the soft agar plate assay. The plates contained malate (10mM) and ammonium chloride (18.7 mM) as carbon and nitrogen sources, respectively, and were incubated for 5 days at 28ºC before being photographed. The plasmids carried by the strains are derivative of the broad host range pRK415 and are indicated on the images. The chemotaxis defect of the *ΔcheA4* mutant strain can be rescued by expressing a wild type CheA4 but not CheA4H54Q. (D) Functional complementation of the aerotaxis defect of the ΔcheY4 mutant. The photographs were taken 10 min after placing the suspension of motile cells within the capillary tubes. The plasmids carried by the strains are indicated on the images. The aerotaxis defect of the *ΔcheY4* mutant strain can be rescued by expressing a wild type CheY4 but not CheY4D57N. The number of cells were equivalent in all tubes and all strains were motile. The images were taken 5 minutes after placing the cells within the capillary tubes. The formation of a stable band of motile cells is indicated by *
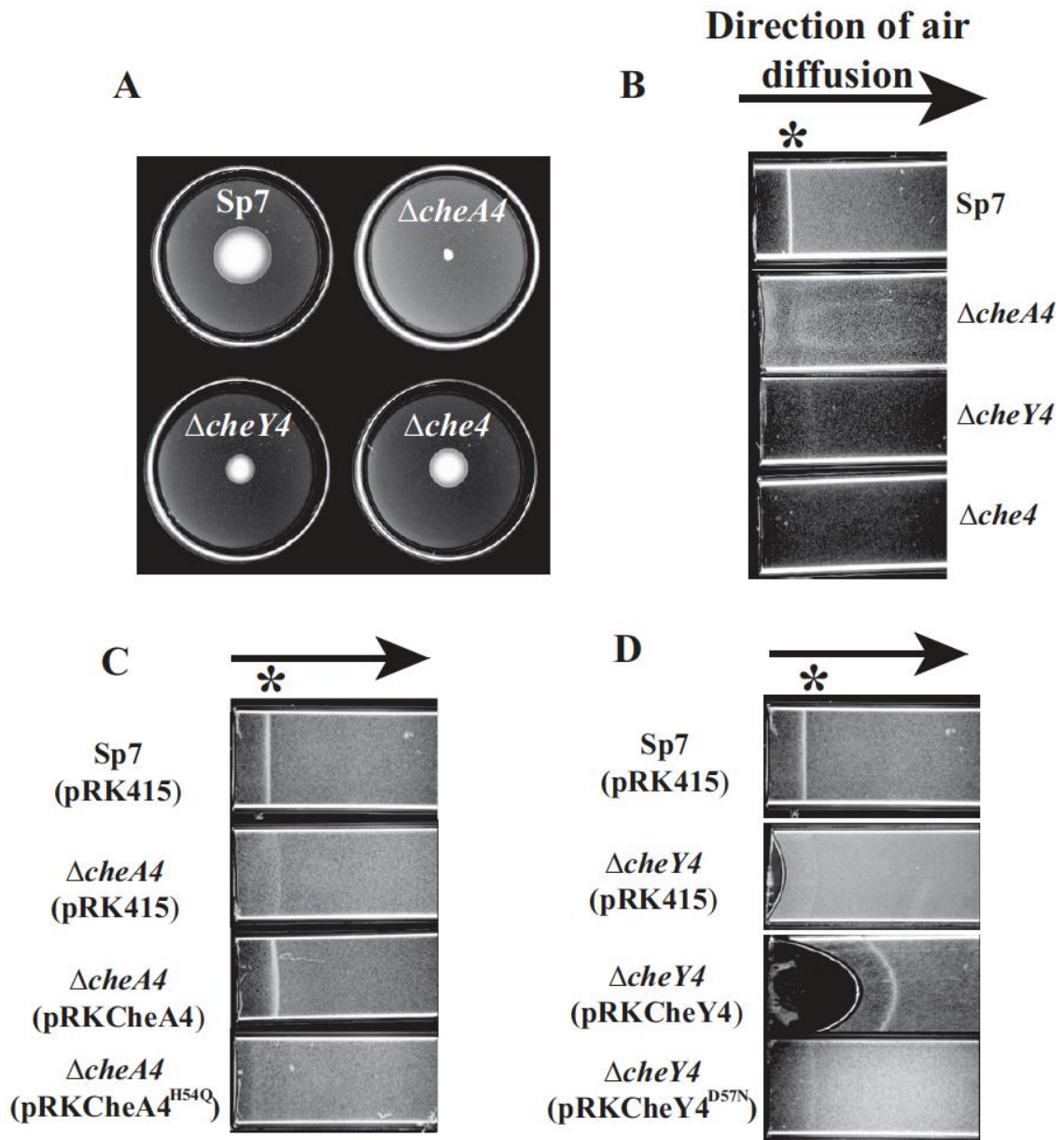
further suggest that signaling from Che4 plays a major role in controlling the changes in the direction of flagellar rotation during swimming reversals.

The signaling output from Che4 is the control of the swimming reversal frequency

The presence of chemotaxis rings in the soft agar assay could suggest that the mutants are still able of chemotaxis under these conditions but not under the condition of the aerotaxis assay. The signaling output of a bacterial chemotaxis pathway ultimately controls the swimming motility pattern by modulating the probability of changes in the swimming direction. In other words, mutants unable to chemotax are expected to either constantly run or constantly change swimming direction. We assessed the swimming motility patterns of the *Δche4*, the *ΔcheA4* and, the *ΔcheY4* mutants under steady state conditions (Fig. 9). The wild type strain swam with long runs interrupted by instances of changes in the swimming direction, with an average probability of changes in the swimming direction of about 0.5 reversals/sec (Fig. 10A). Compared to the wild type, mutants lacking CheA4 swam in straight runs and did not changes swimming direction (Fig. 9-10A). The *ΔcheY4* mutant had a surprisingly different phenotype from the *ΔcheA4* mutant in that it also swam with fewer instances of reversals in the swimming direction compared to the wild type strain (Fig. 9) but it clearly was still able to change swimming direction (Fig. 10A). The strain lacking the *che4* cluster (*Δche4*) displayed a frequency of reversals in the swimming direction that was not significantly different from that of the wild type strain (0.6

A
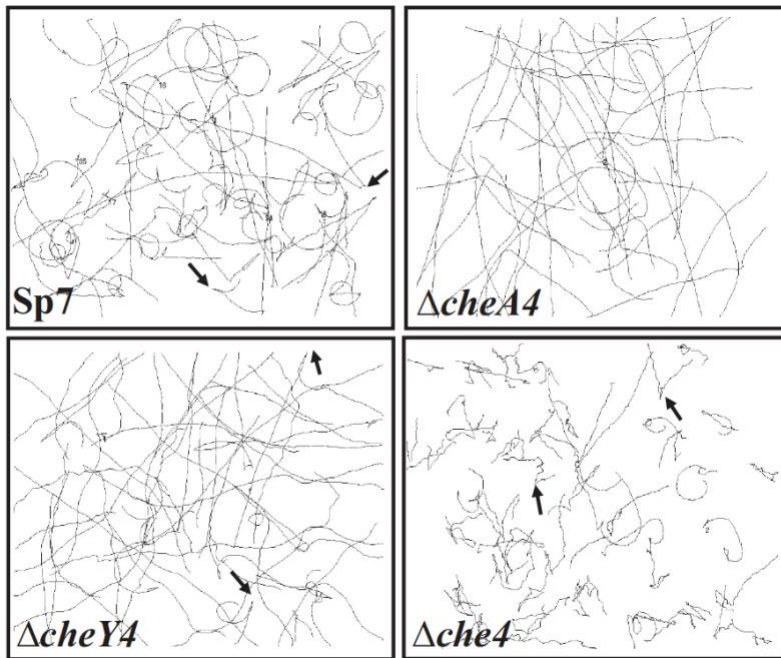
Figure 9. Tracks of free-swimming cells of *A. brasilense* and its *che4* mutant derivatives.

The tracks were obtained from digital recordings and computerized motion analysis. Representative tracks are shown. The arrows point to instances of reversals in the swimming direction.
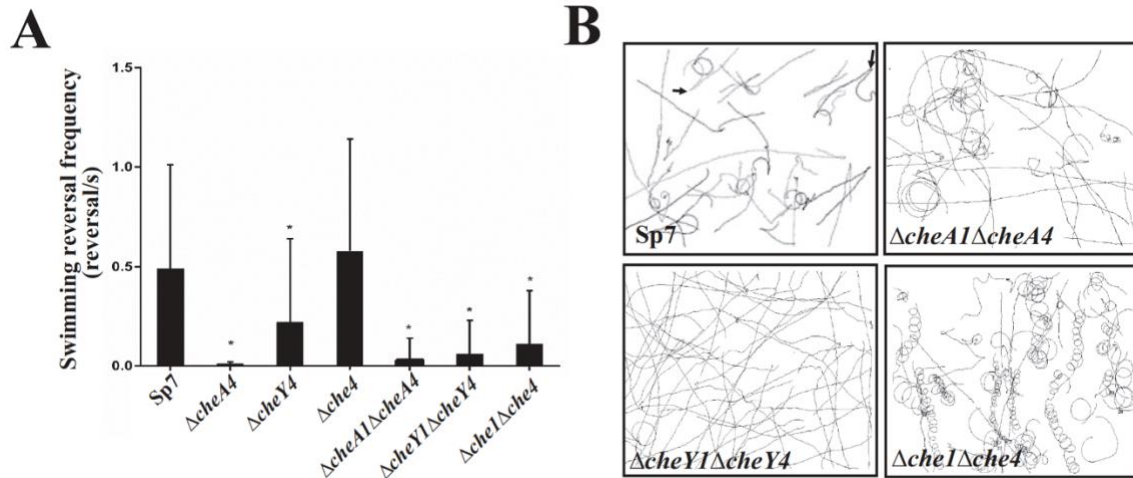
Figure 10. Swimming behavior of *A. brasilense* wild type and mutant derivatives lacking *che4* genes or lacking a combination of *che4* and *che1* genes.

(A) Reversals in the swimming direction (swimming reversals) were determined by computerized motion analysis, from tracks of at least 75 free-swimming cells, from 3 independent cultures. The results showed are the average numbers of swimming reversals per second for each strain analyzed with standard deviation. Statistically different values compared to the wild type strain (t-test; $p < 0.05$) are indicated by *. (B) Tracks of free-swimming cells of *A. brasilense* and its derivatives lacking both *che1* and *che4* genes. The tracks were obtained from digital recordings and computerized motion analysis (CellTrack). Representative tracks are shown. The arrows point to instances of reversals in the swimming direction.

reversal/sec) (Fig. 9) (Fig. 10A). Analysis of free-swimming cells of the Δ*che4* strain also revealed a significantly erratic ('jiggly") motility pattern (Fig. 9).

This analysis thus confirms that CheA4 is essential for the cells to reverse swimming direction. The lack of CheY4 or Che4 severely impaired but did not affect (Che4) or completely abolish (CheY4) the probability of reversals in swimming direction, indicating that CheY4 (and thus Che4) has a major, but not unique role in this behavior.

Che1 and Che4 together contribute to regulating the swimming pattern

The distinct swimming pattern of the *ΔcheY4* and *Δche4* strains compared to the *ΔcheA4* was unexpected since all three strains should display the same phenotype, if the signaling output of the Che4 pathway controls reversals in the swimming direction. The proposed role of Che1 in chemotaxis and the putative functional interaction between Che1 and the pathway affecting swimming reversals characterized previously (99), suggesting to us that Che1 may be responsible for the residual swimming reversal ability of the *ΔcheY4* and the *Δche4* mutants. To test this possibility, we constructed strains lacking both *che1* and *che4* (*Δche1Δche4*; strain AB143), both *cheA1* and *cheA4* (*ΔcheA1ΔcheA4*; strain AB141) and both *cheY1* and *cheY4* (*ΔcheY1ΔcheY4*; strain AB142) and analyzed their swimming patterns (Fig. 10B). We found that mutating *cheY1* and *che1* in the *ΔcheY4* and *Δche4* mutant backgrounds yielded cells unable to reverse swimming direction, similar to the motility pattern observed for the *ΔcheA4* strain or, as expected, for the *ΔcheA1ΔcheA4* strain (Fig. 10A-10B). Disabling Che1 in the *Δche4* mutant (strain AB143) background

also abolished the erratic swimming behavior of the *Δche4* strain, suggesting that signaling from Che1 caused this behavior (Fig. 10A-10B). The *Δche1Δche4* mutant strain and to a lesser extent, the *ΔcheA1ΔcheA4 strain* also persisted and swam in circles close to the surface of the coverslip (Fig. 10B). This behavior has been associated with smooth swimming close to surfaces in *E. coli* (100, 101) and is thus consistent with the lack of swimming reversals in these strains. However, we do not know why this behavior is more preeminent in these two mutants but not in the *ΔcheY1ΔcheY4* strain. Since Che1 affects the swimming speed, we also analyzed this motility parameter for mutants lacking *che4* genes alone or in combination with mutations in *che1* genes and found that only the *ΔcheA4* and the *Δche4* mutants had a reduced swimming speed compared to the wild type strain (Fig. 11). This phenotype was absent in the *ΔcheA1ΔcheA4* and *Δche1Δche4* strains, implicating Che1 in the reduced swimming speed. These results also suggest that it is the combination of reduced swimming speed while maintaining the ability to change swimming direction that caused the erratic swimming pattern of the *Δche4* mutant strain (Fig. 9). Together, the data confirm the role of Che1 and Che4 in regulating the motility patterns of swimming cells and to the chemotaxis response and further support the hypothesis of a functional signaling interaction between Che1 and Che4.
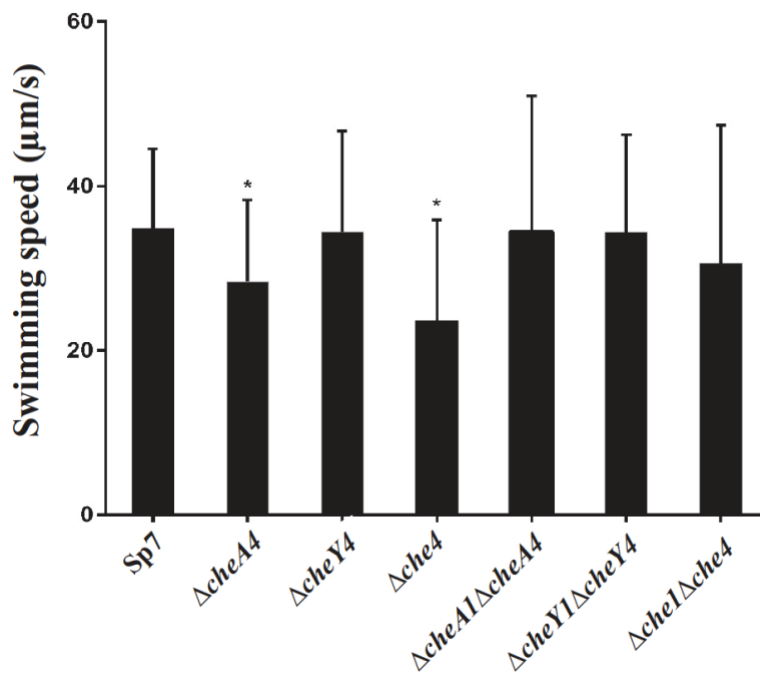
Figure 11. Swimming speed of free-swimming cells of *A. brasilense* wild type and its mutant derivatives lacking *che4* genes or lacking a combination of *che4* and *che1* genes.

The values showed are averages of swimming speed determined by motion tracking of at least 75 cells, from three independent cultures, with standard deviation. Statistically different values compared to the wild type strain (t-test; $p<0.05$) are indicated by *

Che4 control plant association

The major role of Che4 in controlling chemotaxis and the swimming pattern suggested it should also play a significant role in the ability of cells to colonize the roots of cereals, such as wheat, a common host plant for *A. brasilense*. When inoculated alone to sterile wheat plants, the wild type and its *Δche4* mutant derivative were able to colonize sterile wheat roots (Fig. 12A), albeit at a relatively reduced level, compared to the wild type. Given that chemotaxis provides bacteria with a competitive advantage, we hypothesized that the colonization defects of the mutants would become apparent in competition experiments against the wild type strain and thus compared the competitive index of the *Δche4* mutant when inoculated at a 1:1 ratio with the wild type strain (Fig. 12B). The competition experiments showed that lack of *che4* significantly impaired the competitive ability of the strains for colonization of the wheat root surfaces, confirming the major role of this pathway in the lifestyle of *A. brasilense* in the rhizosphere.
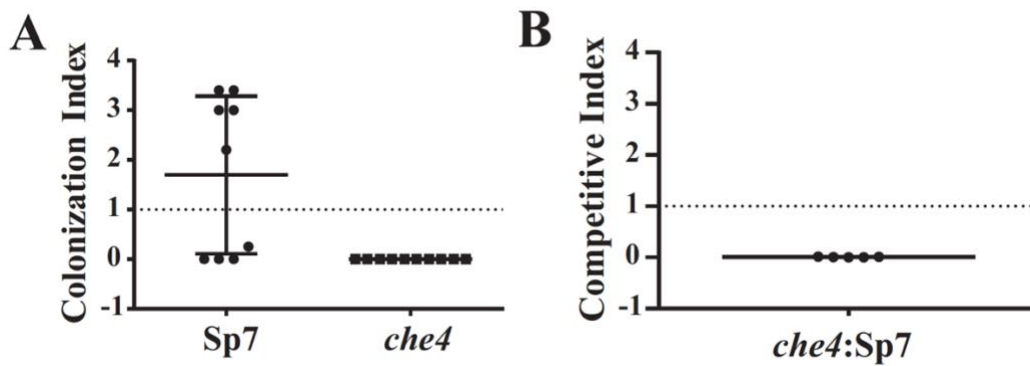
Figure 12. Role of Che4 in the *A. brasilense* root surface colonization of wheat.

(A) The colonization index was determined from *A. brasilense* and its *Δche4* mutant derivative inoculated alone to sterile wheat plantlets. The dots represent the colonization index for a set of four plants (one chamber) inoculated with the strain indicated, horizontal bars represent the mean and the vertical lines are the standard deviation. The broken gray horizontal line represents a colonization index of 1, indicating that all inoculated cells are recovered from the plant root surface. The index is > 1 for Sp7 likely because of growth on the roots. The colonization index of the wild type and the *Δche4* were statistically significant (Student's *t* test; p<0.0001). (B) The competitive index was determined as the ratio of the mutant to the wild type recovered from root after being inoculated at a 1:1 ratio (mutant/wild type). The dots represent the competitive index for four plants (one plant chamber) inoculated with the strains indicated at a 1:1 ratio, the horizontal bars represent the mean and the vertical lines, the standard deviation. The broken line represents a competitive index of 1, corresponding to strains equally competitive for root surface colonization.

The chemotactic advantage of coordinated regulation of swimming speed and reversals

We wondered what the advantage for motile and chemotactic *A. brasilense* cells in could be using two distinct chemotaxis signaling systems regulating two different parameters of swimming motility to modulate taxis responses. Che1, via signaling through CheY1 (84, 85) regulates transient increases in swimming speed and is still capable of chemo- and aerotaxis. Che4, via signaling through CheY4, controls reversals in the swimming direction, as shown here.

We hypothesized that a transient increase in the swimming speed that would accompany a suppression of changes in the swimming direction during response to an attractant should enhance the net movement of cells in this gradient. To test this hypothesis, we compared aerotaxis in a spatial gradient assay of the wild type strain with that of its *ΔcheY1* and *ΔcheY4* mutant derivatives in a time course experiment (Fig. 13). As expected, the *ΔcheY4* strain did not form an aerotactic band although cells were fully motile. The wild type strain starts forming an aerotactic band after 90 seconds and a stable aerotactic band is formed at 150 sec. The initiation of the aerotactic band took almost twice as much time for the *ΔcheY1* strain, which formed a stable aerotactic band, at 300 sec post-inoculation in the capillary tubes. This delay in the formation of the aerotactic band by the *ΔcheY1* cells relative to the wild type strain was consistent. These results suggest that the control of swimming speed by Che1 enhances the response of *A. brasilense* cells to a gradient of a major attractant, oxygen.

45
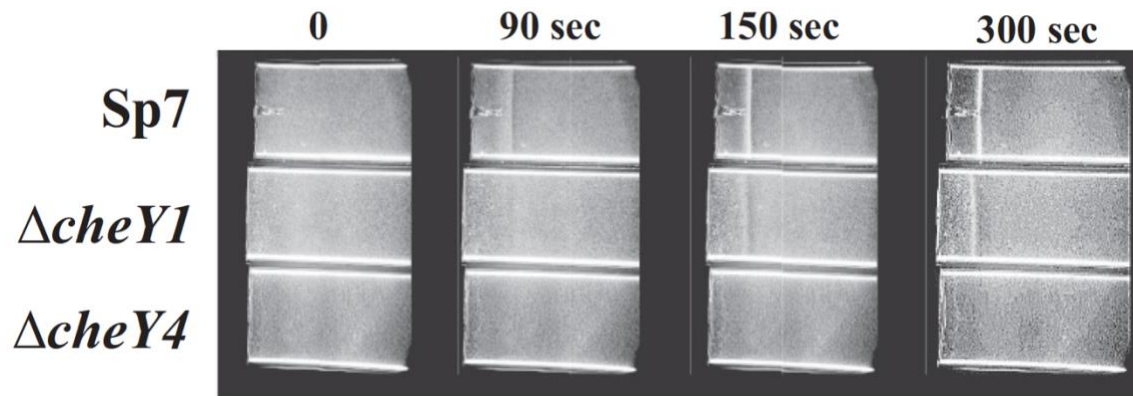
Figure 13. Time course of aerotactic band formation in *A. brasilense* wild type, its Δ*cheY1* and its Δ*cheY4* mutant derivatives.

Cell suspensions adjusted to equivalent numbers were placed in the capillary tubes and recording, shown at the upper left of each panel, was started immediately (t=0). All cells were motile throughout the experiments. Representative images are shown.

DISCUSSION

Experimental evidence obtained here show that Che4 signaling controls reversals in the swimming direction in *A. brasilense* and that it is the major pathway for all taxis responses in this species. As expected from its major function in regulating chemotaxis responses, Che4 is essential for competitive root surface colonization in *A. brasilense*. The *A. brasilense* Che4 pathway is orthologous to the major pathway controlling all chemotaxis responses in *S. meliloti* (102, 103) and *R. leguminosarum* (98) where this chemotaxis system is also essential for plant root colonization. Che4 is present in the genomes of all *Azospirillum* strains sequenced to date (91-93), but absent from the phylogenetically related sediment-dwelling *R. centenum* (94). In *R. centenum*, the Che1 chemotaxis system controls all chemotaxis responses (95) while its homolog in *A. brasilense* (Che1) controls swimming speed and has only a minor role in chemotaxis. Furthermore, mutations in the *A. brasilense che1* did not affect the ability to colonize the surface of wheat roots, indicating that this pathway does not contribute to the rhizosphere lifestyle of this organism (104). Lateral gene transfer (LGT) is considered a major driving force in the evolution of prokaryotes, including the acquisition of functions for adaptation to new niches (105). The *A. brasilense* Che4 pathway was previously identified as one of the functions acquired by lateral gene transfer (LGT) by the ancestors of *Azospirillum* spp. that were proposed to have contributed to the adaptation to the rhizosphere (94). The role for Che4 in root surface colonization characterized here is thus consistent with this hypothesis. Che4 is a representative of the F7 class of chemotaxis systems (77) that was shown to be enriched in

47

rhizosphere bacterial communities relative to those found in soil (88). The F7 chemotaxis systems such as the *A. brasilense* Che4 may thus be advantageous in this environment. However, the specific competitive advantage(s) that signaling via such a chemotaxis pathway provides cells with remains to be identified.

The acquisition of Che4 by LGT in the ancestor of *Azospirillum* spp. did not cause Che1 to lose its function in chemotaxis. Indeed, our results indicate that both Che1 and Che4 have a role in the regulation of the swimming pattern of motile *A. brasilense* cells and thus chemotaxis. However, the contribution of Che1 and Che4 to this behavior is significantly different. As shown previously and in the present study, Che1 controls transient increases in swimming speed (85) and has a minor role in chemotaxis while Che4 controls the probability of swimming reversals and plays a major role in all taxis responses. Our data indicate that signaling via Che4 controls most swimming reversals with Che1 modulating this behavior via direct effects on speed. This is in contrast to the role of two chemotaxis pathways in *R. sphaeroides*, a bacterial species that has been extensively studied in this respect (106). Two chemotaxis systems, named CheOp2 and CheOp3, are implicated in the control of chemotaxis in motile *R. sphaeroides* and the signaling output from both chemotaxis pathways controls stops in the rotation of flagellar motors (107, 108). Consistent with a single signaling output, inactivation of either CheOp2 or CheOp3 abolishes chemotaxis in *R. sphaeroides* because both signaling pathways ultimately affect the activity of a common set of CheY response regulators which bind the flagellar motors to stop their rotation (32, 78). This is in contrast with the results obtained here for *A.*

brasilense that suggest that signaling output from both Che1 and Che4, likely mediated via CheY1 (85) and CheY4, respectively, alter different parameters of flagellar motor activity. The control of chemotaxis by two Che pathways in *A. brasilense* thus illustrates a distinct strategy by which signaling input from multiple Che pathways regulates chemotaxis.

Several lines of experimental evidence also support the hypothesis of signal integration via functional interaction between Che1 and Che4. First, inactivation of *cheA4* completely suppressed reversals in the swimming direction and it also caused the cells to swim at a reduced speed compared to the wild type strain (99, 109). Second, strains lacking CheY4 or Che4 function were significantly impaired but not null for chemotaxis unless CheY1 or Che1, respectively were deleted in these strains. The discrepancy between the swimming speed phenotype of the *ΔcheA4* and *ΔcheY4* strains indirectly supports the hypothesis of functional interaction between Che1 and Che4 because a *ΔcheA1* strain, but not a *ΔcheY1* strain also swam at a slower speed than the wild type *A. brasilense* (85). The lack of observable swimming speed defects in strains lacking CheY1 or CheY4 could either result from functional redundancy between CheY1, CheY4 and any of the 5 other CheY homologs encoded in the genome (94) or some other unidentified interactions between Che1 and Che4 proteins. The mechanism by which signaling from Che1 and Che4 is integrated to affect swimming speed and reversals in the swimming direction remains to be elucidated but previous data suggested that chemotaxis receptors and adaptation proteins may be involved in this process (90, 109). This was also suggested for the role of Che1 and

Che2 in *Rhizobium leguminosarum bv. viciae* chemotaxis (98) and demonstrated as an existing mechanism in *R. sphaeroides* (107, 108).

Increased swimming speed during chemotaxis provides an advantage for marine bacteria in the exploitation of transient sources of nutrients in the oceans (110). Like the ocean, the soil is a heterogeneous environment characterized by plethora of nutrient gradients that change rapidly in space and time (111). In contrast to the ocean, the soil is less limiting in many essential nutrients and as a result, it harbors abundant and diverse microbial communities (112). Oxygen may be particularly limiting in the rhizosphere where microbial cell densities and microbial activities are greatest (113, 114), making oxygen a potential modulator of microbial activities and competition in this environment. Consistent with this hypothesis, a major chemotaxis receptor for sensing oxygen and other metabolism-related parameters is critical for the ability of *A. brasilense* to colonize the wheat root surface (115). Results obtain here suggest that *A. brasilense* derives an aerotactic advantage from increased swimming speed, which is expected to be significant in the competitive environment of the rhizosphere. The additive roles of two chemotaxis systems controlling distinct motility parameters illustrated here by the *A. brasilense* Che1 and Che4 suggests a potential benefit that the control of chemotaxis by two (or more) pathways provide motile bacteria with in a competitive environment. Given the ubiquitous distribution of multiple chemotaxis pathways in the genomes of rhizosphere bacteria, we expect this strategy to be widespread.

EXPERIMENTAL PROCEDURES

Bacterial Strains and Growth Conditions

Bacterial strains used in this study are listed in table 1. The *A. brasilense* strains were grown at 28°C with shaking (200 rpm). The MMAB (<u>m</u>inimal <u>m</u>edium for <u>A</u>. <u>b</u>rasilense) medium was prepared as described previously (116, 117). Cells were induced for nitrogen fixation by growing them in liquid MMAB to the desired optical density (O.D. $_{600nm}$) followed by three to four washes of the cell pellet in sterile chemotaxis buffer before resuspension in liquid MMAB medium lacking any nitrogen source. Cells were induced for nitrogen fixation by growth overnight at 28°C, without shaking to ensure low aeration conditions. All culture stocks were routinely maintained on solid tryptone-yeast medium (10 g bacto tryptone, 5 g yeast extract and 15 g noble agar per liter) or solid MMAB medium lacking nitrogen and incubated under nitrogen fixation with antibiotics supplementation, when appropriate.

Mutagenesis

To construct a strain deleted for the *cheA4* gene, a 843 bp upstream fragment including 126 bp of *cheA4* and a downstream 825 bp sequence including 232 bp at the end of *cheA4* were PCR amplified using *cheA*4Up-F, *cheA*4Up-R, *cheA*4Dwn-F and *cheA4*Dwn-R (Table 1). These primers were engineered to include 5' XbaI (*cheA4*Up-F) and 3'HindIII (*cheA4*Dwn-R) restriction sites for first cloning into pUC19 digested with these enzymes as well as a BamHI sites (present at the 5' end of *cheA*4Up-R and at the 3' end of

51

*cheA*4Dwn-F) to permit subsequent insertion of a gentamycin resistance (Gm^r) cassette isolated from p34S-Gm by BamHI restriction digestion (Table 2). After verification by sequencing, the Δ*cheA4*::Gm^r region present on the pUC19 vector was isolated by restriction digestion with XbaI and HindIII and inserted into the suicide vector pSUP202 (Table 2) digested with the same enzymes, yielding pSUPΔ*cheA4*::Gm^r. The pSUPΔ*cheA4*::Gm^r vector was transformed into *E.coli* S17-1 for biparental mating with strains *A. brasilense* Sp7 and its Δ*cheA1* mutant derivative for allelic exchange, as previously described (117). For constructing a mutant lacking *cheY4*, an upstream fragment encompassing the first 6 bp of *cheY4* and an additional 577 bp of upstream DNA sequence as well as a downstream fragment including the last bp of *cheY4* and an additional 584 bp downstream of the stop codon were amplified using the primer pair *cheY4*Up-F and *cheY4*Up-R and *cheY4*Dwn-F and *cheY4*Dwn-R which were designed to include restriction sites to facilitate cloning into an EcoRI and HindIII digested pUC19 vector (Table 2). The fragments were also engineered to include a BamHI site for insertion of a chloramphenicol cassette isolated from a p34S-Cm BamHI-digested vector. The *cheY*4 deletion insertion construct was verified by sequencing using universal primers that anneal on the pUC19 vector and isolated as a EcoRI and HindIII digested fragment and cloned into the pKGmobGII suicide vector to yield pKGΔ*cheY4*::Cm^r (Table 2), which was then transformed into *E.coli* S17-1 cells and transferred into *A. brasilense* Sp7 or its Δ*cheY1* mutant derivative by biparental mating (117). Strains carrying appropriate deletions were verified by PCR. To construct a strain deleted for most of the *che4* sequence, we first used

PCR amplification of a 698 bp fragment encompassing the first gene of the *che4* cluster (Fig. 7) and upstream DNA sequence using *che4*Up-F and *che4*Up-R (Table 1) and a 722 bp fragment overlapping the last gene of *che4* (Fig. 7) and including additional downstream DNA sequence using *che4*Dwn-F and *che4*Dwn-R (Table 1). The primers *che4*Up-R and *che4*Dwn-F were designed to include 12 bp of overlapping DNA sequence that were used in a second round of SOE PCR (118) to produce a 1420 bp fusion product between the upstream and downstream PCR fragments. The 1420 bp product was restriction digested with PstI and XbaI which were engineered in the *che4*Up-F and the *che4*Dwn-R primers, respectively (Table 1), and cloned into pUC19 digested with the same enzymes. The fusion construct cloned in pUC19 was further digested with SalI in order to insert a SalI-digested gentamycin resistance cassette isolated from the p34S-Gm vector and yield a Δ*che4*::Gm^r construct cloned in pUC19. After verification by sequencing, the Δ*che4*::Gm^r region was isolated as a PstI and XbaI fragment which was then cloned into the suicide vector pSUPPOL2SCA (119) digested with the same enzymes. The suicide vector carrying the che4 deletion insertion construct was transformed into *E. coli* strain S17-1 followed by allelic exchange after transfer to *A. brasilense* wild type strain Sp7 and its Δ*che1* mutant derivative by biparental mating. Mutants carrying the correct deletion insertions were identified by PCR.

Table 1. Primers used in chapter 2

Primer	Sequence
*cheA*4Up-F	TCTAGAAAGGAGACGGGCGGTGAC
*cheA*4Up-R	GGATCCGATGGCGTTGACCTCGTCG
*cheA*4Dwn-F	GGATCCGACCCCACCCGCGCGCTG
*cheA*4Dwn-R	AAGCTTAGGGCCTTGGTCGCCGAG
*che*4Up-F	AAAACTGCAGGTGACTTTGATCAAGTGGAGC
*che*4Up-R	TCTTGTCCAGCCGCAGACCTTCTGAACGAC
*che*4Dwn-F	GTCTGCGGCTGGACAAGACCATGGACAGC
*che*4Dwn-R	GCTCTAGATCAGTCCTCGATCGTGACGAT
*cheA*4FwdEcoRI	TCGTAGTACATGAATTCAGGAGGGGCCCGTATGGACGGGGTGCGCAACAAC
*cheY*4FwdEcoRI	TCGTAGTACATGAATTCAGGAGGGGCCCGTATGGAGCCAAGCGTGAAG
*cheY*4DNRevHindIII	TCGTAGTACATAAGCTTTCAGCCGCAGACCTTCTG
*cheA*4RevHindIII	TCGTAGTACATAAGCTTTCAGACCGGTTCGAGTGCG
*cheY*4RevHindIII	TCGTAGTACATAAGCTTTCAGCCGCACACCTTCTG

Table 2. Strains and plasmids used in chapter 2

Strain or plasmid	Genotype, relevant characteristics	Reference
Strains		
Azospirillum brasilense		
Wild type	Wild type strain (Sp7)	ATCC29145
AB101	Δ(*cheA1*)::*gusA-Km* (Km^r)	(99)
AB102	Δ(*cheY1*)::*Km* (Km^r)	(99)
AB103	Δ(*cheA1-cheR1*)::*Cm* (Cm^r)	(99)
AB401	Δ(*cheA4*)::Gm (Gm^r)	This work
AB402	Δ(*cheY4*)::Cm (Cm^r)	This work
AB403	Δ(*cheX4-cheD4*):: Gm (Gm^r)	This work
AB141	Δ(*cheA1*)Δ(*cheA4*)	
	::*gusA-Km* (Km^r), Gm (Gm^r)	This work
AB142	Δ(*cheY1*)Δ(*cheY4*)	
	:: *Km* (Km^r), Cm (Cm^r)	This work
AB143	Δ(*che1*)Δ(*che4*)	
	:: *Cm* (Cm^r), Gm (Gm^r)	This work
Escherichia coli		
TOP10	General cloning strain	Invitrogen
S17-1	*thi endA recA hsdR* with	
	RP4-2Tc::Mu-Km::Tn7	(120)
	integrated in chromosome	
Plasmids		
pRK415	Cloning vector (121)	(121)
pRK-cheA4	pRK415 containing *cheA4*	This work
pRK-cheA4$_{H54Q}$	pRK415 containing *cheA4*	This work
	with mutation replacing codon	This work
	for H54 to Q	
pRK-*cheY4*	pRK415 containing *cheY*4	This work
pRK-*cheY4*$_{D57N}$	pRK415 containing *cheY4*	This work
	with mutation replacing codon	

Table 2 continued

Strain or plasmid	Genotype, relevant characteristics	Reference
	for D57 to N	
pSUP202	Suicide vector, pBR325 *mob* Tc^R Amp^R Cm^R	(120)
pSUPΔ*cheA4*::Gm^r		This work
pKGmobGII	Km^r, mobilizable suicide vector	
pKGΔ*cheY4*::Cm^r		
p34S-Gm	ori ColEI Amp^R Gm^R cassette	(122)
p34S-Cm	ori ColEI Amp^R Cm^R cassette	(122)
pUC19		(123)
pSUPPOL2SCA	Derivative of pSUP202, oriT of RP4, Tc^r	(119)

Complementation and site-specific mutations of *cheA4* and *cheY4* genes

Functional complements of the mutants were generated by cloning each parental gene locus into pRK415 (Table 2) downstream of the plasmid-born *lac* promoter with engineered restriction sites and a ribosome binding site to ensure expression (85). Each gene was amplified from the genomic DNA of the wild type strain, using a set of forward and reverse primers (Table 2). The kinase inactive CheA4H252Q and inactive CheY4D12N were synthesized by Genscript (http://www.genscript.com/gene_synthesis.html) and cloned into pUC57 between EcoRI and HindIII sites. The *cheA4* and *cheY4* inserts were subcloned into pCR2.1 by TOPO cloning according to the manufacturer's instructions (Invitrogen, CA) for sequencing verification, as well as digested with EcoRI and HindIII to isolate the sequence-verified genes. Next, the isolated DNA fragments were cloned into the pRK415 vector linearized by digestion with EcoRI and HindIII. Recombinant plasmids were isolated from transformed *E. coli* TOP10 cells, prior to being transferred into *E. coli* S17-1 for biparental mating with *A. brasilense* recipient strains, as described above. An empty pRK415 vector was transferred to *A. brasilense* Sp7 and its mutant derivatives and used as controls for functional complementation.

Behavioral assays

For the capillary assay for aerotaxis, cells were grown to O.D. $_{600nm}$ of 0.4-0.6 (exponential phase of growth) in MMAB medium supplemented with malate (10 mM) and ammonium (18.7 mM) and antibiotics as needed. Cultures were adjusted to an equivalent number of

cells (estimated via O.D. $_{600nm}$ measurements) by dilution in chemotaxis buffer (10 mM phosphate buffer [pH 7.0], 1 mM EDTA) and then the cells were gently washed three to five times with chemotaxis buffer, by low speed centrifugation (5000 rpm) and re-suspended in 100µl MMAB containing malate as a carbon source (10mM). All cells were motile under these conditions. Cells were transferred to an optically flat capillary tube (Vitro Dynamics, Inc., Rockaway, N.J.) by dipping one end of the capillary tube in the eppendorf containing cells. Aerotaxis was visualized under the light microscope, as the formation of a stable band of motile cells at a distance from the air-liquid interface (meniscus). An aerotaxis band typically forms within 2-3 minutes and is stable for a minimum of 25 minutes under these conditions (124). The assay was performed on triplicates with independent cultures.

To test chemotaxis in soft agar plates, MMAB plates solidified with 0.3% agar and supplemented with malate as a carbon source (10mM) and ammonium chloride as nitrogen source (18.7mM) as well as antibiotics as needed. Cells were grown as indicated above for aerotaxis and adjusted to an equivalent number of cells prior to being inoculated in the center of the soft agar plates. The diameter of the chemotactic rings formed by the motile cells after incubation at 28°C was measured at 48 hours post inoculation. The experiment was performed in triplicate for each strain and the results were expressed as fraction of the wild type chemotaxis, taken as 1.

Computerized motion tracking of free-swimming cells

Cells were cultured as indicated above for aerotaxis and soft agar plate assays until O.D. $_{600nm}$ of 0.4-0.6. Videos of free-swimming cells were recorded with a SONY HyperHAD monochrome camera at a rate of 30 frames per seconds and the videos were converted to a digital format using IC Capture2 software (The Imaging Source, Charlotte, NC) before being analyzed using CellTrak 1.5 software (Motion Analysis, Santa Rosa, CA). Changes in swimming parameters (velocity and reversal frequency) were determined on a minimum of 75 cells, recorded from at least 2 different fields of view and 3 independent cultures. Velocity is expressed as micrometer per second and reversal frequency as the number of changes in direction per second and per cell.

Plant Inoculation

Wheat seeds (*Triticum aestivum*) were surface sterilized and germinated as previously described (104). Nest, 50mL of Fahraeus medium (CaCl$_2$, 100mg l^{-1}, MgSO$_4$.7H$_2$0, 120mg l^{-1}, KH$_2$PO$_4$, 100mg l^{-1}, Na$_2$HPO4, 150 mg l^{-1} and ferric citrate 5 mg l^{-1}) solidified with 0.6% agar was placed in a 6.5 cm diameter growth chamber. Four sterile germinated seeds were placed into the edge of the growth chambers and inoculation was performed at the center of the chamber (see below). Eight chambers were prepared for each trial yielding a minimum of 8 replicates. For competitive and non-competitive inoculations, strains were grown in MMAB supplemented with malate and ammonium chloride to an O.D. $_{600nm}$ of 0.5. Two mL of the culture were washed 3 times with a sterile 0.8% KCl solution by

centrifugation at 5000 rpm for 3 minutes to pellet the bacteria and re-suspended in 400μL of sterile 0.8% KCl. Twenty μL of this cell suspension was inoculated into the center of the growth chambers. The number of cells in the inoculum was determined by CFU counts. For competitive root colonization assays, the strains to be compared were prepared as indicated above and mixed in a 1:1 ratio prior to inoculation into the chambers. The chambers were incubated at 25°C for 24 hours after which the plants were removed, and the roots excised. For each chamber, the roots of the four plantlets were homogenized with 5 mL 0.8% KCl and serial dilutions followed by plating on selective media (MMAB, supplemented with antibiotics for isolation of the mutant strains) were performed to determine CFU. Root colonization was calculated as a colonization index for plants inoculated with a single strain and as a competitive index for the plants inoculated with two strains. The competitive index for individual strains is the Log_{10}(strain output/strain input), where the number of CFU extracted from roots after incubation is normalized to the CFU measured in the inoculated input. The competitive index is a ratio calculated as follows: Log_{10} (mutant output/wild-type output)/(mutant input/wild-type input).

Acknowledgements

CHAPTER III

DISTINCT CONTRIBUTION OF CHEY HOMOLOGS OF *AZOSPIRILLUM BRASILENSE* TO REVERSALS AND TRANSIENT PAUSES REVEAL UNIQUE FEATURES OF THE FLAGELLAR MOTOR

Text and figures were taken from the following:

Author contributions to this work included: **TM and GA** designed research; **TM, LV** performed research; **ME and TH wrote codes in MATLAB and Python;** **TM, ME, TH and GA** analyzed data; **TM, TH and GA** wrote the paper.

ABSTRACT

Chemotaxis together with motility helps bacteria foraging in their habitat. Motile bacteria exhibit a variety of motility patterns, often controlled by chemotaxis, to promote dispersal Motility in many bacteria is powered by a bidirectional flagellar motor. The flagellar motor has been known to briefly pause during rotation due to incomplete reversals or stator detachment. In addition, transient pauses were previously observed in bacterial strains lacking CheY and these events could not be explained by incomplete motor reversals or stator detachment. Here we systematically analyzed swimming trajectories of various chemotaxis mutants of the monotrichous soil bacterium, *Azospirillum brasilense*. Like other polar flagellated bacterium, the main swimming pattern in *A. brasilense* is run and reverse. *A. brasilense* also uses run-pauses and putative run-reverse-flick-like swimming patterns during swimming though these are rather rare events. *A. brasilense* mutant

derivatives lacking the chemotaxis master histidine kinase, CheA4 or the main response regulator, CheY7 also showed transient pauses. Strikingly, the frequency of transient pauses increased dramatically in the absence of CheY4. Furthermore, though the duration of transient pauses increased in all chemotaxis mutants analyzed except for those lacking CheY1 that were unaffected, turning angles did not increase. Our findings collectively suggest that reversals and pauses are controlled through signaling by CheY homologs, and thus are likely to be functionally important in the lifestyle of this soil organism. The control of the pause events is likely involving additional proteins, yet to be identified, though evidence suggest these candidates should have features allowing them to interact with CheY homologs and structural components of the flagellar motor.

INTRODUCTION

Bacteria swim using polar or lateral flagella, and chemotaxis signal transduction controls the swimming pattern in most of these motile bacteria. The most extensively studied *Escherichia coli* possess peritrichous flagella powered by bidirectional motors and its swimming pattern consists of straight runs interrupted by tumbles that re-orient the cell in a new direction (Berg, 1972, Chemotaxis in *E. coli* analyzed by three-dimensional tracking). When all the flagellar motors rotate counter clockwise (CCW), the rigid flagellar filaments flagella form a bundle that propels the cell forward in a "run." When any of the flagellar motors switches rotation from CCW to clockwise (CW), the flagellar bundle is disrupted (24, 125), resulting in a "tumbling" event. This swimming pattern is referred to as "run and tumble" (126).

Many motile bacteria have one or more polar flagella, including 90% of motile marine bacteria (25). For most of these polarly flagellated bacteria, the swimming pattern has not been characterized. In bacteria with polar monotrichous flagella powered by a bi-directional motor such as the alphaproteobacterium *Azospirillum brasilense*, the rotation of the flagellar motor in the CCW direction causes cells to move forward by pushing the cells whereas CW rotation of the flagellar motor results in a backward movement (24, 83). Regardless of the number of flagella, the probability of reversals in the direction of rotation of the flagellar motors is controlled by chemotaxis signaling (127).

In contrast to tumbles, the run and reverse swimming pattern of monotrichous flagellated bacteria could in theory lead to endless retracing of the trajectory, with reorientation in a new swimming direction depending only on Brownian motion. This represents a rather inefficient way of seeking nutrients or escaping noxious conditions by chemotaxis (125, 128). The unproductive nature of this backtracking for exploration during chemotaxis led to the hypothesis that monotrichous flagellated bacteria have developed mechanism(s) to overcome this limitation. In agreement with this notion, Xie (28) found that the monotrichous flagellated bacterium *Vibrio alginolyticus* could abruptly change swimming direction around ~ 90° angle with a flick of its unique polar flagellum. In this bacterial species, flicking of the flagellum occurs when the cells resume a forward run after a brief backward run, causing the flagellum to buckle at the hook (28, 30). This buckling of the flagellum, which depends on the swimming speed (30) and cell size (31), leads to broad re-orientation of the cells at an angle centered around 90°. The flick was recently proposed

64

to result from a dynamic instability on the flagellar hook and filament (30, 129). In contrast to tumbles and reversals in the direction of rotation of flagellar motors, flicking of the flagellum is not controlled by chemotaxis signaling in *V. alginolyticus* since non-chemotactic mutants remained able to flick (30).

In chemotaxis, a motile organism navigates chemical gradients in the environment and directs its movement toward higher concentrations of an attractant or lower concentrations of a repellent. Motile and flagellated bacteria accomplish chemotaxis by biasing their swimming pattern in order to move toward favorable niches in the environment. In *E. coli* and other bacteria, chemotaxis signaling functions to alter the probability of swimming tumbles or reversals. This signaling is initiated when a stimulus is detected by chemoreceptors causing a conformational change that ultimately alter the phosphorylation state of the associated histidine kinase CheA. Phosphorylated CheA transfers its phosphoryl group to its cognate response regulator, CheY, increasing its affinity for the flagellar motor. Binding of phosphorylated CheY to the flagellar motor triggers a switch in the direction of motor rotation, causing a tumble or swimming reversal (56). In *A. brasilense,* chemotaxis is controlled via two chemotaxis signaling pathways, named Che1 and Che4 (85, 86). Che1 and thus CheA1 and CheY1 control transient changes in the swimming speed (85) while Che4 and its histidine kinase-response regulator pair, CheA4 and CheY4, regulate the probability of swimming reversals (86). In addition to CheY1 and CheY4, the genome of *A. brasilense* encodes two additional chemotaxis systems that do not control flagellar motility but other cellular functions, as well as two other CheY

65

homologs, named CheY6 and CheY7 whose function is not known (94). Here we characterize additional features of the swimming pattern of *A. brasilense*, including pause events that are controlled by chemotaxis signaling. By characterizing the role of different CheY in modulating the swimming pattern we also identify distinct roles for the CheY homologs that suggest novel features of the flagellar motor in this organism.

RESULTS

Distinct reversal and pause swimming patterns in *A. brasilense*

To characterize the swimming patterns of *A. brasilense*, we first examined the distributions of the angles during the turning events (defined based on abrupt increase in angular velocity and significant directional change. See methods for details.) in wildtype strain Sp7 (Fig. 14A). The distribution of the turning angles is centered at 180˚, with a long tail extended below 90˚. This pattern suggests that the majority of turning events are 'reversals' during which the bacteria completely switched their swimming directions. One example of such events is shown in Fig 14B. In this example, bacteria made three abrupt turns (Fig. 14B, yellow track segments) with angles close to 180˚. Together with the straight motion before the turning events, these events constitute the 'run-reverse' swimming patterns that were well-characterized before (130). We surmise they correspond to reversals of the direction of rotation of the polar flagellar motor from CCW to CW, which were observed in other bacteria and in *A. brasilense* (83, 130). Unlike bacteria which have three step swimming pattern of run-reverse-flick and have a broad peak centered around 90° (28), we did not observe a distinct population of turning events with angles centered around 90˚ (Fig. 14A).

66

Nonetheless, we found that a minor population of the turning events exhibit the flick pattern (run-reverse-flick), and it is possible that flicking events with angles distributed broadly around 90˚ (Figs. 14A-15) occurred. This suggests the possibility that *A. brasilense* uses flicking as a secondary swimming strategy.

We next characterized the events in which the bacteria have abrupt decreases in swimming speed (see method for details). The turning angles during these events have a remarkable bimodal distribution (Fig. 14C). We observed significant number of events with turning angles distributed around each of the modes at 180˚ and 0˚. Based on this bimodal distribution, we classified these events into two categories: those with turning angles less than 90˚ are defined as 'transient pauses' (Fig. 14C, blue population. See example in Fig. 14D), and the rest of them are defined as 'reversals' (Fig. 14C, red population) because they are strongly correlated with the abrupt turning events (Fig. 14B, yellow segments and red dots. Fig. 14E, Pearson correlation coefficient: 0.89; p-value < 0.0001). For those transient pauses, *A. brasilense* decreased its swimming speed abruptly during a swimming run, and then resumed the swim in the same direction (Fig. 14D, run-pause, pauses labeled as red dots). Note that we use 'reverals' to refer to the events with both detected sharp decrease in speed and significant directional change (red population in Fig. 14C) for convenience, but it is possible to use the term to describe the abrupt turning events (Fig. 14A) because of their strong correlation (Fig. 14E). This strong correlation between reversal frequency and abrupt turns is also true for all chemotaxis mutants used in this study (Fig. 16). Hence, all of our conclusions are not sensitive to this choice of terminology.

The examples shown in Fig. 14B and Fig. 14D suggest that the transient pauses and the reversals are distinct swimming patterns. We asked whether this distinction is generally true in the tracked cells. We found that the frequencies of observing the transient pauses and observing the reversals are not correlated among the tracks (Fig. 14F). Notably, there are significant numbers of tracks that have either transient pauses only or reversals only (Fig. 14G, data points on the x or y axis). This result indicates that the transient pauses may not simply correspond to incomplete motor reversal events that were described earlier (58), and they might be controlled by mechanisms distinct from those controlling the reversals. In summary, we found that free-swimming *A. brasilense* cells display distinct run-reverse and run-pause patterns, and we also observed infrequent run-reverse-flick events in these cells. We next performed detailed analysis on this remarkable diverse swimming patterns, in particular, on the transient pauses that were not well-characterized in previous studies.

Signaling through CheA4 and CheY4 controls frequency of transient pauses

While analyzing the swimming behavior of chemotaxis mutants, we found some strains pausing more or less than the wild type strain, suggesting that chemotaxis signaling could alter the frequency of these transient pauses. There are two changes associated with chemotaxis in *A. brasilense*: transient changes in the swimming speed and in the reversal frequency (85, 86). To further establish the role of chemotaxis signaling, we first
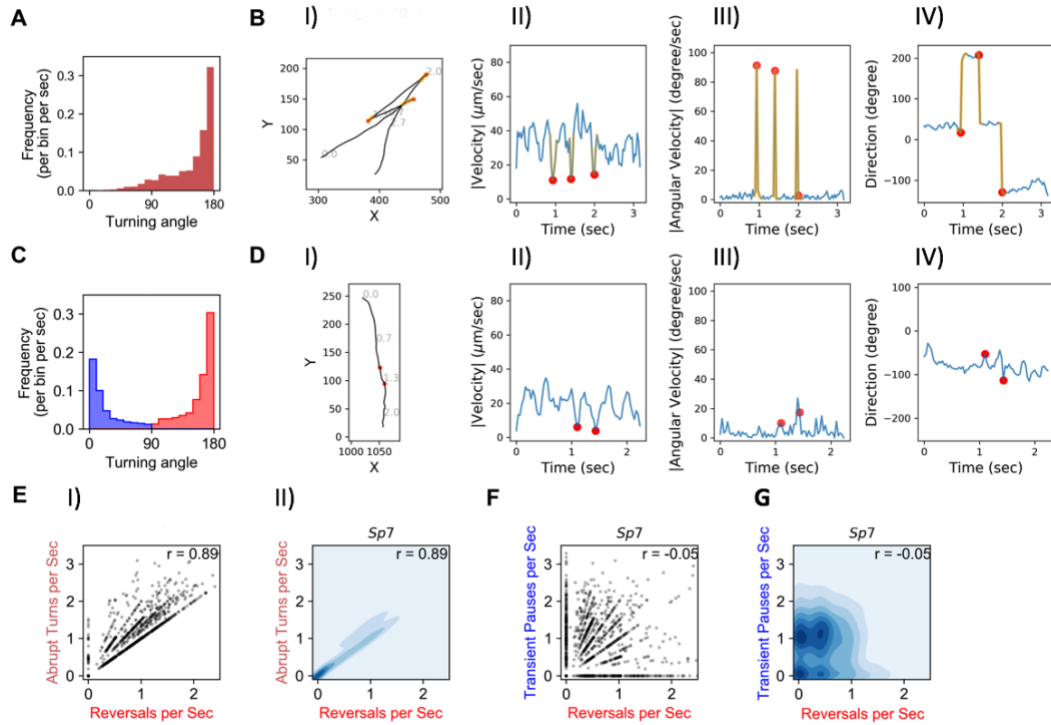
Figure 14. Quantification and presentation of different aspects of the swimming patterns in wildtype *A. brasilense*.

A) Distribution of turning angles during swimming in wildtype *A. brasilense* B) I) Run-reverse swimming pattern as seen in wildtype *A. brasilense*. II) instantaneous speed, III) angular velocity and IV) direction of travel for same trajectory are shown in separate horizontal panels. C) Distribution of events with transient pause and reversals as classified based on turning angle cut off. D) A typical trajectory with two consecutive transient pauses. E) Correlation of abrupt turns per sec vs reversals per sec. F) and G) Correlation of abrupt turns per sec vs transient pauses per sec. The yellow color in B and D represents the frames involved in turning event where as red dot represents a transient pause.

69
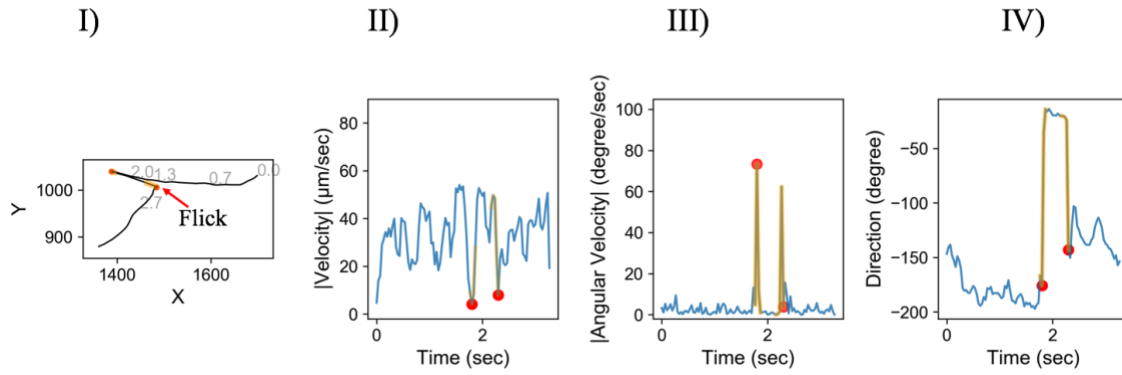
Figure 15. A run-reverse-flick like event as seen during swimming of wildtype *A. brasilense*.

II) Instantaneous speed, III) angular velocity and IV) direction of travel for same trajectory are shown in separate horizontal panels. The yellow color in B and D represents the frames involved in turning event where as red dot represents a transient pause.

systematically analyzed the swimming trajectories of chemotaxis mutants having varying degree of impairment in the ability to reverse swimming direction, i.e. having different frequency of reversals (Fig. 17).
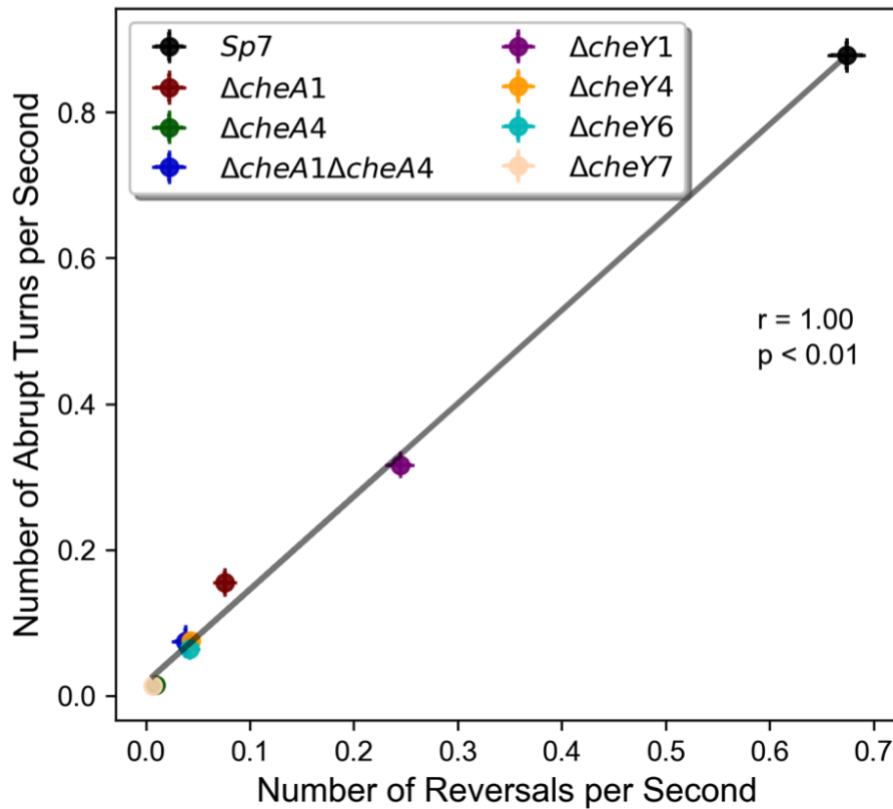
Figure 16. Correlation of abrupt turns per sec vs reversals per sec for all the chemotaxis strains used in this study.

A very strong correlation is seen with Pearson correlation coefficient of 1 (p-value < 0.01).

We found that the swimming reversal frequency did not correlate with the frequency of transient pauses in any of these mutants (Fig. 17-18). Furthermore, a ΔcheA4 mutant, that is unable to reverse swimming direction and is null for chemotaxis (86), also displayed instances of transient pauses (Figs. 17-18). Next, we determined the frequency of transient pauses in those mutants relative to that of the wild type. The average frequency of transient pauses for the wild type strain was 0.53 sec^{-1}, however, it was unaffected in the ΔcheA1 mutant and significantly decreased in the ΔcheA4 (0.22 sec^{-1}) and $\Delta cheA1\Delta che$A4 (0.31 sec^{-1}) mutant strains which are unable to reverse swimming directions (Fig. 19). Together these results suggest that signaling through the CheA4 pathway controls the frequency of transient pauses, and that signaling through CheA1 does not affect these events. However, the frequency of transient pauses in the $\Delta cheY1$ mutant of the Che1 pathway was significantly reduced compared to that of the wildtype strain (Fig. 19). In contrast, the $\Delta cheY4$ mutant that lacks CheY4 encoded in the *che4* gene cluster had a reduced reversal frequency and it also displayed an unexpected increase in the frequency of transient pauses compared to the wild type strain (Fig. 19). Together, these results indicate that CheA1 have no role in controlling the frequency of transient pauses while CheA4 is essential. Our results also suggest that CheY4 functions to suppress pauses while it also increases the frequency of reversals, suggesting that these two events are distinct in *A. brasilense*.

Additional CheY homologs affect both frequency of pauses and of reversals

Our previous work suggested that CheY homologs other than CheY4 contributed to the control of the swimming reversal frequency in A. brasilense (86). Of the other CheY homologs found outside of the Che1 and Che4 clusters on the genome, two have all the hallmarks of functional CheY homologs: that includes the conserved aspartate residue for phosphorylation (aspartate 57 in *E. coli* CheY) and the residues involved in Y-T coupling (corresponding residues to tyrosine 106 and threonine 87 for *E. coli* CheY). We constructed mutant strains lacking CheY6 or CheY7 and analyzed the effect on the frequency of swimming reversals and transient pauses. We found that the *Δche*Y6 mutant had a low but not null reversal frequency and that the *ΔcheY7* completely lacked the ability to reverse swimming direction (Fig. 19). These results establish that CheY7 is the major CheY homolog that regulates swimming reversals in *A. brasilense* while both CheY4 and CheY6 have a major but non essential role. Both the *Δche*Y6 and the *Δche*Y7 mutants had significantly reduced, yet not null frequency of transient pauses, with *Δche*Y7 having a lower frequency of transient pauses compared to that of the *Δche*Y6 mutant (0.62-fold, $p < 10^{-4}$) (Fig. 19). Together, these data indicate that a lower reversal frequency is associated with a lower probability of transient pause in strains lacking CheY6 and CheY7. However, lack of CheY4 decreases the reversal frequency but also causes an increase in the frequency of transient pauses suggesting that the pauses are additional features of the flagellar motor that are controlled by CheY homologs.

73

Pause duration is affected by chemotaxis but not related to the turning angle

Given the role of chemotaxis signaling in the frequency of transient pauses, we also determined the role of the different CheY homologs on the duration of both reversal and transient pauses. Duration of reversals and transient pauses varied from 0.1sec to as high as 0.6 sec (Fig. 20-21) with an average duration of 0.25 sec for thee wildtype (Fig. 21). The reversal duration was significantly reduced in the *ΔcheY1* mutant (Fig. 21). CheY1 was previously found to control transient increase in swimming speed and we surmise that its effect of the reversal duration result from this function (85), the target of which is not known to date. In *A. brasilense*, the duration of the pause events did not correlate with the turning angle (Fig. 20) in the wild type or any of the non-chemotactic mutants (Fig. 20). This suggests that the duration of the pause events do not contribute to increased turning angle, further implying that the duration of transient pauses does not contribute to direction changing.
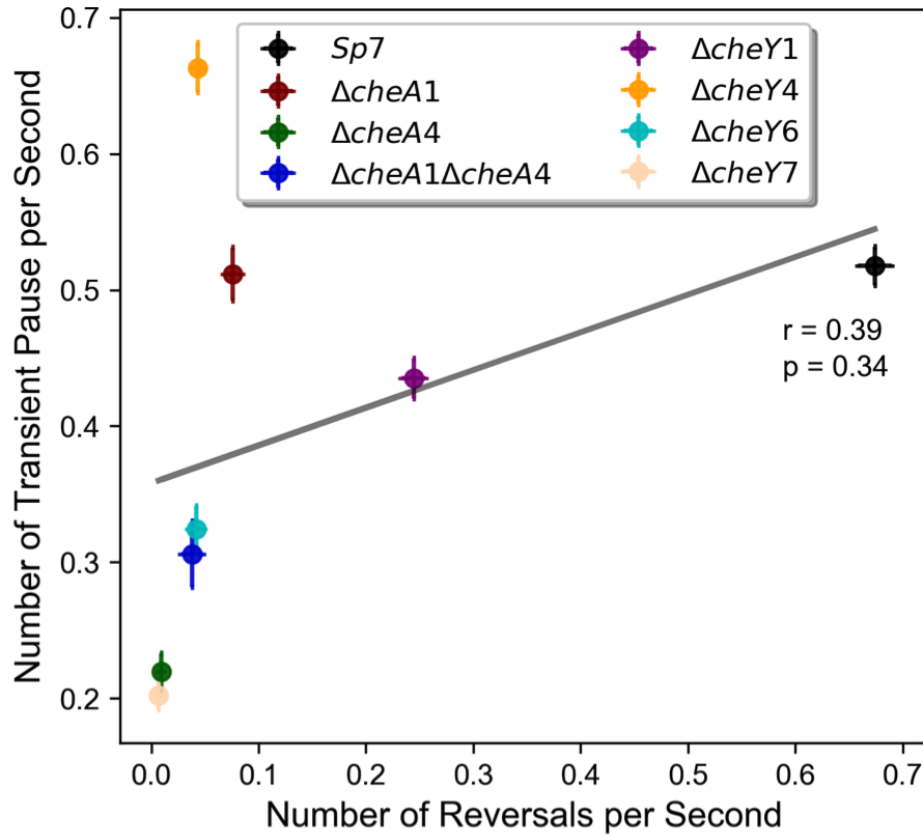
Figure 17. Frequency of transient pauses do not correlate with reversals frequency.

Correlation of transient pauses per sec vs reversals per sec for all the chemotaxis strains used in this study. A weak correlation is seen with Pearson correlation coefficient of 0.39 (p-value =0.34).
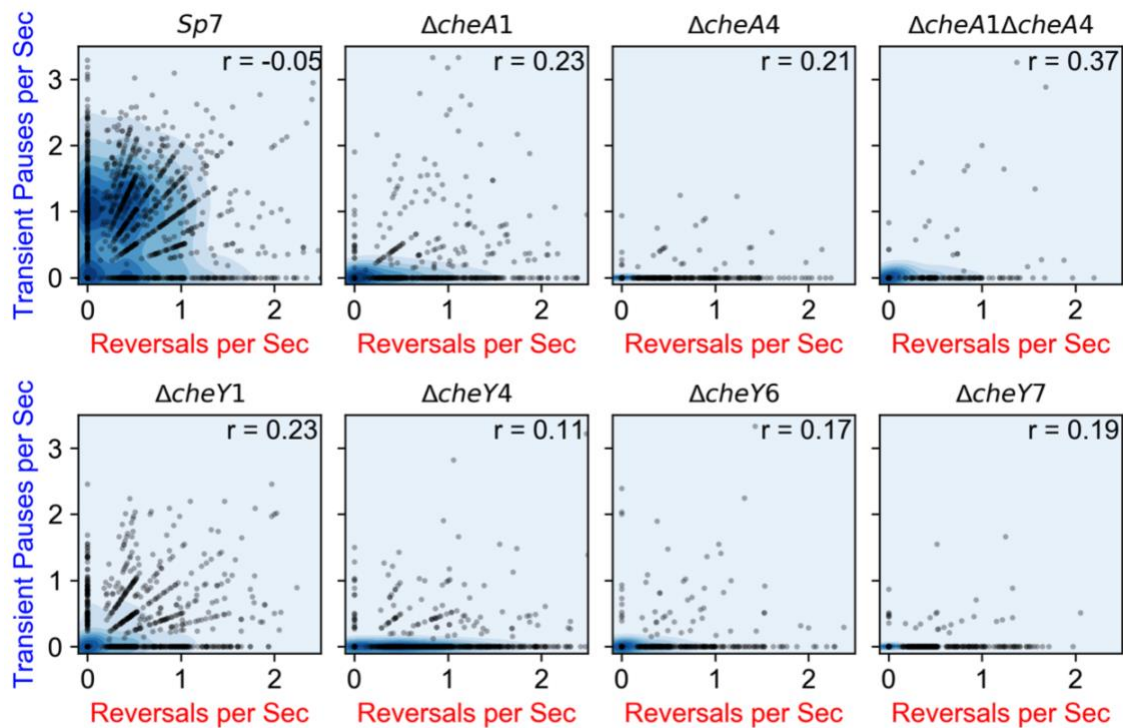
Figure 18. Correlation of transient pauses per sec vs reversals per sec for all the chemotaxis strains used in this study shown individually.

Correlation between transient pauses per sec vs reversals per sec vary from no relationship (r = -0.05) in wildtype (Sp7) to a weak positive linear relationship in *ΔcheA1Δche*A4 with Pearson correlation coefficient of 0.37. p-value for each of the strains are provided in their respective panels.
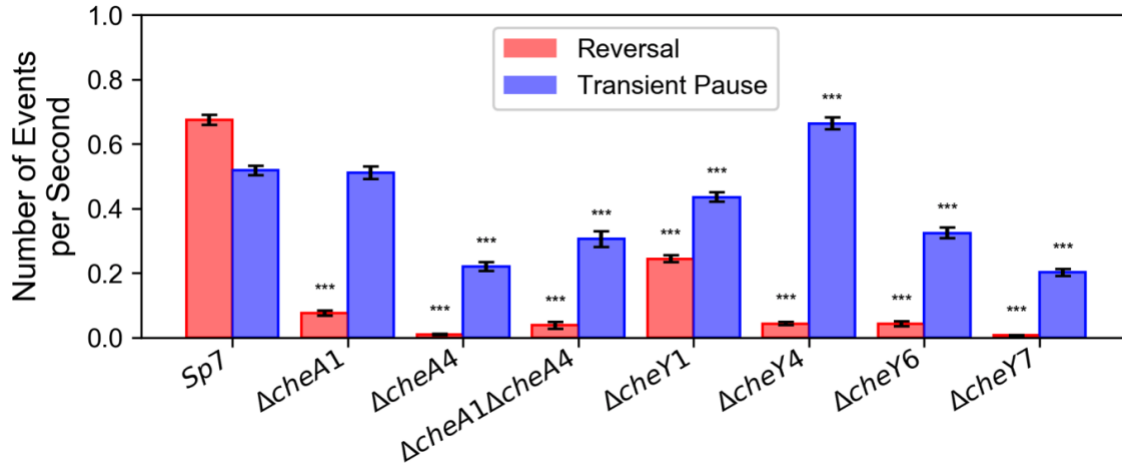
Figure 19. Frequency of transient pauses (blue) and reversals (red) for each of the chemotaxis mutants tested in this study.

Number of tracks analyzed for each strain are presented in Table 3. Pairwise comparison was done for each strain with wildtype (Sp7) for statistical significance separately for reversal frequency and transient pause frequency. An (***) represent statistically significant differences at the $p < 0.001$ levels (Student's t test).
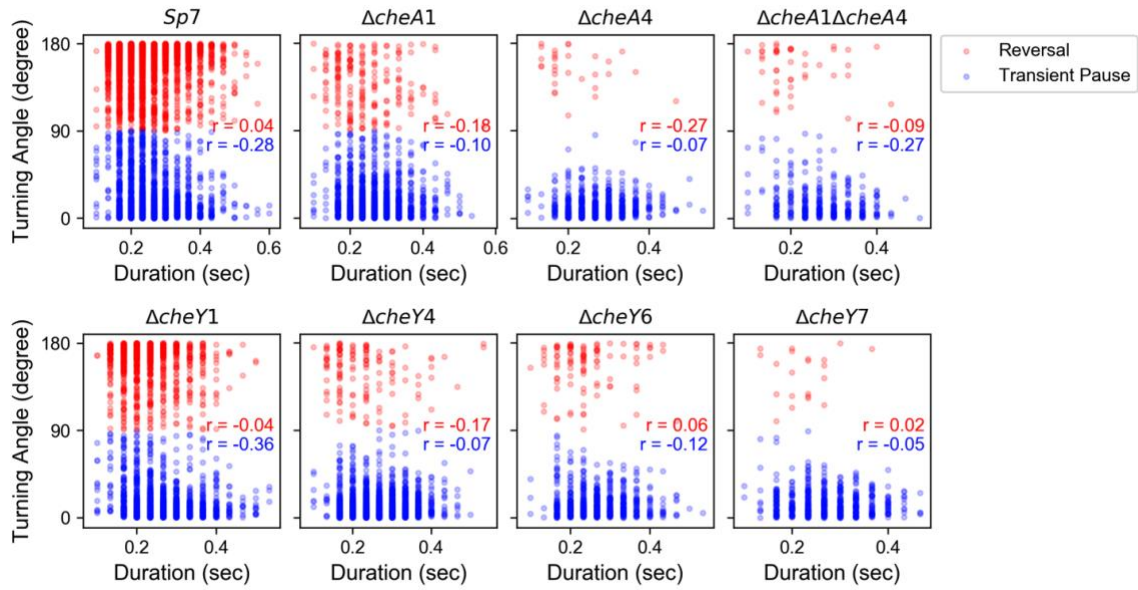
Figure 20. Turning angle do not correlate with duration of transient pauses or reversals.

Correlation of turning angle vs duration of transient pause (blue solid circle) and reversals (red solid circle) for all the chemotaxis strains used in this study shown individually. Pearson correlation coefficient (r) is denoted in red for reversals and blue for transient pauses in each panel. p-value for each of the strains are provided in their respective panels.
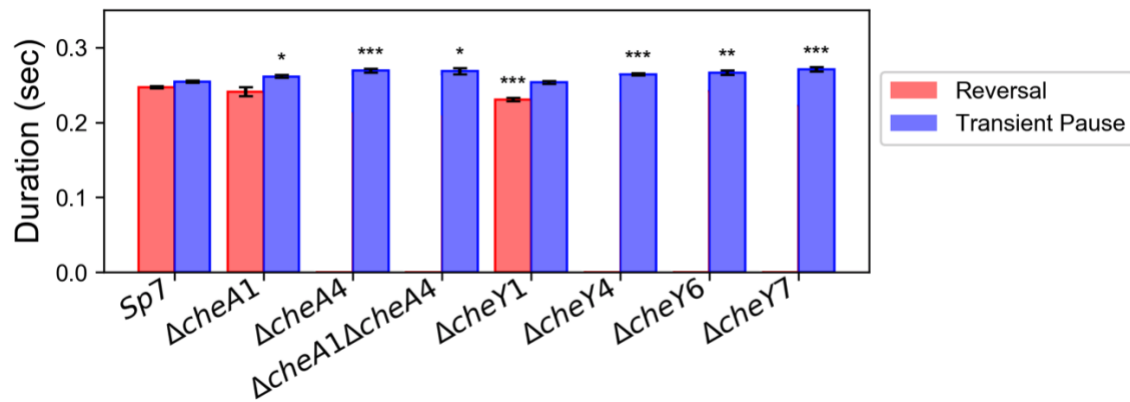
Figure 21. Duration of transient pauses or reversals for different chemotaxis strains used in this study.

Duration of reversals is denoted by red bars for each strain whereas duration of transient pauses is denoted by blue bars. An (*), (**) or (***) represent statistically significant differences at the $p < 0.05$, $p < 0.005$ or $p < 0.001$ levels, respectively using Student's t test.

DISCUSSION

Here, we identified three swimming patterns of free-swimming *A. brasilense* cells: run-reverse, run-pause and run-reverse-flick. These different patterns of swimming allow a population of swimming *A. brasilense* cells to sample its environment by changing direction at angles spanning 0° to 180°. Although most directional changes were observed around 180° angles under the conditions used here, this behavior may increase competitiveness in the soil environment. Indeed, the soil is a spatially and temporally heterogenous structure comprised of aggregates of varying sizes and pore spaces that create a range of chemical gradients (131). The ability of a motile cell to explore the surroundings using a broad range of angles could be advantageous.

The run-reverse swimming pattern is ubiquitous in polarly flagellated bacteria and observed in 70% marine bacteria (25, 26). The run-reverse-flick pattern was first identified in the marine bacteria *V. aliginolyticus* and *P. haloplanktis* which both have a single polar flagellum that rotates at high swimming speed of up to ~70 μm/sec (30). Son et al increased the Na concentration in the liquid medium which increased the swimming speed of the sodium driven motor of *V. aliginolyticus* and measured the number of cells that flicked (30). They came to the conclusion that the flicking probability increases with speed more than 35μm/sec (30). Motile soil-dwelling bacteria that have been studied thus far swim slower than marine bacteria because of their proton driven motor and flicks have not been identified conclusively as was the case of the soil *Pseudomonas oryzihabitans* (132). The average speed of motile *A. brasilense* cells is 30 μm/sec (86) with the maximum speed we

detected at 60µm/sec. Since not all *A. brasilense* cells have speed higher than 35µm/sec, it may be the case that not all cells were involved in flicking. *A. brasilense* may show a speed dependent phenotypic heterogeneity where cells with higher speed have greater tendency to flick and thus more chemotactically efficient. Cells size was also shown to be a factor in determining the flicking angle (31) but we did not analyze this parameter here.

Our results indicate that chemotaxis proteins CheA4 controls transient pauses and all reversals, most likely by signaling through CheY7 who displays a similar phenotype. These observations would suggest that transient pauses correspond to incomplete reversals in the direction of rotation of the flagellar motor, that were also observed in *E. coli* (133, 134). These pause events were associated with changes in the direction of rotation of the flagellar motor during a tumble because non-chemotactic mutants, including a mutant lacking CheY, that are unable to tumble, no longer pause (134, 135). In *E. coli*, these transient pauses were later observed experimentally (58, 134). Transient pauses during swimming were also observed in two *Pseudomonas* species (*P. putida* and *P. aeruginosa*) and the dependence on motor reversal was found to be similar to that of *E. coli* (45, 136). Transient stator detachment was proposed as one possible mechanism for swimming pauses in *E. coli* (137). Recently, tethering experiments carried out at high angular and temporal resolution to characterize flagellar motor rotation in *E. coli* revealed that a cell lacking CheY paused with a frequency of 1about 0 pauses per sec with each pause event averaging 5 ms. The pause duration range varied from 5 to 33 ms in 90% of the pauses analyzed but these were not accompanied by any evidence of stator displacement (138). These observations led the

authors to hypothesize that most pause events in *E.coli* are caused by a mechanism other than stator displacement or incomplete reversals (138). Our time-scale resolution for the pauses detected here is 33 ms and above. Therefore, we cannot conclude on any particular molecular event responsible for these pauses.

In contrast to *E.coli* and *Pseudomonas* species, the transient pauses are not strictly associated with changes in the direction of flagellar motor rotation because a strain lacking CheY4 had a low frequency of reversals but an increased frequency of transient pauses. This suggests that transient pauses can be regulated independently of swimming reversals and that signaling through CheY4 is a major regulator. The phenotype of the CheY4 is unexpected for several reasons. First, CheA4 and CheY4 are produced from the *che*4 cluster and function together to control reversals (86). Unlike the control of swimming reversals, CheY4 has a divergent role on the control of the transient pauses, suggesting that either CheY4 binds the flagellar switch complex differently than any other CheY, which is unlikely given its role in reversals and the overall amino acid sequence conservation, or that CheY4 and perhaps all or only some of the other CheY homologs, regulate the pause frequency through interaction with an additional protein or protein(s). Together these data suggest that the direction of rotation as well as the pauses exhibited by the polar flagellar motor of *A. brasilense* are regulated, and thus likely have a functional role. We hypothesize that the pause events likely involve unidentified additional proteins, that may have features allowing them to interact with CheY homologs and structural components of the flagellar motor.

EXPERIMENTAL PROCEDURES

Bacterial strains and culture conditions

The bacterial strains used in this study are listed in Table 1. Minimal medium for *A. brasilense* (MMAB) with malate (10 mM) as a carbon source and with or without nitrogen in the form of sodium chloride (18.7 mM) (+/−N) and Che (Chemotaxis) buffer were prepared as described previously (117, 139). Stocks of individual strains at -80˚C were directly streaked on am agar-solidified MMAB-N+C plate, since *A. brasilense* is a diazotroph (Tarrand et al., 1978). A single colony from the freshly streaked plate was inoculated into 5ml liquid MMAB+N+C media with proper antibiotic concentrations. The *A. brasilense* wild type (Sp7) and mutant strains were grown at 28°C, with shaking (200 rpm). The culture was re-inoculated at least once more until 0.6 OD_{600} before recording swimming of the bacteria for motion tracking analyses purposes. The culture was then harvested and washed in 1 ml of Che buffer, 3 times at 3000 rpm, for 3 min. The samples were left undisturbed for at least 30 minutes to ensure cells were adapted to the drop of nutrients. All recordings were completed within 2 hours of collecting the initial culture to avoid starving of the cells. The strains used in this study are listed in Table 2. Unless stated, the required antibiotics were used at the following concentrations: ampicillin (Amp) 200 µg/ml, carbenicillin (Cb) 50 µg/ml, kanamycin (Km) 25 µg/ml, gentamycin (Gm) 20 µg/ml, and chloramphenicol (Cm) 20 µg/ml.

Mutagenesis

Construction of deletion mutants except for *ΔcheY6* and *ΔcheY7* were previously reported elsewhere and are referenced in the Table 3. The strain carrying a *ΔcheY6* deletion was made using an allelic exchange method (117). A 418 bp sequence including the first 39 bases of *cheY6* was amplified from the upstream region of c*heY6* using primers 1F and 1R (Table 4). Similarly, 410 bp was amplified from the downstream region of *cheY6* including last 33 bases of *cheY6* using primers 2F and 2R (Table 4). Then these two fragments were fused using **s**plicing by **o**verlap **e**xtension PCR (SOECheY6) using primers 1F and 2R and cloned into pCR2.1 resulting in pCRSOECheY6 and then digested with EcoRI and ligated into suicide vector pK18mobsacB which was also digested with EcoRI. The resulting vector pK18SOECheY6 was transformed into *E. coli* S17-1 cells and mobilized into Sp7 through biparental mating following previously described protocol (117). To construct the *ΔcheY7* mutant strain, a 164 bp internal fragment of *cheY7* was amplified using primers Inter_CheY7_FwdBamHI and Inter_CheY7_RevBamHI (Table 4). The resulting fragment was cloned into the pCR2.1 vector to generate pCRInterCheY7. The pCRInterCheY7 vector and the suicide vector pKNOCK(Gm^r) were then digested with BamHI (140). The BamHI digested internal fragment of *cheY7* was then ligated into BamHI digested pKNOCK(Gm^r) to generate pKNOCKInterCheY7. pKNOCKInterCheY7 plasmid was then transformed into DH5-α λpir and helper plasmid pRK2013 was transformed into

84

Table 3. Strains and plasmids used in this study.

Strains	Genotype	References
Azospirillum brasilense		
Wild-type	Wild-type strain Sp7	ATCC 29145
ΔcheY1	ΔcheY1::Km (Km^r)	(99)
ΔcheY4	ΔcheY4::Cm (Cm^r)	(86)
ΔcheA1	ΔcheA1::gusA-Km (Km^r)	(99)
ΔcheA4	ΔcheA4::Gm (Gm^r)	(86)
ΔcheA1ΔcheA4	ΔcheA1ΔcheA4::gusA-Km-Gm (Km^r Gm^r)	(86)
ΔcheY7	ΔcheY7::Gm (Gm^r)	This work
ΔcheY6	markerless deletion that also includes first 39 bp and last 33bp of the open reading frame of *cheY6*	This work
Escherichia coli		
S17-1	*thi endA recA hsdR* strain with RP4-2Tc::Mu-Km::Tn7 integrated in chromosome	(120)
HB101	General cloning strain	Invitrogen
DH5-α λpir	DH5-α derivative containing *pir* gene	(141)
Plasmids		
pCR2.1	TOPO Cloning Vector	Invitrogen
pKNOCK	Mobilized suicide plasmid for insertional deletion (pBLS63 derivative carrying RP4 *ori*T and R6K γ-*ori,* Gm^r)	(140)
pRK2013	Helper plasmid for triparental mating (ColE1 replicon, Tra, Kan)	(142)
pK18mobsacB	Suicide vector for gene disruption; *lacZ mob sacB* Km^r	(143)
pCRSOECheY6	pCR2.1 with SOECheY6 fragment	This work
pK18SOECheY6	pK18mobsacB with SOECheY6	This work
pCRInterCheY7	pCR2.1 with 164 bp internal fragment of *cheY7*	This work
pKNOCKInterCheY7	pKNOCK vector with internal fragment of *cheY7* cloned into the BamHI sites	This work

Table 4. List of primers used in this study.

Primers	Sequence (5'-3',)
1F	ACCATGCGGAAGCAGAAGATCCAGGCC
1R	ATCTCGAAGGACGCGCGTTCG
2F	GATCATCGACTGAGGGACATG
2R	CCGCATGGTGGCGTAGTCATCGACGAC
Inter_CheY7_FwdBamHI	TGTACA<u>GGATCC</u>CGTCGACGACTCCAAGACCA
Inter_CheY7_RevBamHI	TGTACA<u>GGATCC</u>GACCGTCCATGCCCGGCATG
DelY7ChkFwd	CTGGTCCTTCGCCTATTCGCATC
DelY7ChkRev	AGCAGAGCAGCGTGACCCAGAG
pKNOCK_SK	CGCTCTAGAACTAGTGGATC

E. coli HB101 cells. pKNOCKInter-CheY7 was then mobilized into wild-type *A. brasilense*, by triparental mating as previously described (117).

Video tracking of free-swimming cells

All recordings were done using a Concavity Microscope Slide from Thermo Fisher scientific (cat no-1518006). These slides have a concave depression with 5 (bottom)-18mm (top) diameter well and are 0.6-0.8 mm deep. A 10 µl drop of culture in Che buffer was placed in the middle of the depression well and covered with a coverslip (Corning, #1 Cover Glass, cat no-2975-223). The coverslip in addition to the necessary contrast also provided a setting where there was little or no perturbation due to air flow. The recording was done using a Nikon E200 upright microscope equipped with a 20X long working distance objective (Nikon, Plan Fluor ELWD, X 20, NA 0.45). The microscope was focused such that the focal plane was at least 300-400 µM away from the surface (Fig. 22). All recordings of free-swimming cells were captured using a Leica MC120HD digital camera, at 30fps (frames per second) at a 1920 X 1080 resolution.
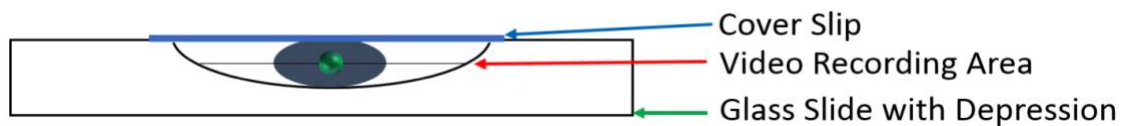
Figure 22. Experimental setup for recording video of swimming cells.

The bigger elliptical drop represents the liquid culture containing *A. brasilense* cells. The green dot represents the area where the microscope was focused for recording video.

Image processing and Cell tracking

Video recordings were processed using a custom software written in MATLAB, to extract and analyze individual cell trajectories. A bandpass filter using Gaussian average for each nearby pixel was applied to all frames to reduce the random noise from individual pixels. A background image was then constructed by calculating the mean pixel intensities of the frames over the image sequence and subtracted from each image in the image stack to exclude nonmoving cells. A 3 x 3 median filter was then applied to the background free frames. In each frame, cells were segmented by an automatically selected intensity threshold, which was dependent on the brightest pixels in the frame. The locations of all cells in each frame were determined by calculating the centroid (center of mass) of the brightest pixels in frames. Cells were linked from frame to frame by identifying the nearest neighbor in later frame for each cell in the prior frame. frame to frame by identifying the nearest neighbor in later frame for each cell in the prior frame. A MATLAB version of the particle tracking algorithm was used to link the positions of cells in each frame to reconstruct trajectories in time and space (144).

Post-processing

Only trajectories with a tracked duration greater than 2 seconds were considered for final analysis. Trajectories with an average speed of fewer than 15 µm/sec were also discarded to avoid including dead, dividing and slow-moving cells in the analysis. Trajectories of colliding cells were discarded manually. Cells tend to change swimming direction at the

beginning and end of each trajectory since this is the most common way to enter or leave the focal plane. Thus, we eliminated the first and last five frames of each recorded track, in order to avoid overestimating the reversal frequency. The tracks with highest median curvature were removed since these tracks performed reversal for a very long time. The trajectories were smoothed with 3-frames running average and all the statistics were applied to these smoothed trajectories.

We recorded 1360 swimming tracks for wildtype *A. brasilense* (Sp7) under steady state condition in quasi 2D and after initial processing as mentioned above, 1317 tracks were used for further analysis (Table 5). Similar screening was performed for the tracks of the various chemotaxis mutants of *A. brasilense* and an average number of at least 1000 processed trajectories were used for each strain for final analysis (Table 5). We selected only 361 tracks for the *ΔcheA1ΔcheA4* mutant because these cells tend to stick to surface under the conditions of this experiment and thus to lose motility rapidly under the microscope. From the cell trajectories, we computed multiple aspects of cell movement, including average run speed, maximum speed, minimum speed, average run time, acceleration, frequency of reversal, average angle of reversal, pause frequency, average pause time, and mean square displacement of bacteria. Turning events were identified by rapid changes in speed and/or direction of motion as discussed in Theves *et al* (46).

Table 5. Strains used in this study with total number of tracks initially recorded for each strains and tracks retained after deleting.

Strains	Tracks before deletion	Tracks after deletion
Sp7	1360	1317
Δche4	880	776
ΔcheA1	1034	844
ΔcheA1ΔcheA4	374	361
ΔcheA4	1103	1029
ΔcheY1	1104	1098
ΔcheY4	1192	1029
ΔcheY6	840	708
ΔcheY7	1226	1065

Cell speed was measured as the scalar quantity representing the distance moved between consecutive frames, divided by the time elapsed in between. Given the position $(x(t), y(t))$ of a cell at time t, its speed at time t is calculated as

$$v(t) = \frac{\sqrt{(x(t) - x(t - \Delta t))^2 + (y(t) - y(t - \Delta t))^2}}{\Delta t}$$

where Δt is the time interval between two consecutive frames.

$x(t)$ = x-coordinate of the cell

$y(t)$ = y-coordinate of the cell

Angular velocity is calculated as

$$\omega(t) = \frac{\Theta(t) - \Theta(t - \Delta t)}{\Delta t}$$

where $\Theta(t) = \arctan(\frac{\Delta y}{\Delta x})$, $\Delta y(t) = y(t + \Delta t) - y(t)$ and $\Delta x(t) = x(t + \Delta t) - x(t)$.

Turn and pause detection

To detect the events where the cells make abrupt turns and/or pauses, we used the method described previously by Masson *et al.* and Theves *et al.* (46, 145). To identify angular velocity changes, we first detected local maxima in the absolute value of the angular velocity. The time where a local maximum was achieved is denoted by t_{max}. The location of two closest local minima immediately before and after t_{max} are denoted respectively by t_1 and t_2. If the total change in direction over the interval $[t_1, t_2]$ was sufficiently larger than a threshold, which depends on the rotational diffusivity ($|\Delta\Theta| > 7\sqrt{D_r(t_2 - t_1)}$ where $D_r = 0.1\frac{rad^2}{s}$, we considered the bacterium is undergoing directional change during the time interval around t_{max} such that the angular speed $\omega(t)$ satisfied the condition

$$|\omega(t_{max})| - |\omega(t)| \leq 0.7\,\Delta\omega$$

with

$$\Delta\omega = \max(\omega(t_{max})| - |\omega(t_1)|, |\omega(t_{max})| - |\omega(t_2)|)$$

To identify abrupt changes in speed, we first detected local minima of the instantaneous velocity, the time where a local minimum was achieved is denoted by t_{min}. The location of two closest local maxima immediately before and after t_{min} are denoted respectively by t_1 and t_2. We computed the relative change in speed as,

$$\frac{\Delta v}{v(t_{min})}$$

where

$$\Delta v = \max(v(t_1) - v(t_{min}), v(t_2) - v(t_{min}))$$

If the relative change of velocity was sufficiently large,

$$\frac{\Delta v}{v(t_{min})} > 2$$

we considered the bacterium was undergoing change in speed (defined as 'pausing events') during the time interval around t_{min} such that

$$v(t) \leq v(t_{min}) + 0.2\ \Delta v$$

The threshold parameters for pauses and reversals are similar to previous studies (46, 145). We confirmed the validity of these parameters by visual inspection of the trajectories (see Figs. 14-15 for examples). We manually checked the two different types of pauses identified by the algorithm and fine-tuned the parameters before subsequent analysis.

Based on the bimodal distributions (centered at 0˚ and 180˚) of the directional changes during the pauses, we partitioned the 'pausing events' into transient pauses (<90˚) and reversals (≥90˚). As such, the reversal events exhibit both abrupt decrease of speed and a significant change of directions. As expected, the reverals are very strongly correlated with abrupt turns (Fig. 14E), which are defined by the criteria on angular velocties in stead of speed as mentioned above.

CHAPTER IV

EVIDENCE OF CROSS TALK THROUGH FUNCTIONAL INTEGRATION OF ORPHAN CHEYS IN CHEMOTAXIS SYSTEM OF *AZOSPIRILLUM BRASILENSE*

ABSTRACT

The *Escherichia coli* chemotaxis pathway has been extensively studied. However, unlike *E. coli*, most chemotactic bacteria have multiple CheY homologues. *Azospirillum brasilense* encodes several CheY homologs, and here, we show that CheY3, CheY5, CheY6 and CheY7 may have been horizontally acquired, with sequence analysis suggesting that CheY3 and CheY5 do not function to regulate the swimming pattern during chemotaxis. Preliminary data obtained here suggest different and novel roles for the multiple CheY homologs of *A. brasilense* that should be further characterized in the future.

INTRODUCTION

Chemotaxis is the ability of bacteria and other cells to sense chemical gradients and respond to the concentration of attractant or repellent by moving to the most favorable concentration of chemicals optimal for their growth (146). *E. coli* chemotaxis has been extensively studied and represents a model for bacterial signal transduction (56). Any change in the chemical environment is sensed in the periplasm by membrane spanning receptors. These receptors upon activation leads to CheA trans-autophosphorylates a conserved histidine residue using phosphoryl group from ATP and then transfer the phosphoryl group CheY and CheB (a methyl esterase). Phosphorylated CheY has higher affinity for the flagella motor switch complex compared to unphosphorylated CheY, thereby increasing the chances of binding to the FliM motor protein causing a switch in the flagellar direction of rotation (147). The switch in the direction of flagellar rotation causes a change from smooth swimming to tumble in case of *E. coli*, allowing the bacteria to

95

redirect swimming in a new direction. Therefore, binding of CheY~P increases the rate of switching frequency of the flagellar motor and thus the tumbling frequency.

A. brasilense, an alpha proteobacterium, lives in soils, or in close associations with plants in the rhizosphere (the area right next to the roots of plants). One of the chemotaxis operons in *A. brasilense* named Che1, was shown to regulate this transient increase in swimming speed that accompanies suppression in the swimming reversals (85) and is dispensable for chemotaxis (104). Recent study in our lab suggests that signaling via Che4 is the major chemotaxis operon that controls the swimming reversals and it functions together with Che1 to regulate chemotaxis in *A. brasilense* (86). The study also showed that CheA4 is the major histidine kinase required for chemotaxis. Che4 was also shown to be the major chemotaxis pathway required for plant root colonization (86). CheY4 from the Che4 operon has a major, but not unique, role in chemotaxis since the *ΔcheY4* strains had residual reversal frequency. However, neither *ΔcheY1ΔcheY4* nor *Δche1Δche4* are perfect smooth swimmers and these strains had residual reversals. The observation that two distinct pathways, each possessing a single CheY response regulator (CheY1 and CheY4), contribute to taxis suggest that multiple CheY~P may interact with the flagellar motor protein FliM to modulate the signaling output. The genome of *A. brasilense* also encodes additional CheY homologs whose role in chemotaxis is not known. Here we provide preliminary evidence for different roles of the CheY homologs in *A. brasilense*. We found that two of the CheYs that may have been acquired outside the class of alpha proteobacterium integrates with signaling by the two main chemotaxis pathways of *A.*

96

brasilense. We also found that there may be cross-regulation between Che1 and Che4 pathway via CheYs.

RESULTS

Orphan CheYs of *A. brasilense* may have been horizontally acquired

A thorough genomic study by Wuichet *et al* using all the microbial genomes sequenced till 2010, classified the chemotaxis system based on four phylogenomic markers to at least 18 classes including ACF (Alternate Cellular Functions) (F1-F17) (77). Out of the four phylogenomic markers used in this previous study, genomic context and genetic organization were criteria used to classify bacterial chemotaxis systems. According to this classification, Che1, Che2, Che3 and Che4 of *A.* brasilense are representatives of the F5, ACF, F9 and F7 chemotaxis system classes, respectively. Unlike CheA homologues that are very rarely found outside a Che (chemotaxis) operon, *cheY* homologues are commonly found separated from other *che* genes (77). *A. brasilense* genome has seven predicted CheY homologues. The primary sequences of these CheY homologs range from 121 to 132 amino acids. Most functional CheY homologs are 120-129 amino acids in length (148). This suggests that CheY3 and CheY5 may not be true CheY homologs with role in chemotaxis.

Out of the seven CheYs, only CheY1, CheY2 and CheY4 are in operons and have putative cognate histidine kinases encoded in the same operon. However, the four other CheYs, namely, CheY3, CheY5, CheY6 and CheY7 are not in operon and cannot be associated with any cognate histidine kinase from genomic context analysis alone (Fig. 23). The

comparison of the amino acid sequences for these CheY homologs showed that CheY6 has the highest sequence identity (56%) to the *E. coli* CheY followed by CheY4 at 41%. In contrast, CheY3 and CheY5 have only 18% sequence identity to the *E. coli* CheY, suggesting they are significantly divergent.

Next, the presence of key residues that were shown in *E. coli* to contribute to CheY function and that are conserved in sequences from other organisms were compared. This analysis showed that CheY2, CheY3 and CheY5 are missing from 1 to 4 key residues implicated in conformational change induced by phosphorylation of CheY in *E. coli* (aspartate89, trytophan58, methionine85, and tyrosine106) (75)(Figs. 23-24). These findings suggest that CheY6 and CheY7 may have putative roles in chemotaxis while CheY2, CheY3 and CheY5 are unlikely to regulate the swimming pattern of *A. brasilense* in chemotaxis (Figs. 23-24).

Taking advantage of the classification of the chemotaxis systems by Wuichet *et al*, we also analyzed the phylogenetic relationship of the seven CheYs (77). As expected, this phylogenetic analysis revealed that CheY1 and CheY4 cluster with homologs that belong to the F5 and F7 classes, respectively (Fig. 25). CheY7 clusters in the same clade as CheY4. This cluster includes CheY homologs from bacteria other than alphaproteobacteria, although the bootstrap values are very low and thus, inconclusive. These hints that both CheY4 and CheY7 may have evolved independently from a common ancestor. Including more sequences from the alpha, beta, gamma proteobacteria would be required to draw any reliable conclusion with confidence.
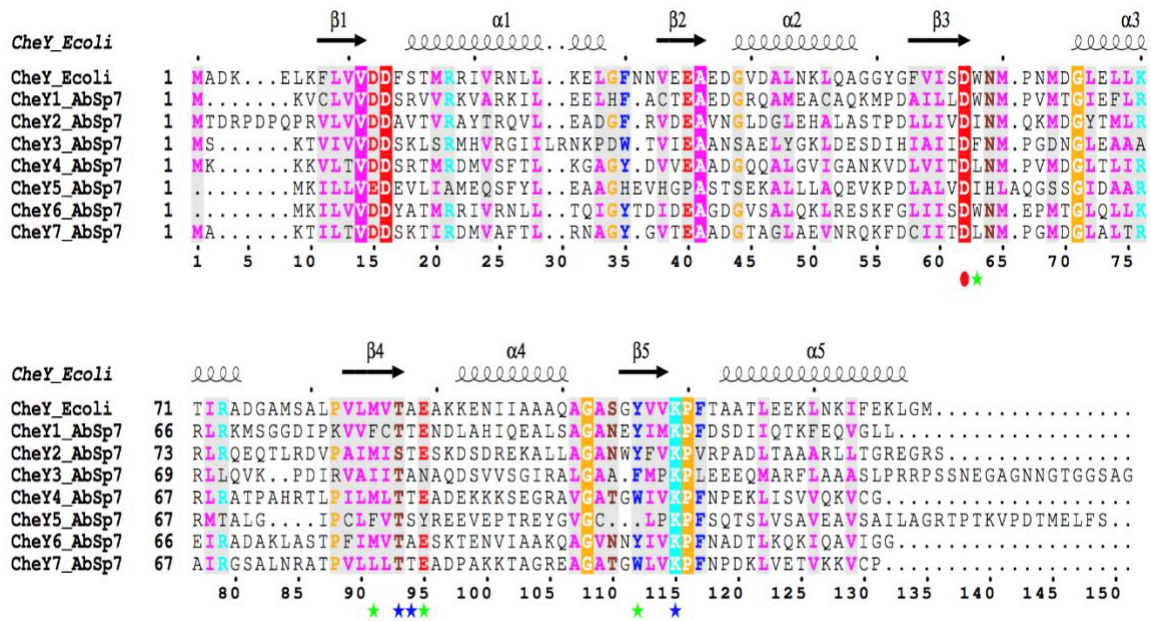
Figure 23. Sequence alignment for all the seven CheYs in *A. brasilense* with *E. coli* CheY structure as reference.

The residues important for activation and interaction with CheA are summarized in Fig. 24. the figure was generated in ESPript 3 using *E. coli* CheY crystal structure (3CHY) (149, 150). AbSP7 - *A. brasilense* Sp7. Secondary structure of the *E. coli* CheY is presented on the top of the alignment whereas residue number are at the bottom. Grey colored background depicts regions of similarity based on global similarity score of 0.7. Residues within the grey colored blocks are color coded according to their physicochemical properties only. Green stars underneath the alignment depict the allosteric quartet and blue stars phosphorylation sensor with reference to *E. coli* CheY (75). A red solid circle denotes the site of phosphorylation at the conserved aspartate residue.

Residues in *E. coli*	T87	A88	K109	E89	W58	M85	Y106
	"Phospho-Sensor"			"Conformational Change Inducer"			
CheY1_AbSp7	T82	T83	K104	E84	W53	F80	Y101
CheY2_AbSp7	S89	T90	K111	E91	I60	M87	Y108
CheY3_AbSp7	T83	A84	K104	N85	F56	I81	F101
CheY4_AbSp7	T83	T84	K105	E85	L54	M81	W102
CheY5_AbSp7	T77	S78	K98	Y79	I53	F77	C95
CheY6_AbSp7	T82	A83	K104	E84	W53	M80	Y101
CheY7_AbSp7	T83	T84	K105	E85	L54	L81	W102

Figure 24. Residues important for activation of CheY mapped in *A. brasilense* using *E. coli* CheY crystal structure (PDB-3CHY).

Multiple sequence alignment was performed using *E. coli* CheY and all the CheY homologs of *A. brasilense* as shown in Fig. 23. White Box- Different residue in CheYs of *A. brasilense* at the corresponding position for *E. coli* CheY. Bright Green Box- Same residue in CheYs of *A. brasilense* at the corresponding position for *E. coli* CheY.

Figure 25. Phylogenetic tree of CheYs.

A maximum likelihood rooted phylogenetic tree was generated using 59 CheY sequences from 19 different species using Phylip package using 100 bootstrap values. The tree was edited in iTOL webserver (151). Chemotaxis class are denoted by solid circles (F5-Orange, F7-Red, F9-Green). Gene neighborhood if positive are denoted by stars (filled/unfilled) (YZ/YZZ-Orange filled star/Orange unfilled star, YC-Purple filled star, YM-Blue Filled star). Y = CheY, Z=CheZ (a phosphatase), C=CheC (a phosphatase), M= MCP (**M**ethyl accepting **c**hemotaxis **p**rotein - receptor). Taxonomic classes of the bacteria are denoted by alpha, beta, gamma for the different classes of proteobacteria.

F5 (Che1)   F7 (Che4)   F9 (Che3)   YZ / YZZ   YC   YM   **(Taxonomic Class)**

Taxon	F5 (Che1)	F7 (Che4)	F9 (Che3)	YZ / YZZ	YC	YM	(Taxonomic Class)
CheY T. Maritima							Thermotogae
CheY3 B. burgdorferi							Spirochaetes
CheY1 B. burgdorferi							Spirochaetes
CheY B. subtilis							Firmicutes
CheY6 R. rubrum			●				Alpha
CheY6 R. sphaeroides		●					Alpha
CheY3 B. mallei					★		Beta
CheY4 B. mallei					★		Beta
CheY3 A. brasilense					★		Alpha
CheY2 V. cholerae			●				Gamma
CheY2 R. centenum			●				Alpha
CheY4 R. rubrum			●				Alpha
CheY2 A. brasilense			●				Alpha
CheYII C. crescentus		●					Alpha
CheY2 R. meliloti		●					Alpha
CheY2 R. leguminosarum		●					Alpha
CheYIV C. crescentus	●						Alpha
CheY1 R. rubrum	●						Alpha
CheYIV C. crescentus	●						Alpha
CheY1 R. centenum	●						Alpha
CheY1 A. brasilense	●						Alpha
CheY C. jejuni							Epsilon
CheY H. pylori							Epsilon
CheY S. typhimurium							Gamma
CheY E. coli		●					Gamma
CheY3 V. cholerae							Gamma
CheY P. putida							Gamma
CheY P. aeruginosa							Gamma
CheY P. fluorescens							Gamma
CheY2 B. mallei		●					Beta
CheY2 R. sphaeroides		●					Alpha
CheY6 A. brasilense				★			Alpha
CheY6 R. centenum	●			★			Alpha
CheY2 R. rubrum	●			★			Alpha
CheYII C. crescentus	●						Alpha
CheYI C. crescentus	●						Alpha
CheYIII C. crescentus							Alpha
CheY1 V. cholerae						★	Gamma
CheY7 R. centenum				☆			Alpha
CheY5 R. rubrum			●				Alpha
CheY3 R. centenum							Alpha
CheY5 A. brasilense							Alpha
CheY7 A. brasilense						★	Alpha
CheY1 B. mallei		●					Beta
CheY2 P. aeruginosa		●					Gamma
CheY3 R. leguminosarum							Alpha
CheY3 R. rubrum							Alpha
CheY4 A. brasilense		●					Alpha
CheY2 B. burgdorferi							Spirochaetes
CheY3 P. fluorescens		●					Gamma
CheY2 P. fluorescens		●					Gamma
CheY4 R. sphaeroides						★	Alpha
CheY5 R. sphaeroides		●					Alpha
CheY3 R. sphaeroides							Alpha
CheY4 V. cholerae		●					Gamma
CheY1 R. sphaeroides		●					Alpha
CheYI C. crescentus		●					Alpha
CheY1 R. meliloti		●					Alpha
CheY1 R. leguminosarum		●					Alpha

Branch support/length values: 0.4, 0.19, 0.24, 0.03, 0.19, 0.01, 0.16, 0.11, 0.32, 0.04, 0.37, 0.77, 0.03, 0.17, 0.47, 0.44, 1, 0.03, 0.95, 0.99, 0.05, 0.21, 0.89, 0.4, 0.72, 0.09, 0.22, 0.02, 0.74, 0.26, 0.7, 0.07, 0.05, 0.73, 0.01, 0.04, 0.18, 0.14, 0.44, 0.04, 0.84, 0.5, 0.06, 0.12, 0.32, 0.6, 1

The phylogenetic analysis indicates that the CheY6 sequence may have diverged from that of CheY1 early in evolution. Interestingly, the two clades containing CheY1 and CheY6 include CheY members predicted to belong to the F5 system. As expected from previous work (116), the CheY1 of *A. brasilense* clusters with CheY1 of the closely related *Rhodospirillum centenum* also predicted to belong to the F5 system (77), with a maximum possible bootstrap value of 1 (a bootstrap value of 100 out of 100 is denoted as 1). Similarly, CheY6 of *R. centenum,* predicted to be in the F5 class was found to be in the same branch with a high boot strap value of 0.74 with CheY6 of *A. brasilense*. These combined evidences lead us to hypothesize that CheY6 may be functioning with the F5 chemotaxis system, i.e., Che1.

CheY6 and CheY7 are required for reversing directions in liquid media

In order to further characterize the role of CheY6 and CheY7 suggested to function during chemotaxis above, we next analyzed the effect of deletion of *che*Y6 and *che*Y7 on the swimming motility patterns of the corresponding mutants. We found that the Δ*che*Y7 mutant was totally unable to reverse swimming direction, similar to the phenotype of the Δ*che*A4 mutant (Fig. 26A) (86). The Δ*che*Y6 mutant still had a reversal frequency value similar to that of a Δ*che*Y4 mutant, reported previously (86)(Fig. 26A). Next, we analyzed the directionality ratio that measures the straightness of swimming trajectories and, thus provides information about the ability of a motile cell to explore its surroundings. This is the ratio of straight-line displacement between the start point and the endpoint of the swimming trajectory to the length of the entire trajectory which decays over time (152).

This ratio reaches 1 for a straight trajectory and approaches 0 for a highly tortuous trajectory. As expected form the reversal frequency phenotypes of the mutants, we found that the directionality ratio for the Δ*che*Y7 mutant was close to 1 over a 4 sec long trajectory, indicating that the Δ*che*Y7 mutant swims in straight trajectories, i.e., it cannot change the direction of swimming (Fig. 26B). The Δ*che*Y6 and Δ*che*Y4 mutant strains shared a similar directionality ratio, consistent with their similar reversal frequency (Fig. 26B). Together, these data indicate that CheY6 and CheY7 are both required for controlling the swimming reversal frequency and that CheY7 is the major CheY homolog controlling reversals in *A. brasilense*.

CheY6 is required for swimming in liquid media but not in swim plate

Next, we used spatial gradient assays to analyze the role of CheY homologs in chemotaxis. We first used the swim plate assay, where cells move through a low agar medium (0.3% w/v) and form rings away for the inoculation site after a few hours. As expected from its null reversal frequency, the *ΔcheY*7 mutant was significantly impaired in swimming in this assay. In contrast, the *ΔcheY*6 mutant, which has a reduced reversal frequency relative to the wild type strain, did not display any visible defect in this assay and it formed a ring of a diameter similar to that formed by the wild type strain (Fig. 27).

The role of chemotaxis in swarming, which is the movement across a semi-solid surface using lateral flagella, differ from organism to organism (153). It has not been analyzed in *A. brasilense* to date. The lack of phenotype of the *ΔcheY*6 mutant in the swim plate assay,
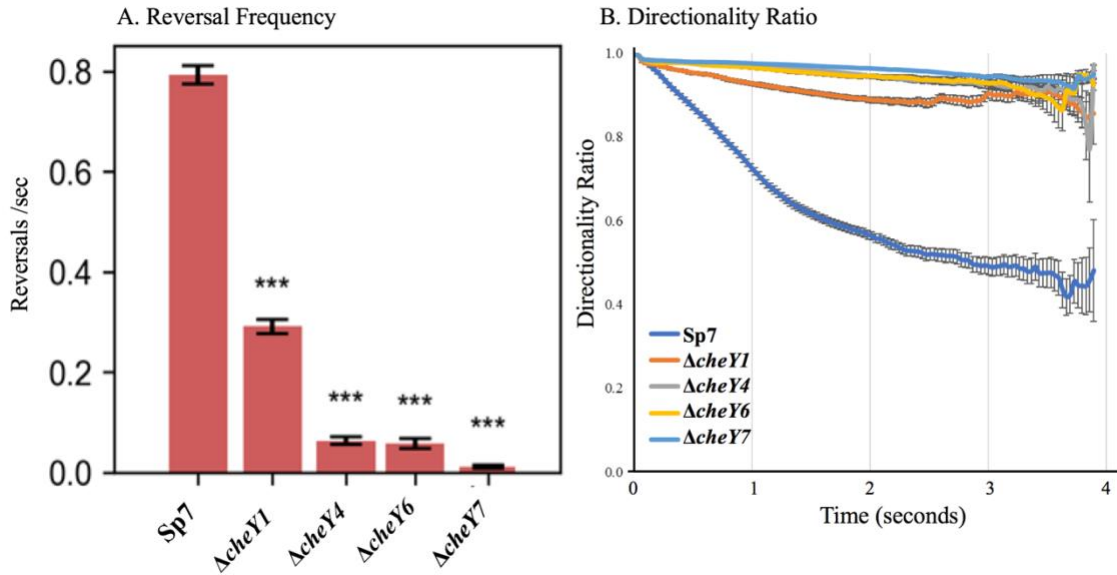
Figure 26. Reversal frequency and directionality ratio of various *ΔcheY*s mutants.

A) Reversal frequency calculated for wildtype and the *ΔcheY* mutants of *A. brasilense* analyzed here B) Directionality ratio calculated for all the trajectories of wildtype *ΔcheY* mutants of *A. brasilense*. At least 1000 trajectories were analyzed by computerized motion analysis for each strain. A value of 1 indicates a straight trajectory. The directionality ratio was calculated using DiPer program (152). Reversal frequency data for *ΔcheY1* and *ΔcheY4* have been earlier published in (86) and (99) using recording for swimming cells performed close to the surface.
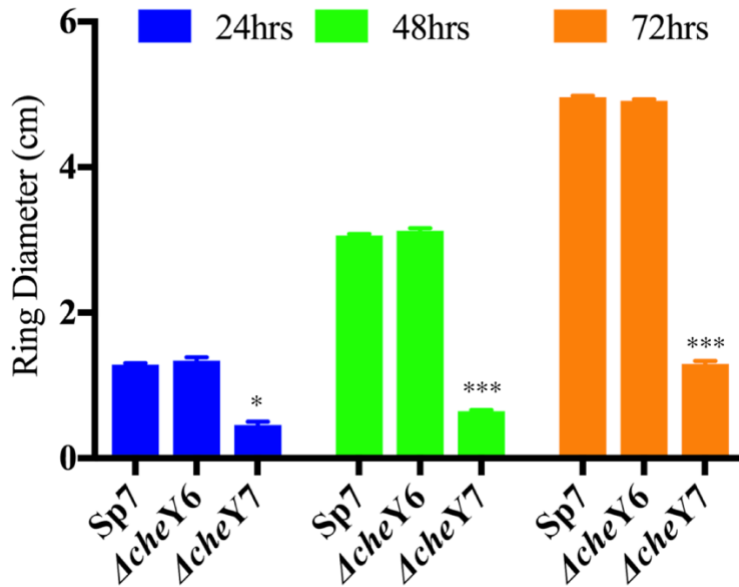
Figure 27. Swim plate assay (0.3% agar) showing ring diameter.

despite its reduced reversal frequency, prompted us to test the role of CheY6 in swarming, using the swarm plate assay.

The swarm plate assay uses media solidified with 0.6% agar. Preliminary observations suggested that the *ΔcheY*6 mutant swam faster than the wild type strain (data not shown). We used scanning transmission electron microscopy (STEM) to determine whether the *ΔcheY*6 mutant constitutively produce lateral flagella but did not find any difference (data not shown).

Interactions of CheA1 and CheA4 with CheY1, CheY4, CheY6 and CheY7 in the BACTH assay

CheA homologs are known to physically interact with CheY, albeit transiently, to mediate chemotaxis through phospho-transfer between CheA~P to CheY (154). Here, we used the BACTH system to perform a preliminary analysis of the potential physical interactions between the *A. brasilense* CheY and CheA homologs that function in chemotaxis (CheA1, CheA4, CheY1, CheY4, CheY6 and CheY7).

Using the BACTH, we found that CheA1 interacts with CheY1, and it also interacts with CheY6, consistent with the phylogenetic analysis above (Figs. 25, 28). Interestingly, in this assay, CheA1 interacted more strongly with CheY6 than with CheY1, although CheA1 and CheY1 are within the same operon and function together (Fig. 28). The most surprising result was interaction of CheA1 (Che1 system) with CheY4 (Che4 system), although this interaction was weaker than the interaction of CheA1 with CheY6 and CheY1 (Fig. 28).

In this assay, CheA4 interacted with all the CheY homologs, suggesting the possibility of physical interactions between these proteins. These results suggest that CheA1 and CheA4 from the Che1 and Che4, respectively, could potentially cross-talked with all CheYs, although this possibility must be further explored with biochemical assays.
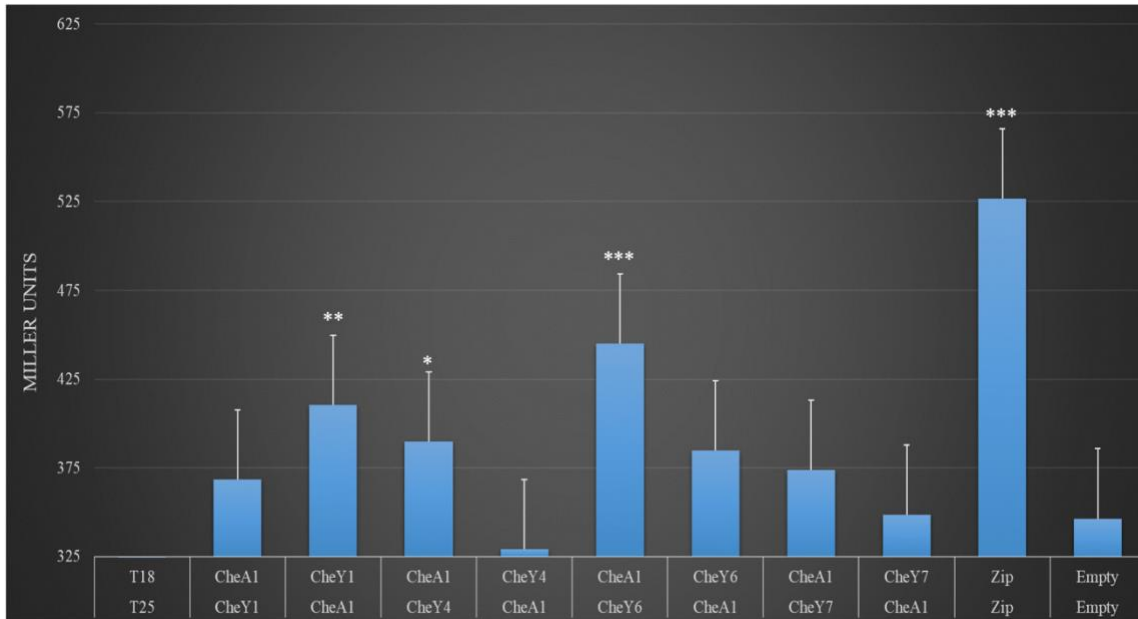
Figure 28. Bacterial Two Hybrid Assay for interaction between CheA1 and CheYs

Each gene of interest was cloned into either pKNT25 (low copy plasmid) or pUT18 (high copy plasmid) and all interactions were quantified using a beta-galactosidase assay. Each gene was cloned into both pKNT25 and pUT18 to assess differences in interactions based of plasmid copy number. * denotes p value < 0.05; ** denotes p value < 0.005. Significance for each interaction is relative to the negative control (interaction between empty pKNT25 and empty pUT18 vectors) ran alongside it on its individual 96-well plate.
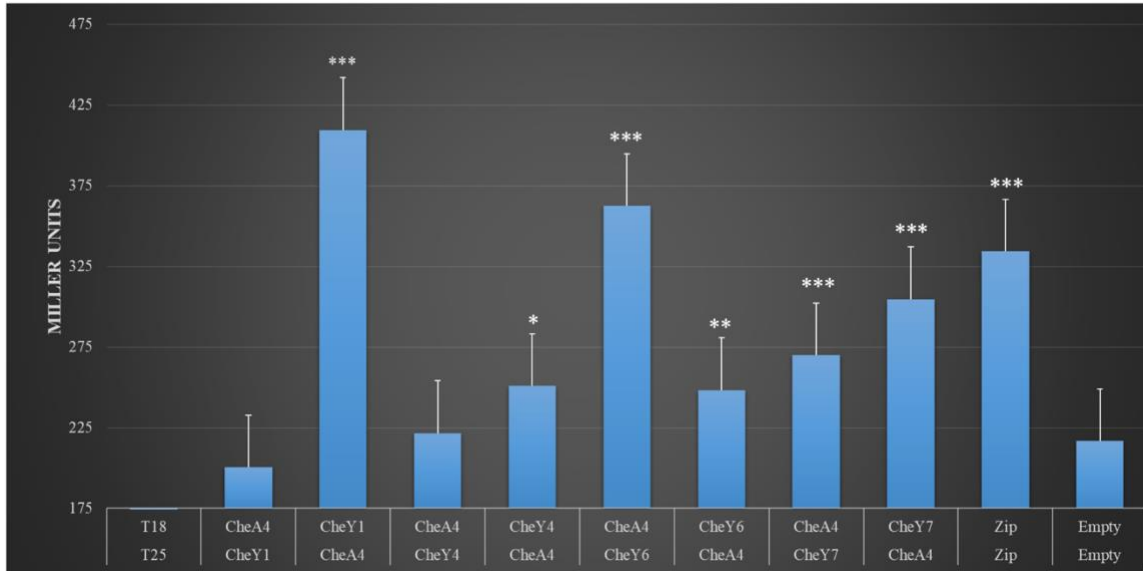
Figure 29. Bacterial Two Hybrid Assay for interaction between CheA4 and CheYs

Each gene of interest was cloned into either pKNT25 (low copy plasmid) or pUT18 (high copy plasmid) and all interactions were quantified using a beta-galactosidase assay. Each gene was cloned into both pKNT25 and pUT18 to assess differences in interactions based of plasmid copy number. * denotes p value < 0.05; ** denotes p value < 0.005. Significance for each interaction is relative to the negative control (interaction between empty pKNT25 and empty pUT18 vectors) ran alongside it on its individual 96-well plate.

DISCUSSION

The data presented here provide some evidence, albeit preliminary, that some CheYs may function in cross-regulation between Che1 and Che4 through CheAs in *A. brasilense*. In her thesis work, Gullett showed co-binding between proteins of Che1 and Che4 (Gullett Unpublished work) at the receptor levels. The histidine kinase (HK) and response regulator (RR) that together form the two-component system (TCS) are encoded in the same operon and the HK almost every time will phosphorylate its cognate RR. If unwanted and potentially detrimental communication occur between two TCSs through cross-phosphorylation of noncognate response regulator (RR), it is called crosstalk (155). Although there are hundreds of TCSs encoded in microbial genomes, very few examples of cross- regulation between two TCSs are known till date. The three main ways that cross talk is avoided between TCSs are i) specificity in molecular recognition between cognate HK and RR pair, ii) phosphatase activity of HK, iii) competition between RR for a particular HK for phosphorylation where only the cognate RR gets phosphorylated faster (156). In addition to the above three mechanism of reducing the chances of cross-talk, spatial and temporal restriction of pathways also helps in avoiding unwanted cross-talk (156). On the other hand, if cross-talk is of physiological significance to an organism as in integration of signals, it is then referred to as cross-regulation (155). Cross-regulation can occur either through cross-phosphorylation as in cross-talk, or by differential regulation of promoters or through a connector protein to integrate signals.

The observation that Gullett made in her thesis work (Gullett *et al* unpublished results) regarding co-binding of chemotaxis paralogs at the level of the receptor baseplate may allow for signal integration without cross-talk. In fact, one of the ways that cross-regulation can happen is that if the two HKs from the two TCSs physically and strongly interact with each other. The question then remains that if signal integration happens at the receptor level, how do these signals are relayed to the flagellar motor through the set of phosphorylated CheYs functioning in chemotaxis in *A. brasilense*.

EXPERIMENTAL PROCEDURES

Bacterial strains and growth condition

All bacterial strains used in this study are described in Table 1. Bacterial strains available from previous studies were stored at -80°C as 30% glycerol stocks. Minimal medium for *Azospirillum brasilense* (MMAB) with and without nitrogen source (N) or carbon (C) were prepared as previous described (139). The *A. brasilense* strains were inoculated in MMAB +N +C medium with appropriate antibiotics and grown at 28°C in water-bath incubator shaking at 200 rpm. The *E. coli* strains were inoculated in LB medium with appropriate antibiotics and grown at 37°C in incubator shaking at 200 rpm (in exception for bacterial two-hybrid and beta-galactosidase assay). Unless stated, the required antibiotics were used at the following concentrations: ampicillin (Amp) 200 ug/ml, carbenicillin (157) 50 ug/mL, kanamycin (Km) 25 ug/ml, gentamycin (158) 20 ug/ml, and chloramphenicol (Cm) 20 ug/ml.

111

For bacterial conjugation experiment, *A. brasilense* strains and *E. coli* strains were grown, as described above, until they reached exponential growth phase (OD$_{600}$ = 0.4-0.6). Cells were collected via centrifugation at 3000 rpm, following by being washed for three times and resuspended in 0.8% KCl buffer (0.8 g KCl per 1000 mL water) to remove traces of antibiotics. Appropriate combinations of *A. brasilense* and *E. coli* strains were mixed and plated on D-medium without antibiotics. The cell mixtures were grown for 12 hours in a humid environment at 28°C. The colonies on D-medium plate were then scraped and resuspended in 0.8% KCl buffer. The cell mixtures were spread on MMAB -N +C agar plates with appropriate antibiotics and incubated at 28°C for 6 to 7 days. *A. brasilense* were selected by re-streaking on MMAB -N + C agar plates with appropriate antibiotics and re-incubating at 28°C for 6 to 7 days. This re-streaking and re-incubating process were repeated 3 times to eradicate *E. coli* contamination.

For recording swimming video and behavioral assays, *A. brasilense* strains were either inoculated from glycerol stocks or single colonies from routinely maintained MMAB -N + C agar plates. The strains were grown in condition described above.

Plasmids construction

All the base plasmids and primers used in making constructs for this study are listed in Table 1 and Table 2 respectively. To construct plasmids for the bacterial two-hybrid assay, the genes *cheA4, cheY1, cheY4, cheY6,* and *cheY7* were PCR amplified from *A. brasilense* (Sp7) genomic DNA with appropriate primers listed in Table 2. The primers were designed to have 5' BamHI and 3' KpnI restriction sites as well as extraneous 11-bp upstream from

the 5' BamHI restriction site to improve the efficiency of restriction digest. The PCR products and base plasmids (pKNT25, pKT25, pUT18, and pUT18C) were digested with BamHI and KpnI, following by phenol-chloroform extraction and ethanol precipitation. Appropriate combinations of digested plasmid and digested PCR products were ligated via T4 ligation for 16 hours. The ligated products were transformed into XL1-BLUE competent cells and plated on LB agar plates with appropriate antibiotics. Screening of positive clones was performed using colony PCR with appropriate primers. Plasmids from positive clones were extracted and subsequently sent to sequencing with BACTH-T25T18Fwd and BACTH-T25T18Rev primers.

Mutagenesis

Strains used in this study are described in the previous chapter.

Bacterial two-hybrid assay

The detections of *in vivo* protein-protein interactions between response regulators CheYs (CheY1, CheY4, CheY6, and CheY7) and major histidine kinases CheAs (CheA1 and CheA4) were performed using Bacterial Two Hybrid Assay kit from Euromedex. The proteins of interest were fused with both T25 and T18 fragments of adenylate-cyclase at both N and C terminus. This was done by inserting the genes of interest in appropriate plasmids (pKT25, pKNT25, pUT18, and pUT18C). The resulting plasmids used in this experiment are listed in Table 1. Different combinations of T25 and T18 vectors were co-transformed into *E. coli* strain BTH101 and transformants were spread on LB agar with kanamycin (50 µg/mL) and carbenicillin (50 µg/mL). The plates were incubated in 30°C

for 48 hours. Following the incubation, several colonies of each transformant were inoculated in LB with the same antibiotics and grown at 30°C shaking at 200 rpm for 12 hours. The cultures were then re-inoculated the next day and grown until exponential growth phase (OD600 = 0.4-0.6). The cultures were spotted on MacConkey (50 g/L MacConkey, 1% lactose) agar plate and let dry near sterile environment. The plates were then incubated at 30°C for 48-72 hours. For every 24 hours increments, color changes were recorded for each sample and the plates were photographed. This experiment was repeated two times: each sample had six technical replicates and two biological replicates.

Following the 48-72 hours incubation of the MacConkey agar plates, colonies from each sample were inoculated in LB with the same antibiotics and grown at 30°C shaking at 200 rpm for 12 hours. If the samples showed positive interaction, colonies that showed color changes were inoculated. If the sample showed negative interaction, random colonies were inoculated. On the next day, the cultures were reinoculated and grown until exponential growth phase (OD600 = 0.4-0.6). 100 uL of cultures were then distributed on each well of round bottom 96-wells plates. Cell densities (OD600) of the samples on the 96-wells plate were measured by microplate reader. After measurement, the 96-wells plates were wrapped in parafilm and stored in -80°C.

When ready to perform beta-galactosidase assay, the 96-wells plate was defrosted in 37°C for 30 minutes and subsequently placed back into -80°C for 30 minutes. This process was repeated three times to ensure beta-galactosidases exposure to ONPG solution. 20 mg/ml ONPG solution (20 mg ONPG for 1 mL of sterile water) was prepared during the freeze-

thaw process. After the freeze-thaw process, 20 μL of the ONPG solution was added onto each sample using multi-channel pipette. The final solution in each well had 4 mg/mL of ONPG. Immediately after adding the ONPG solution, the 96-wells plate was placed into the microplate reader. The microplate reader was set to record OD420 of each well after 30 minutes incubation at 30°C with shaking at 200 rpm. This experiment was repeated two times: each sample has six technical replicates and two biological replicates.

Behavioral Assay

For swim plate assays, 0.3 % soft agar MMAB +N +C plates were prepared with appropriate antibiotics (with 1mM IPTG if needed). *A. brasilense* strains were grown in condition described above until they reached exponential growth phase (OD600 = 0.4-0.6). The number of cells for each strain were normalized by OD600 readings and pelleted by centrifugation at 3000 rpm. The pellets were washed with chemotaxis buffer (10 mM phosphate, 1 mM EDTA, pH= 6.85-7) for three times to remove any trace of nitrogen and carbon sources in MMAB +N +C medium. The chemotaxis buffer was made as described previously (139). The pellets were then resuspended in 100 μL of chemotaxis buffer and inoculated in the center of the soft agar plates with 3 μL of culture. The inoculated plates were incubated at 28°C for 48 hours before being photographed. The ring size formed by each of the *A. brasilense* strains were measured and recorded for subsequent statistical analysis. The experiment was performed in two technical replicates and three biological replicates for each strain.

For the swarm plate assay, we generally followed recommendations by Kearns (159). A total of 250ml of media containing Difco nutrient broth (NB) with 0.6% Difco agar w/v was made each time. the media was boiled gently and then autoclaved for 20 mins exactly. After autoclave, the media is cooled to 50ºC to avoid loss of water during pouring by condensation. Exactly 25ml of the semisolid medium was used for each plate and cooled at room temperature for 20 minutes. The plate is used immediately following solidification and incubated at 28 ºC for 24-48hrs. Taking readings for swarm diameter after 48 hrs is not recommended as the plates can dry and loose water.

Statistical Analysis

For comparing the reversal frequency of wild-type and mutant phenotypes, we determined average values from at least three independent experiments performed in duplicate and performed one-way analysis of variance (alpha level, 0.05), followed by pairwise two-sample t tests assuming equal variances (alpha level, 0.05) using Prism (version 6) software (GraphPad Software Inc., San Diego, CA).

Table 6. Strains and plasmids used in chapter 3

Strains	Genotype	References
Azospirillum brasilense		
Wild-type	Wild-type strain Sp7	ATCC 29145
Δ*cheY1*	Δ*cheY1*::Km (Km^r)	(99)
Δ*cheY4*	Δ*cheY4*::Cm (Cm^r)	(86)
Δ*cheA1*	Δ*cheA1*::*gusA*-Km (Km^r)	(99)
Δ*cheA4*	Δ*cheA4*::Gm (Gm^r)	(86)
Δ*cheA1*Δ*cheA4*	Δ*cheA1*Δ*cheA4*::*gusA*-Km-Gm (Km^r Gm^r)	(86)
Δ*cheY7*	Δ*cheY7*::Gm (Gm^r)	Chapter III
Δ*cheY6*	Δ*cheY6*	Chapter III
Escherichia coli	Description	
XL1-BLUE	General cloning strain	Invitrogen
TOP10	General cloning strain	Invitrogen
S17-1	*thi endA recA hsdR* strain with RP4-2Tc::Mu-Km::Tn7 intergrated in chromosome	(120)
HB101	General cloning strain	Invitrogen
BTH101	F−, *cya*-99, *ara*D139, *gal*E15, *gal*K16, *rps*L1 (Strr), *hsd*R2, *mcr*A1, *mcr*B1; BACTH reporter strain	Euromedex
DH5-α λpir	DH5-α derivative containing *pir* gene	(141)

Table 6 continued

Plasmids	Description	
Bacterial Two Hybrid Assay		
pKT25	pSU40 derivative with T25 fragment (1-224 amino acid of CyaA), P*lac* promoter, MCS is at C-terminal of T25, Km^r, Ori p15A	Euromedex
pUT18C	pUC19 derivative with T18 fragment (225-399 amino acid of CyaA), P*lac* promoter, MCS is at C-terminal of T18, Amp^r, Ori p15A	Euromedex
pKNT25	pSU40 derivative with T25 fragment (1-224 amino acid of CyaA), P*lac* promoter, MCS is at N-terminal of T25, Km^r, Ori p15A	Euromedex
pUT18	pUC19 derivative with T18 fragment (225-399 amino acid of CyaA), P*lac* promoter, MCS is at C-terminal of T18, Amp^r, Ori p15A	Euromedex
pT25Zip	pT25 with gene that code for leucine zipper region of GCN4 in yeast (positive control)	(160)
pT18Zip	pT18 with gene that code for leucine zipper region of GCN4 in yeast (positive control)	(160)

Table 6 continued

pKNT25CheA1	pKNT25 with *cheA1*	(Aksenova's Thesis)
pKNT25CheA4	pKNT25 with *cheA4*	This work
pUT18CheA1	pUT18 with *cheA1*	(Aksenova's Thesis)
pUT18CheA4	pUT18 with *cheA4*	This work
pKT25CheY1	pKT25 with *cheY1*	This work
pKT25CheY4	pKT25 with *cheY4*	This work
pKT25CheY6	pKT25 with *cheY6*	This work
pKT25CheY7	pKT25 with *cheY7*	This work
pU18TCheA1	pUT18 with *cheA1*	This work
pU18TCheA4	pUT18 with *cheA4*	This work
pUT18CCheY1	pUT18C with *cheY1*	This work
pUT18CCheY4	pUT18C with *cheY4*	This work
pUT18CCheY6	pUT18C with *cheY6*	This work
pUT18CCheY7	pUT18C with *cheY7*	This work

Table 7. Primers used in chapter 3

Primers	Sequence
Bacterial Two-Hybrid	
CheY1 BamHI-Fwd	TCGTAGTACATGGATCCATGAAAGTTTGTCTGGTCGTC
CheY1 KpnI-Rev	TCGTAGTACATGGTACCCAGCAGCCCGACCTGCTCGAAC
CheY4 BamHI-Fwd	TCGTAGTACATGGATCCATGGAGCCAAGCGTGAAGAAG
CheY4 KpnI-Rev	TCGTAGTACATGGTACCGCCGCACACCTTCTGCACGAC
CheY6 BamHI-Fwd	TCGTAGTACATGGATCCATGAAGATCCTTGTCGTCGAT
CheY6 KpnI-Rev	TCGTAGTACATGGTACCCCCGCCGATGACGGCCTGGAT
CheY7 BamHI-Fwd	TCGTAGTACATGGATCCGTGGCCAAGACCATTCTGAC
CheY7 KpnI-Rev	TCGTAGTACATGGTACCCGGGCAGACCTTCTTCACGGT
CheA4 BamHI-Fwd	TCGTAGTACATGGATCCATGGAAGACCTGAGCCGGTTC
CheA4KpnIRevBACTH	TCGTAGTACATGGTACCGACCGGTTCGAGTGC
BACTH-T25T18Rev	AGAGTGCACCATATTACTTAG
BACTH-T25T18Fwd	ACAATTTCACACAGGAAACAG

CHAPTER V

CONCLUSIONS

In this thesis work, I unraveled some astonishing features of motility and chemotaxis in *A. brasilense* which left me with more questions unanswered. The finding that *A. brasilense* utilizes two chemotaxis pathways regulating distinct motility parameters (speed and reversal frequency), likely to enhance its chemotactic advantage in its natural environment was in itself intriguing. The genome of *A. brasilense* encodes seven CheYs but their role was not known at the time I initiated this thesis work. Combining genetic and high throughput single cell tracking allowed fine nuances in the swimming patters of each of these CheYs to be detected. Surprisingly, some of our results suggest the intriguing possibility that CheY6 would contribute to swarming but not swimming. This finding should be followed through.

The finding that CheY4 helps in suppressing the transient pauses was unexpected. This is because till date CheYs are known to increase the tendency of transient pauses during swimming and transient pauses during swimming observed thus far are related to reversal of the direction of rotation of the flagellar motor. The relationship of the transient pauses during swimming have not yet been studied in a bacterium with more than one chemotaxis system and thus with more than one CheYs. It will be really interesting to determine the exact mechanism generating transient pauses in *A. brasilense*. Swimming patterns in bacteria contribute to chemotaxis and dispersal (50-52). Mathematical modelling of the swimming patterns of the *A. brasilense* strains analyzed here suggest that the swimming pattern of *A. brasilense* has features that combine some detected in *Pseudomonas* species (*P. putida* and *P. aeruginosa*) and *V. aliginolyticus*. The model should be refined by

understanding the physiological significance of transient pause, perhaps through high resolution tracking of swimming behavior in a microfluidics chamber with attractant or repellent gradients. Mutant strains of *A. brasilense* with similar reversal frequency, but different frequency of transient pauses is available as in chapter III could provide insight into the physiological significance of transient pauses. At this point, I speculate that, yet another unidentified protein(s) connects some of the CheY and the flagellar motor for controlling transient pauses. Interestingly, bioinformatic analysis showed that *A. brasilense* does not encode any brake like cyclic-di-GMP (c-di-GMP) binding protein such as the *E. coli* YcgR in the genome. YcgR in *E. coli* was shown to inhibit flagellar motor rotation through interaction with FliG and FliM (161).The second messenger molecule c-di-GMP was also shown to play a role in modulating flagellar rotation through CheY-like (Cle) proteins in *C. crescentus* (79). However, in that case the Cle proteins are longer than typical CheYs (*E. coli* CheY – 129 amino acids long) with an arginine rich region in the C terminal region for c-di-GMP binding (79). BLAST search against *A. brasilense* with Cle proteins does show presence of such Cle proteins albeit with 29% identity but their role in transient pauses is yet to be investigated for *A. brasilense*. It should be also noted that all the seven CheYs encoded in the genome do have the conserved aspartate (D57 in *E. coli* CheY) needed for phosphorylation. It may be possible that these CheYs (CheY3 and CheY5) may compete for the phosphorylation from CheA1/CheA4 and serve as phosphate sink. Conclusive evidence for a mechanism such as stator exchange or involvement of any brake- or clutch-like protein in the transient pauses can only come from analyzing the rotational

behavior of different chemotaxis mutants in tethering experiments, preferably with imaging using a higher resolution camera.

One of the other interesting finding was that our tracking data suggested the existence of flick "like" movement during swimming in *A. brasilense*. It is quite tempting to conclude that the pattern shown in Fig. 15 forms a cyclic three step run-reverse-flick. This is because a near 90° change in swimming direction is very rare owing to the expected effect of reversal of direction of motor rotation in polarly flagellated bacteria, which should mostly occur around 180°. In addition, if the reversal of direction of motor rotation could generate changes in swimming direction others than around 180°, then most of bacteria with polar flagella and bidirectional motors would show a broad distribution around 90°. However, this is not the case and the turning angle distribution for swimming *Pseudomonas* species does not show such a distribution (46, 136). To confirm the presence of flick events in swimming *A. brasilense* cells, the flagellum could be stained and visualized under microscope connected to a high-speed camera. Run-reverse is very common in bacteria with polar flagella (25, 26) but flicking has only been observed in a handful of bacteria. Work by others with marine bacteria have showed that the flicking probability increases with swimming speed exceeding 35µm/sec (30). Flicking is thought to occur because of the force exerted on the cell body by water's drag and the opposing force from the rotating flagellum. These opposing forces cause the hook to buckle when the cells change from backward to forward swimming. Thus, marine bacteria which usually have higher swimming speed, may more commonly swim in a cyclic three step pattern of run-reverse-

124

flick. On the other hand, soil-dwelling bacteria like *A. brasilense* are usually slower with the average speed of *A. brasilense* at about 30 μm/sec (86). Since most swimming *A. brasilense* cells have maximum speed around n 35μm/sec, it may be that only a subset of swimming cells can flick. Cell size was also shown to be a factor in determining the flicking angle (31) and could thus perhaps contribute to rare flicking events. The effect of cell size, swimming speed and turning angle should be should be systematically analyzed to conclusively established if and how flicks occur in *A. brasilense*.

REFERENCES

1. Morimoto YV & Minamino T (2014) Structure and function of the bi-directional bacterial flagellar motor. *Biomolecules* 4(1):217-234.
2. Altegoer F, Schuhmacher J, Pausch P, & Bange G (2014) From molecular evolution to biobricks and synthetic modules: a lesson by the bacterial flagellum. *Biotechnol Genet Eng Rev* 30(1-2):49-64.
3. Minamino T & Imada K (2015) The bacterial flagellar motor and its structural diversity. *Trends Microbiol* 23(5):267-274.
4. Wolgemuth CW (2015) Flagellar motility of the pathogenic spirochetes. *Semin Cell Dev Biol* 46:104-112.
5. Lauga E & Powers TR (2009) The hydrodynamics of swimming microorganisms. *Reports on Progress in Physics* 72(9).
6. Terashima H, Kawamoto A, Morimoto YV, Imada K, & Minamino T (2017) Structural differences in the bacterial flagellar motor among bacterial species. *Biophys Physicobiol*), Vol 14, pp 191-198.
7. Oster G & Wang H (2003) Rotary protein motors. *Trends Cell Biol* 13(3):114-121.
8. Larsen SH, Adler J, Gargus JJ, & Hogg RW (1974) Chemomechanical coupling without ATP: the source of energy for motility and chemotaxis in bacteria. *Proc Natl Acad Sci U S A* 71(4):1239-1243.
9. Imae Y & Atsumi T (1989) Na+-driven bacterial flagellar motors. *Journal of bioenergetics and biomembranes* 21(6):705-716.
10. Mandadapu KK, Nirody JA, Berry RM, & Oster G (2015) Mechanics of torque generation in the bacterial flagellar motor. *Proc Natl Acad Sci U S A* 112(32):E4381-4389.
11. Thomas DR, Francis NR, Xu C, & DeRosier DJ (2006) The three-dimensional structure of the flagellar rotor from a clockwise-locked mutant of Salmonella enterica serovar Typhimurium. *J Bacteriol* 188(20):7039-7048.
12. Beeby M, *et al.* (2016) Diverse high-torque bacterial flagellar motors assemble wider stator rings using a conserved protein scaffold. *Proc Natl Acad Sci U S A* 113(13):E1917-1926.
13. Zhou J, Lloyd SA, & Blair DF (1998) Electrostatic interactions between rotor and stator in the bacterial flagellar motor. *Proc Natl Acad Sci U S A* 95(11):6436-6441.
14. Gotz R & Schmitt R (1987) Rhizobium meliloti swims by unidirectional, intermittent rotation of right-handed flagellar helices. *J Bacteriol* 169(7):3146-3150.
15. Armitage JP & Macnab RM (1987) Unidirectional, intermittent rotation of the flagellum of Rhodobacter sphaeroides. *J Bacteriol* 169(2):514-518.
16. Kojima M, Kubo R, Yakushi T, Homma M, & Kawagishi I (2007) The bidirectional polar and unidirectional lateral flagellar motors of Vibrio alginolyticus are controlled by a single CheY species. *Mol Microbiol* 64(1):57-67.
17. Ryu WS, Berry RM, & Berg HC (2000) Torque-generating units of the flagellar motor of Escherichia coli have a high duty ratio. *Nature* 403(6768):444-447.

18. Nord AL, Sowa Y, Steel BC, Lo CJ, & Berry RM (2017) Speed of the bacterial flagellar motor near zero load depends on the number of stator units. *Proc Natl Acad Sci U S A* 114(44):11603-11608.

19. Sowa Y, Hotta H, Homma M, & Ishijima A (2003) Torque-speed relationship of the Na+-driven flagellar motor of Vibrio alginolyticus. *J Mol Biol* 327(5):1043-1051.

20. Li G & Tang JX (2006) Low flagellar motor torque and high swimming efficiency of Caulobacter crescentus swarmer cells. *Biophys J* 91(7):2726-2734.

21. McCarter LL (2004) Dual flagellar systems enable motility under different circumstances. *J Mol Microbiol Biotechnol* 7(1-2):18-29.

22. Merino S, Shaw JG, & Tomas JM (2006) Bacterial lateral flagella: an inducible flagella system. *FEMS Microbiol Lett* 263(2):127-135.

23. Berg HC (2013) CELL MOTILITY Turning failure into function. *Nature Physics* 9(8):460-461.

24. Elgeti J, Winkler RG, & Gompper G (2015) Physics of microswimmers--single particle motion and collective behavior: a review. *Rep Prog Phys* 78(5):056601.

25. Leifson E, Cosenza BJ, Murchelano R, & Cleverdon RC (1964) Motile Marine Bacteria. I. Techniques, Ecology, and General Characteristics. *J Bacteriol* 87:652-666.

26. Johansen JE, Pinhassi J, Blackburn N, Zweifel UL, & Hagstrom A (2002) Variability in motility characteristics among marine bacteria. *Aquat Microb Ecol* 28(3):229-237.

27. Lauga E (2016) Bacterial Hydrodynamics. *Annual Review of Fluid Mechanics, Vol 48* 48:105-130.

28. Xie L, Altindal T, Chattopadhyay S, & Wu XL (2011) From the Cover: Bacterial flagellum as a propeller and as a rudder for efficient chemotaxis. *Proc Natl Acad Sci U S A* 108(6):2246-2251.

29. Stocker R (2011) Reverse and flick: Hybrid locomotion in bacteria. *Proc Natl Acad Sci U S A* 108(7):2635-2636.

30. Son K, Guasto JS, & Stocker R (2013) Bacteria can exploit a flagellar buckling instability to change direction. *Nature Physics* 9(8):494-498.

31. Taute KM, Gude S, Tans SJ, & Shimizu TS (2015) High-throughput 3D tracking of bacteria on a standard phase contrast microscope. *Nat Commun* 6:8776.

32. Pilizota T*, et al.* (2009) A molecular brake, not a clutch, stops the Rhodobacter sphaeroides flagellar motor. *Proc Natl Acad Sci U S A* 106(28):11582-11587.

33. Packer HL, Lawther H, & Armitage JP (1997) The Rhodobacter sphaeroides flagellar motor is a variable-speed rotor. *Febs Letters* 409(1):37-40.

34. Attmannspacher U, Scharf B, & Schmitt R (2005) Control of speed modulation (chemokinesis) in the unidirectional rotary motor of Sinorhizobium meliloti. *Mol Microbiol* 56(3):708-718.

35. Fung DC & Berg HC (1995) Powering the flagellar motor of Escherichia coli with an external voltage source. *Nature* 375(6534):809-812.

36. Nierman WC, *et al.* (2001) Complete genome sequence of Caulobacter crescentus. *Proc Natl Acad Sci U S A*), Vol 98, pp 4136-4141.

37. Lele PP, Roland T, Shrivastava A, Chen Y, & Berg HC (2016) The flagellar motor of Caulobacter crescentus generates more torque when a cell swims backward. *Nat Phys* 12(2):175-178.

38. Chaban B, Coleman I, & Beeby M (2018) Evolution of higher torque in Campylobacter-type bacterial flagellar motors. *Sci Rep* 8(1):97.

39. Beeby M (2015) Motility in the epsilon-proteobacteria. *Curr Opin Microbiol* 28:115-121.

40. Lever MA, *et al.* (2015) Life under extreme energy limitation: a synthesis of laboratory- and field-based investigations. *FEMS Microbiol Rev* 39(5):688-728.

41. Son K, Menolascina F, & Stocker R (2016) Speed-dependent chemotactic precision in marine bacteria. *Proc Natl Acad Sci U S A* 113(31):8624-8629.

42. Liu B, *et al.* (2014) Helical motion of the cell body enhances Caulobacter crescentus motility. *Proc Natl Acad Sci U S A* 111(31):11252-11256.

43. Martinez LE, *et al.* (2016) Helicobacter pylori strains vary cell shape and flagellum number to maintain robust motility in viscous environments. *Mol Microbiol* 99(1):88-110.

44. Ping L, Birkenbeil J, & Monajembashi S (2013) Swimming behavior of the monotrichous bacterium Pseudomonas fluorescens SBW25. *FEMS Microbiol Ecol* 86(1):36-44.

45. Qian C, Wong CC, Swarup S, & Chiam KH (2013) Bacterial tethering analysis reveals a "run-reverse-turn" mechanism for Pseudomonas species motility. *Appl Environ Microbiol* 79(15):4734-4743.

46. Theves M, Taktikos J, Zaburdaev V, Stark H, & Beta C (2013) A bacterial swimmer with two alternating speeds of propagation. *Biophys J* 105(8):1915-1924.

47. Vater SM, *et al.* (2014) Swimming behavior of Pseudomonas aeruginosa studied by holographic 3D tracking. *PLoS One* 9(1):e87765.

48. Yang Y, He J, Altindal T, Xie L, & Wu XL (2015) A Non-Poissonian Flagellar Motor Switch Increases Bacterial Chemotactic Potential. *Biophys J* 109(5):1058-1069.

49. Mitchell JG & Kogure K (2006) Bacterial motility: links to the environment and a driving force for microbial physics. *FEMS Microbiol Ecol* 55(1):3-16.

50. Xie L & Wu XL (2014) Bacterial motility patterns reveal importance of exploitation over exploration in marine microhabitats. Part I: theory. *Biophys J* 107(7):1712-1720.

51. Altindal T, Xie L, & Wu XL (2011) Implications of three-step swimming patterns in bacterial chemotaxis. *Biophys J* 100(1):32-41.

52. Taktikos J, Stark H, & Zaburdaev V (2013) How the motility pattern of bacteria affects their dispersal and chemotaxis. *PLoS One* 8(12):e81936.

53. Stocker R, Seymour JR, Samadani A, Hunt DE, & Polz MF (2008) Rapid chemotactic response enables marine bacteria to exploit ephemeral microscale nutrient patches. *Proc Natl Acad Sci U S A* 105(11):4209-4214.

54. Anderson JK, Smith TG, & Hoover TR (2010) Sense and sensibility: flagellum-mediated gene regulation. *Trends Microbiol* 18(1):30-37.

55. Nadeau J, Lindensmith C, Deming JW, Fernandez VI, & Stocker R (2016) Microbial Morphology and Motility as Biosignatures for Outer Planet Missions. *Astrobiology* 16(10):755-774.

56. Wadhams GH & Armitage JP (2004) Making sense of it all: bacterial chemotaxis. *Nat Rev Mol Cell Biol* 5(12):1024-1037.

57. Chaban B, Hughes HV, & Beeby M (2015) The flagellum in bacterial pathogens: For motility and a whole lot more. *Semin Cell Dev Biol* 46:91-103.

58. Bai F*, et al.* (2010) Conformational spread as a mechanism for cooperativity in the bacterial flagellar switch. *Science* 327(5966):685-689.

59. Yuan J, Branch RW, Hosu BG, & Berg HC (2012) Adaptation at the output of the chemotaxis signalling pathway. *Nature* 484(7393):233-236.

60. Branch RW, Sayegh MN, Shen C, Nathan VSJ, & Berg HC (2014) Adaptive remodelling by FliN in the bacterial rotary motor. *J Mol Biol* 426(19):3314-3324.

61. Cluzel P, Surette M, & Leibler S (2000) An ultrasensitive bacterial motor revealed by monitoring signaling proteins in single cells. *Science* 287(5458):1652-1655.

62. Kim EA*, et al.* (2017) Architecture of the Flagellar Switch Complex of Escherichia coli: Conformational Plasticity of FliG and Implications for Adaptive Remodeling. *J Mol Biol* 429(9):1305-1320.

63. Yuan J & Berg HC (2013) Ultrasensitivity of an adaptive bacterial motor. *J Mol Biol* 425(10):1760-1764.

64. Duke TA, Le Novere N, & Bray D (2001) Conformational spread in a ring of proteins: a stochastic approach to allostery. *J Mol Biol* 308(3):541-553.

65. Ma Q, Nicolau DV, Jr., Maini PK, Berry RM, & Bai F (2012) Conformational spread in the flagellar motor switch: a model study. *PLoS Comput Biol* 8(5):e1002523.

66. Welch M, Oosawa K, Aizawa S, & Eisenbach M (1993) Phosphorylation-dependent binding of a signal molecule to the flagellar switch of bacteria. *Proc Natl Acad Sci U S A* 90(19):8787-8791.

67. Sarkar MK, Paul K, & Blair D (2010) Chemotaxis signaling protein CheY binds to the rotor protein FliN to control the direction of flagellar rotation in Escherichia coli. *Proc Natl Acad Sci U S A* 107(20):9370-9375.

68. Sarkar MK, Paul K, & Blair DF (2010) Subunit organization and reversal-associated movements in the flagellar switch of Escherichia coli. *J Biol Chem* 285(1):675-684.

69. Lloyd SA, Tang H, Wang X, Billings S, & Blair DF (1996) Torque generation in the flagellar motor of Escherichia coli: evidence of a direct role for FliG but not for FliM or FliN. *J Bacteriol* 178(1):223-231.

70. Lloyd SA & Blair DF (1997) Charged residues of the rotor protein FliG essential for torque generation in the flagellar motor of Escherichia coli. *J Mol Biol* 266(4):733-744.

71. Fukuoka H, Sagawa T, Inoue Y, Takahashi H, & Ishijima A (2014) Direct imaging of intracellular signaling components that regulate bacterial chemotaxis. *Sci Signal* 7(319):ra32.

72. Zhu X, Volz K, & Matsumura P (1997) The CheZ-binding surface of CheY overlaps the CheA- and FliM-binding surfaces. *J Biol Chem* 272(38):23758-23764.

73. Lee SY*, et al.* (2001) Crystal structure of activated CheY. Comparison with other activated receiver domains. *J Biol Chem* 276(19):16425-16431.

74. Lee SY*, et al.* (2001) Crystal structure of an activated response regulator bound to its target. *Nat Struct Biol* 8(1):52-56.

75. McDonald LR, Whitley MJ, Boyer JA, & Lee AL (2013) Colocalization of fast and slow timescale dynamics in the allosteric signaling protein CheY. *J Mol Biol* 425(13):2372-2381.

76. Cho HS*, et al.* (2000) NMR structure of activated CheY. *J Mol Biol* 297(3):543-551.

77. Wuichet K & Zhulin IB (2010) Origins and diversification of a complex signal transduction system in prokaryotes. *Sci Signal* 3(128):ra50.

78. Porter SL*, et al.* (2006) The CheYs of Rhodobacter sphaeroides. *J Biol Chem* 281(43):32694-32704.

79. Nesper J*, et al.* (2017) Cyclic di-GMP differentially tunes a bacterial flagellar motor through a novel class of CheY-like regulators. *Elife* 6.

80. Sourjik V & Schmitt R (1996) Different roles of CheY1 and CheY2 in the chemotaxis of Rhizobium meliloti. *Mol Microbiol* 22(3):427-436.

81. Sourjik V & Schmitt R (1998) Phosphotransfer between CheA, CheY1, and CheY2 in the chemotaxis signal transduction chain of Rhizobium meliloti. *Biochemistry* 37(8):2327-2335.

82. Szurmant H, Muff TJ, & Ordal GW (2004) Bacillus subtilis CheC and FliY are members of a novel class of CheY-P-hydrolyzing proteins in the chemotactic signal transduction cascade. *J Biol Chem* 279(21):21787-21792.

83. Zhulin IB & Armitage JP (1993) Motility, chemokinesis, and methylation-independent chemotaxis in Azospirillum brasilense. *J Bacteriol* 175(4):952-958.

84. Bible AN*, et al.* (2015) Metabolic adaptations of Azospirillum brasilense to oxygen stress by cell-cell clumping and flocculation. *Applied and Environmental Microbiology*.

85. Bible A, Russell MH, & Alexandre G (2012) The Azospirillum brasilense Che1 chemotaxis pathway controls swimming velocity, which affects transient cell-to-cell clumping. *J Bacteriol* 194(13):3343-3355.

86. Mukherjee T, Kumar D, Burriss N, Xie Z, & Alexandre G (2016) Azospirillum brasilense Chemotaxis Depends on Two Signaling Pathways Regulating Distinct Motility Parameters. *J Bacteriol* 198(12):1764-1772.

87.   Wadhams GH*, et al.* (2002) TlpC, a novel chemotaxis protein in Rhodobacter sphaeroides, localizes to a discrete region in the cytoplasm. *Mol Microbiol* 46(5):1211-1221.

88.   Buchan A, Crombie B, & Alexandre GM (2010) Temporal dynamics and genetic diversity of chemotactic-competent microbial populations in the rhizosphere. *Environ Microbiol* 12(12):3171-3184.

89.   Wuichet K, Alexander RP, & Zhulin IB (2007) Comparative genomic and protein sequence analyses of a complex system controlling bacterial chemotaxis. *Methods Enzymol* 422:1-31.

90.   Stephens BB, Loar SN, & Alexandre G (2006) Role of CheB and CheR in the complex chemotactic and aerotactic pathway of Azospirillum brasilense. *J Bacteriol* 188(13):4759-4768.

91.   Cecagno R, Fritsch TE, & Schrank IS (2015) The plant growth-promoting bacteria Azospirillum amazonense: genomic versatility and phytohormone pathway. *Biomed Res Int* 2015:898592.

92.   Wisniewski-Dye F*, et al.* (2012) Genome Sequence of Azospirillum brasilense CBG497 and Comparative Analyses of Azospirillum Core and Accessory Genomes provide Insight into Niche Adaptation. *Genes (Basel)* 3(4):576-602.

93.   Rivera D*, et al.* (2014) Complete Genome Sequence of the Model Rhizosphere Strain Azospirillum brasilense Az39, Successfully Applied in Agriculture. *Genome Announc* 2(4).

94.   Wisniewski-Dye F*, et al.* (2011) Azospirillum genomes reveal transition of bacteria from aquatic to terrestrial environments. *PLoS Genet* 7(12):e1002430.

95.   Jiang ZY, Gest H, & Bauer CE (1997) Chemosensory and photosensory perception in purple photosynthetic bacteria utilize common signal transduction components. *J Bacteriol* 179(18):5720-5727.

96.   Mohari B*, et al.* (2015) Novel Pseudotaxis Mechanisms Improve Migration of Straight-Swimming Bacterial Mutants Through a Porous Environment. *mBio*), Vol 6.

97.   Wolfe AJ & Berg HC (1989) Migration of bacteria in semisolid agar. *Proc Natl Acad Sci U S A* 86(18):6973-6977.

98.   Miller LD, Yost CK, Hynes MF, & Alexandre G (2007) The major chemotaxis gene cluster of Rhizobium leguminosarum bv. viciae is essential for competitive nodulation. *Mol Microbiol* 63(2):348-362.

99.   Bible AN, Stephens BB, Ortega DR, Xie Z, & Alexandre G (2008) Function of a chemotaxis-like signal transduction pathway in modulating motility, cell clumping, and cell length in the alphaproteobacterium Azospirillum brasilense. *J Bacteriol* 190(19):6365-6375.

100.   Lauga E, DiLuzio WR, Whitesides GM, & Stone HA (2006) Swimming in circles: motion of bacteria near solid boundaries. *Biophys J* 90(2):400-412.

101. Lemelle L, Palierne JF, Chatre E, & Place C (2010) Counterclockwise circular motion of bacteria swimming at the air-liquid interface. *J Bacteriol* 192(23):6307-6308.
102. Armitage JP & Schmitt R (1997) Bacterial chemotaxis: Rhodobacter sphaeroides and Sinorhizobium meliloti--variations on a theme? *Microbiology* 143 (Pt 12):3671-3682.
103. Greck M, Platzer J, Sourjik V, & Schmitt R (1995) Analysis of a chemotaxis operon in Rhizobium meliloti. *Mol Microbiol* 15(6):989-1000.
104. Siuti P, Green C, Edwards AN, Doktycz MJ, & Alexandre G (2011) The chemotaxis-like Che1 pathway has an indirect role in adhesive cell properties of Azospirillum brasilense. *FEMS Microbiol Lett* 323(2):105-112.
105. Koonin EV, Makarova KS, & Aravind L (2001) Horizontal gene transfer in prokaryotes: quantification and classification. *Annu Rev Microbiol* 55:709-742.
106. Porter SL, Wadhams GH, & Armitage JP (2011) Signal processing in complex chemotaxis pathways. *Nat Rev Microbiol* 9(3):153-165.
107. Porter SL, Warren AV, Martin AC, & Armitage JP (2002) The third chemotaxis locus of Rhodobacter sphaeroides is essential for chemotaxis. *Molecular Microbiology* 46(4):1081-1094.
108. Shah DS, Porter SL, Martin AC, Hamblin PA, & Armitage JP (2000) Fine tuning bacterial chemotaxis: analysis of Rhodobacter sphaeroides behaviour under aerobic and anaerobic conditions by mutation of the major chemotaxis operons and cheY genes. *EMBO J* 19(17):4601-4613.
109. Russell MH, *et al.* (2013) Integration of the second messenger c-di-GMP into the chemotactic signaling pathway. *MBio* 4(2):e00001-00013.
110. Stocker R & Seymour JR (2012) Ecology and physics of bacterial chemotaxis in the ocean. *Microbiol Mol Biol Rev* 76(4):792-812.
111. Carvalhais LC, *et al.* (2013) Linking plant nutritional status to plant-microbe interactions. *PLoS One* 8(7):e68555.
112. Philippot L, Raaijmakers JM, Lemanceau P, & van der Putten WH (2013) Going back to the roots: the microbial ecology of the rhizosphere. *Nat Rev Microbiol* 11(11):789-799.
113. Hinsinger P, Bengough AG, Vetterlein D, & Young IM (2009) Rhizosphere: biophysics, biogeochemistry and ecological relevance. *Plant Soil* 321(1-2):117-152.
114. Flessa H (1994) Plant-induced changes in the redox potential of the rhizospheres of the submerged vascular macrophytes Myriophyllum verticillatum L. and Ranunculus circinatus L. *Aquatic Botany* 47(2):119-129.
115. Greer-Phillips SE, Stephens BB, & Alexandre G (2004) An energy taxis transducer promotes root colonization by Azospirillum brasilense. *J Bacteriol* 186(19):6595-6604.
116. Hauwaerts D, Alexandre G, Das SK, Vanderleyden J, & Zhulin IB (2002) A major chemotaxis gene cluster in Azospirillum brasilense and relationships between

chemotaxis operons in alpha-proteobacteria. *Fems Microbiology Letters* 208(1):61-67.

117. Vanstockem M, Michiels K, Vanderleyden J, & Van Gool AP (1987) Transposon Mutagenesis of Azospirillum brasilense and Azospirillum lipoferum: Physical Analysis of Tn5 and Tn5-Mob Insertion Mutants. *Appl Environ Microbiol* 53(2):410-415.

118. Higuchi R, Krummel B, & Saiki RK (1988) A general method of in vitro preparation and specific mutagenesis of DNA fragments: study of protein and DNA interactions. *Nucleic Acids Res* 16(15):7351-7367.

119. Krause A, Doerfel A, & Gottfert M (2002) Mutational and transcriptional analysis of the type III secretion system of Bradyrhizobium japonicum. *Molecular plant-microbe interactions : MPMI* 15(12):1228-1235.

120. Simon R, Priefer U, & Puhler A (1983) A Broad Host Range Mobilization System for In Vivo Genetic Engineering: Transposon Mutagenesis in Gram Negative Bacteria. *Nat Biotech* 1(9):784-791.

121. Keen NT, Tamaki S, Kobayashi D, & Trollinger D (1988) Improved broad-host-range plasmids for DNA cloning in gram-negative bacteria. *Gene* 70(1):191-197.

122. Dennis JJ & Zylstra GJ (1998) Plasposons: modular self-cloning minitransposon derivatives for rapid genetic analysis of gram-negative bacterial genomes. *Appl Environ Microbiol* 64(7):2710-2715.

123. Topfer R, Schell J, & Steinbiss HH (1988) Versatile cloning vectors for transient gene expression and direct gene transfer in plant cells. *Nucleic Acids Res* 16(17):8725.

124. Alexandre G, Greer SE, & Zhulin IB (2000) Energy taxis is the dominant behavior in Azospirillum brasilense. *Journal of Bacteriology* 182(21):6042-6048.

125. Goto T, Nakata K, Baba K, Nishimura M, & Magariyama Y (2005) A fluid-dynamic interpretation of the asymmetric motion of singly flagellated bacteria swimming close to a boundary. *Biophys J* 89(6):3771-3779.

126. Berg HC & Brown DA (1972) Chemotaxis in Escherichia coli analysed by three-dimensional tracking. *Nature* 239(5374):500-504.

127. Berg HC (2000) Motile behavior of bacteria. *Physics Today* 53(1):24-29.

128. Lazova MD, Ahmed T, Bellomo D, Stocker R, & Shimizu TS (2011) Response rescaling in bacterial chemotaxis. *Proc Natl Acad Sci U S A* 108(33):13870-13875.

129. Jabbarzadeh M & Fu HC (2018) Dynamic instability in the hook-flagellum system that triggers bacterial flicks. *Phys Rev E* 97(1-1):012402.

130. Taylor BL & Koshland DE, Jr. (1974) Reversal of flagellar rotation in monotrichous and peritrichous bacteria: generation of changes in direction. *J Bacteriol* 119(2):640-642.

131. Vos M, Wolf AB, Jennings SJ, & Kowalchuk GA (2013) Micro-scale determinants of bacterial diversity in soil. *FEMS Microbiol Rev* 37(6):936-954.

132. Lanfranconi MP, Alvarez HM, & Studdert CA (2003) A strain isolated from gas oil-contaminated soil displays chemotaxis towards gas oil and hexadecane. *Environ Microbiol* 5(10):1002-1008.

133. Lapidus IR, Welch M, & Eisenbach M (1988) Pausing of flagellar rotation is a component of bacterial motility and chemotaxis. *J Bacteriol* 170(8):3627-3632.

134. Eisenbach M, *et al.* (1990) Pausing, Switching and Speed Fluctuation of the Bacterial Flagellar Motor and Their Relation to Motility and Chemotaxis. *Journal of Molecular Biology* 211(3):551-563.

135. Berg HC (2003) The rotary motor of bacterial flagella. *Annu Rev Biochem* 72:19-54.

136. Cai Q, Li Z, Ouyang Q, Luo C, & Gordon VD (2016) Singly Flagellated Pseudomonas aeruginosa Chemotaxes Efficiently by Unbiased Motor Regulation. *MBio* 7(2):e00013.

137. Yuan J & Berg HC (2008) Resurrection of the flagellar rotary motor near zero load. *Proc Natl Acad Sci U S A* 105(4):1182-1185.

138. Nord AL, Pedaci F, & Berry RM (2016) Transient pauses of the bacterial flagellar motor at low load. *New Journal of Physics* 18(11).

139. Gullett J, O'Neal L, Mukherjee T, & Alexandre G (2017) Azospirillum brasilense: Laboratory Maintenance and Genetic Manipulation. *Current protocols in microbiology* 47:3e.2.1-3e.2.17.

140. Alexeyev MF (1999) The pKNOCK series of broad-host-range mobilizable suicide vectors for gene knockout and targeted DNA insertion into the chromosome of Gram-negative bacteria. *Biotechniques* 26(5):824-+.

141. Platt R, Drescher C, Park SK, & Phillips GJ (2000) Genetic system for reversible integration of DNA constructs and lacZ gene fusions into the Escherichia coli chromosome. *Plasmid* 43(1):12-23.

142. Figurski DH & Helinski DR (1979) Replication of an origin-containing derivative of plasmid RK2 dependent on a plasmid function provided in trans. *Proc Natl Acad Sci U S A* 76(4):1648-1652.

143. Schafer A, *et al.* (1994) Small mobilizable multi-purpose cloning vectors derived from the Escherichia coli plasmids pK18 and pK19: selection of defined deletions in the chromosome of Corynebacterium glutamicum. *Gene* 145(1):69-73.

144. Crocker JC & Grier DG (1996) Methods of digital video microscopy for colloidal studies. *J Colloid Interf Sci* 179(1):298-310.

145. Masson JB, Voisinne G, Wong-Ng J, Celani A, & Vergassola M (2012) Noninvasive inference of the molecular chemotactic response using bacterial trajectories. *Proc Natl Acad Sci U S A* 109(5):1802-1807.

146. Sourjik V & Wingreen NS (2012) Responding to chemical gradients: bacterial chemotaxis. *Curr Opin Cell Biol* 24(2):262-268.

147. Hamer R, Chen PY, Armitage JP, Reinert G, & Deane CM (2010) Deciphering chemotaxis pathways using cross species comparisons. *BMC Syst Biol* 4:3.

148. Bourret RB (2010) Receiver domain structure and function in response regulator proteins. *Curr Opin Microbiol* 13(2):142-149.

149. Volz K & Matsumura P (1991) Crystal structure of Escherichia coli CheY refined at 1.7-A resolution. *J Biol Chem* 266(23):15511-15519.

150. Robert X & Gouet P (2014) Deciphering key features in protein structures with the new ENDscript server. *Nucleic Acids Res* 42(Web Server issue):W320-324.

151. Letunic I & Bork P (2016) Interactive tree of life (iTOL) v3: an online tool for the display and annotation of phylogenetic and other trees. *Nucleic Acids Res* 44(W1):W242-245.

152. Gorelik R & Gautreau A (2014) Quantitative and unbiased analysis of directional persistence in cell migration. *Nat Protoc* 9(8):1931-1943.

153. Darnton NC, Turner L, Rojevsky S, & Berg HC (2010) Dynamics of bacterial swarming. *Biophys J* 98(10):2082-2090.

154. Zhao R, Collins EJ, Bourret RB, & Silversmith RE (2002) Structure and catalytic mechanism of the E. coli chemotaxis phosphatase CheZ. *Nat Struct Biol* 9(8):570-575.

155. Laub MT & Goulian M (2007) Specificity in two-component signal transduction pathways. *Annu Rev Genet* 41:121-145.

156. Podgornaia AI & Laub MT (2013) Determinants of specificity in two-component signal transduction. *Curr Opin Microbiol* 16(2):156-162.

157. Jarrell KF & McBride MJ (2008) The surprisingly diverse ways that prokaryotes move. *Nat Rev Microbiol* 6(6):466-476.

158. Abdel-Salam MS & Klingm�ller W (1987) Transposon Tn5 mutagenesis in Azospirillum lipoferum: isolation of indole acetic acid mutants. *MGG Molecular & General Genetics* 210(1):165-170.

159. Kearns DB (2010) A field guide to bacterial swarming motility. *Nat Rev Microbiol* 8(9):634-644.

160. Karimova G, Pidoux J, Ullmann A, & Ladant D (1998) A bacterial two-hybrid system based on a reconstituted signal transduction pathway. *Proc Natl Acad Sci U S A* 95(10):5752-5756.

161. Paul K, Nieto V, Carlquist WC, Blair DF, & Harshey RM (2010) The c-di-GMP binding protein YcgR controls flagellar motor direction and speed to affect chemotaxis by a "backstop brake" mechanism. *Mol Cell* 38(1):128-139.

VITA

Tanmoy Mukherjee was born and raised in a small town within the coal capital of India called Dhanbad. As a high schooler, he was fascinated by the microbial world and how an organism so small to be seen by naked eyes can cause havoc to human and plant health. He completed his schooling in Dhanbad and moved to different parts of India for his bachelor's and master's study. Before coming to USA for his PhD at The University of Tennessee, Knoxville he worked for more than 2 years in one of the premier research institute in India at Institute of Genomics and Integrative Biology, Delhi. He led a team for several projects on microbial diversity and developing molecular markers for rapid and precise identification of pathogenic bacteria. There he developed keen interest in bacterial signaling and importance of evolutionary study in the host-microbe relationship. He joined the lab of Dr. Gladys Alexandre and has focused on bacterial signaling during his tenure as a graduate student. He has presented his work at several conferences including Bacterial Locomotion and Signal Transduction (BLAST) and the Gordon Research Conference. Tanmoy defended his Thesis on July20th 2018.